THÈSE

En vue de l'obtention du

DOCTORAT DE L'UNIVERSITÉ DE TOULOUSE

Délivré par l'Université Toulouse 3 - Paul Sabatier

Cotutelle internationale avec Nara Institute of Science and Technologie (NAIST)

Présentée et soutenue par

Ryosuke ASATO

Le 22 janvier 2021

Design and Synthesis of Multifunctional Terarylenes for Mechano-, Radio- and Thermo-Chemical Responses

---

Ecole doctorale : **SDM - SCIENCES DE LA MATIERE - Toulouse**

Spécialité : **Chimie Moléculaire**

Unité de recherche :

CEMES - Centre d'Elaboration de Matériaux et d'Etudes Structurales

Thèse dirigée par

Gwénaël RAPENNE et Tsuyoshi KAWAI

Jury

Dr. Jeanne CRASSOUS	**Université de Rennes**	Rapporteure
Prof. Joanne XIE	**ENS Paris Saclay**	Rapporteure
Prof. Eric BENOIST	**Université Paul Sabatier Toulouse**	Examinateur
Prof. Shun HIROTA	**NAIST**	Examinateur
Prof. Kenji MATSUDA	**Kyoto University**	Examinateur
Prof. Takuya NAKASHIMA	**NAIST**	Examinateur
Prof. Gwénaël RAPENNE	**Université Paul Sabatier Toulouse**	Directeur de thèse
Prof. Tsuyoshi KAWAI	**NAIST**	Directeur de thèse

CONTENTS OF THESIS

Abstract / Résumé

Molecular switching materials that modulate physical properties through an external trigger have received much attention in the development of new devices. They require precise switching performance and large scale propagation on single and multiple molecular levels. Diarylethene has attracted much attention due to its excellent photoswitching properties. These molecules photocyclize from the open (o) form to the closed (c) form with UV light, with visible light inducing reversion to the o form. Terarylene structures have been optimized in some items including photoreaction quantum yields, thermal stability and desorption of functional groups upon structural change. This thesis is focused on a single photoswitching reaction and the affect this has on local geometry and physical properties. First, this thesis shows that a small number of photoswitching reactions on a terarylene subunit can stop or start dynamic movement, namely the rotation of a molecular motor. The rotation was activated depending on which part of the rotor is approached by an electron injecting STM tip; with light irradiation offering a second independent control input. A new motor containing a terarylene substituent was designed in which the flexible open form can be converted to its rigid closed form to block rotation via steric interactions thus acting as a light-induced brake. With the initial target unit for this motor chosen using computational calculations of these interactions. A new synthetic methodology for the introduction of the photoswiching unit into the motor is presented and then the rotational control was discussed using spectral changes in the NMR upon irradiation. In the second part of this thesis, the effect c to o form isomerization of terarylenes has on nearby molecules through synergetic effects are presented. Work to enhance the quantum yield of the isomerization provides new applications using alternative stimulus without light irradiation. Examples including chemical or electrochemical oxidation proceed with high efficiency in a (electro)catalytic way, with apparent reaction efficiency exceeding 100% through a cascade reaction. By introducing aromatic groups on the reactive carbons of a photoreactive system, the efficiency of the electrocatalytic cycloreversion reaction was increased to 100000% and applied to the amplified detection of a small amount of high energy photons such as X-rays. In the third part, new molecular solar thermal (MOST) fuel is presented using the cascade reaction. MOST fuel systems capture photonic energy, retaining photocurrent in the formed chemical bond, instead of battery based electrochemical storage. The high energy density of MOST fuel offers large heat release, with cycloreversion via bond disassociation at levels equivalent to artificial photosynthesis without environmental impact. A small amount of electrochemical or chemical oxidation can induce the cascade release of stored thermal energy. In addition, a storing process of the light energy optimized by introduction of phenyl rings on the terarylene reactive carbon atoms has been developed. These present high MOST efficiency and the results are supported by a detailed computational study.

Les matériaux photo-commutation moléculaires qui modulent les propriétés physiques via un stimulus externe ont reçu beaucoup d'attention dans le développement de nouveaux appareils. Les diaryléthènes sont particulièrement intéressants en raison de leurs excellentes propriétés de photoswitching. Ces molécules photocyclisent de la forme ouverte (o) à la forme fermée (c) sous rayonnement UV, la lumière visible permettant de revenir à la forme o. Les structures de type terarylène ont été optimisées pour présenter des rendements quantiques de photoréaction important ainsi qu'un bonne stabilité thermique. Dans cette thèse, l'accent est mis sur une seule réaction de photoswitching et son effet sur la géométrie locale et les propriétés physiques de la molécule obtenue. Dans la première partie, cette thèse montre qu'un petit nombre de réactions de photoswitching sur une sous-unité de terarylène peut arrêter ou déclencher le mouvement de rotation d'un moteur moléculaire à deux étages. La rotation est activée par l'injection d'électrons sur le rotor par une pointe STM. La lumière offre donc une deuxième entrée de commande indépendante. Un nouveau moteur contenant un substituant terarylène a été conçu dans lequel la forme ouverte flexible peut être convertie en sa forme fermée rigide pour bloquer la rotation via des interactions stériques agissant ainsi comme un frein induit par la lumière. L'introduction du fragment photochrome a nécessité une nouvelle voie synthétique dans le moteur est présentée et le contrôle de rotation est démontré par RMN à température variable et suivi de l'irradiation par spectroscopie UV-Visible. Dans la deuxième partie de cette thèse, il est démontré que l'isomérisation des terarylènes peut se propager aux molécules voisines. Il est donc possible d'améliorer le rendement quantique de l'isomérisation pour de nouvelles applications sans qu'il y ait besoin de stimulus lumineux. Des exemples comprenant une oxydation chimique ou électrochimique se déroulent avec une efficacité élevée de manière (électro) catalytique, avec une efficacité de réaction apparente dépassant largement 100% par une réaction en cascade. En introduisant des groupes aromatiques sur les carbones réactifs du système photochrome, l'efficacité de la réaction de cycloréversion électrocatalytique a été augmentée à 100 000 %. Un nouveau système thiophényl riche en électrons a aussi été conçu pour augmenter la stabilité cationique. Il permet de détecter de faible quantité de photons à haute énergie tels que les rayons X. Dans la troisième partie est proposé un nouveau système de combustible solaire thermique moléculaire (MOST) utilisant également la réaction en cascade. La plupart des systèmes de carburant capturent l'énergie photonique, conservant le photocourant sous forme de liaison chimique, au lieu d'un stockage électrochimique couramment utilisé dans les batteries. La densité d'énergie élevée du combustible MOST offre un dégagement de chaleur important, avec une cycloréversion par dissociation des liaisons à des niveaux équivalents à la photosynthèse artificielle sans impact environnemental. Une petite quantité d'oxydation électrochimique ou chimique peut induire la libération en cascade de l'énergie thermique stockée. De plus, un procédé de stockage de l'énergie lumineuse optimisé par l'introduction de cycles phényle sur les atomes de carbone réactifs au terarylène a été développé. Ceux-ci présentent une efficacité MOST élevée et les résultats sont soutenus par une étude théorique détaillée.

1. Introduction: Photoswitching molecular material

New technologies and academic disciplines created by the exploration of molecular systems have contributed greatly to the development of modern humanity. In particular, the challenge of controlling macroscopic functions by considering how they operate at the molecular level and creating materials from multifunctional molecules has led to the development of a wide variety of materials in many fields, such as biology, physics, and chemistry. In the latest field, the ability to design novel molecules has been greatly expanded by new synthetic methodologies. For example, the palladium cross-coupling reactions of Richard F. Heck[1], Ei-ichi Negishi[2] , and Akira Suzuki[3], who were awarded the Nobel Prize in Chemistry in 2010, have enabled the synthesis of a wide variety of targets (Scheme 1a). In various molecular designs, the selective control of physical and chemical properties has been a long-held research target and has led to many potential new applications. For instance, structural modulation of organic substances has been demonstrated through reversible isomerization reactions including the reversible cis-trans isomerization of azobenzene which results in dramatic variations in the physical properties of the molecules and macroscopic materials derived from them. External thermal, chemical and physical stimuli such as stress can also be responsible for these changes; with molecules undergoing light-induced reversible isomerization known as photochromes.

In nature, the cis-trans isomerization in a unique, protein Rhodopsin[4] operates as an initial trigger of the vision cascade system. The photoreceptor Rhodopsin is composed of a chromophore unit, 11-cis-retinal, and a protein part, Opsin. The 11-cis-retinal absorbs visible light and

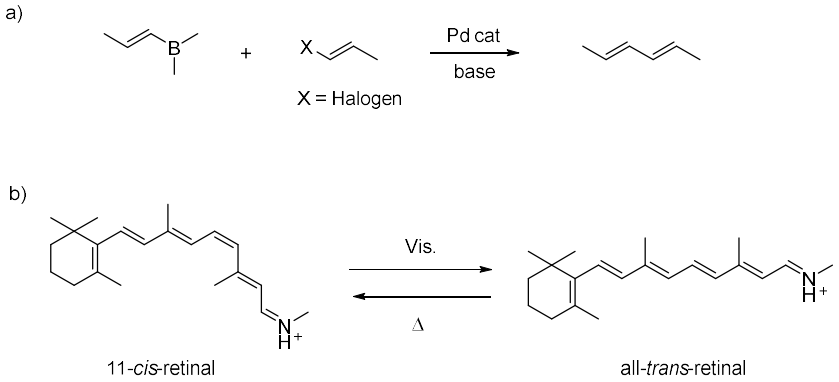

Scheme 1-1 a) The first reported Suzuki-Miyaura cross-coupling reaction[3]

b) Photoisomerization from 11-cis-retinal to all-trans-retinal

isomerizes to the all-trans form, inducing a structural change in the Opsin subunit (scheme 1b). This small structural change affects the higher-order structure of the giant protein and further propagates through the cascade of molecular switches, resulting in the precise and dynamic vision function. The light signals of low photon number are amplified by the dynamic cascade system composed of chromophores, proteins, lipid membranes, and ions. The mechanism is an example of one by which a single photon induces conformational changes in macromolecules and amplifies the input for highly functional photoswitching materials.

On the other hand, photoswitchable human-made molecules readily change their structures with an external light stimuli and display a color change; these molecules are called photochromic molecules and have also been widely studied.[5] The expansion and contraction of π-conjugation upon photoisomerization by light is responsible for the color change of most photochromic molecules. With the development of modern organic synthesis techniques, molecular frameworks such as azobenzene, spiropyran, and diarylethene have been reported as representative examples of organic photochromic molecules (Figure 1-1). The discovery of azobenzene can be dated back to the 1937 report of Hartley et al.[6] However, the recent prominence of photochromism research originates from the study of spiropyrans by Fischer, Hirshberg and others in 1952.[7] Spiropyrans are examples of "T-type" (Thermo reversion type) photochromic molecules, characterized by their ability to undergo both light-induced coloration and thermally-induced rapid fading reactions repeatedly. Meanwhile, diarylethenes[8] were reported by Irie and coworkers in 1988 as typical "P-type" (Photo reversion type) photochromic molecules, showing reversible switching triggered only by light in specific wavelength ranges. The absence of thermally-induced isomerization

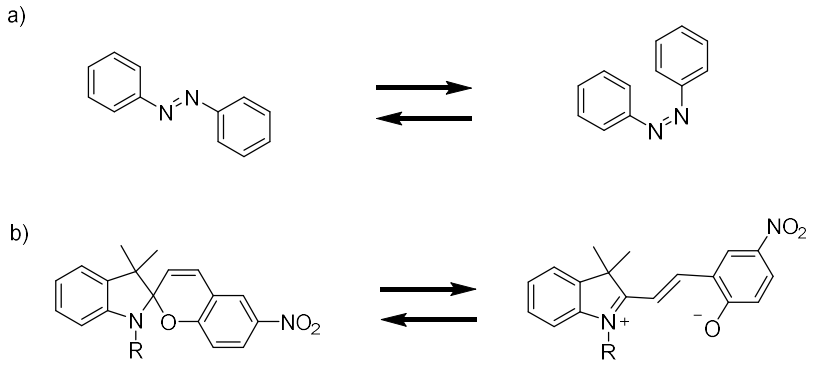

Figure 1-1 a) Photoisomerization of azobenzene[6] b) Photoisomerization of spiropyran.[7]

reactions at room temperature and sometimes even at elevated temperature, is recognized as one of the prominent advantages of diarylethene over other photochromic systems.

1.1 Thermally stable diarylethene derivatives

This class of molecules consists of a framework termed hexatriene, a 6π electron system composed of three π-conjugated bonds, which can undergo an electrocyclic reaction (Figure 1-2a)[9]. The electrocyclic reaction generates or breaks σ-bonds at both ends of a conjugated π-electron system leading to a ring-closing or reverse ring-opening, respectively. This can be interpreted on the basis of frontier orbitals and using Woodward-Hoffman rules, which state in the orbital symmetry conservation principle[10] that the symmetry of the molecule must be conserved in the reaction process and as such the p-orbitals must be of the same symmetry as the HOMO of the product.[10,11]

As schematically illustrated in Figure 1-2, the reaction proceeds by the rotation of the p-orbitals located on the terminal carbon atoms either in the same direction (conrotatory) or in the opposite direction (disrotatory) to each other. In the conrotatory process, the rotational symmetry about the C_2 axis is maintained throughout, while the σ_v reflection plane is maintained in the

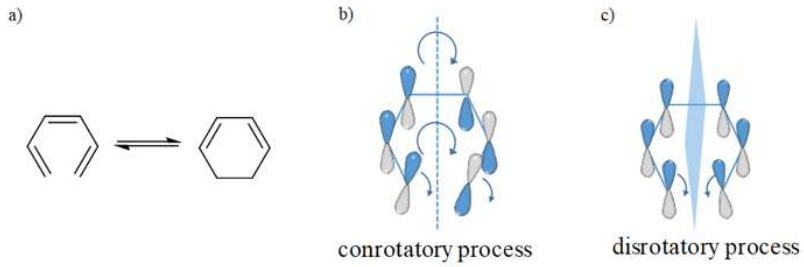

Figure 1-2 a) Electrocyclic reaction of hexatriene. The orbital symmetry conservation principle in the b) conrotatory process, the rotational symmetry about the C_2 axis is satisfied, while c) in disrotatory process, the σ_v reflection plane is satisfied.

disrotatory process (Figure 1-2b, 1-2c). Based on the orbital symmetry conservation principle, in the ground state, the maximum orbital overlap is available in the disrotatory process and which is symmetry allowed process (Figure 1-3). The bonding orbitals may have less overlap in the conrotatory process which is thus symmetry forbidden in the ground state. This means the thermal

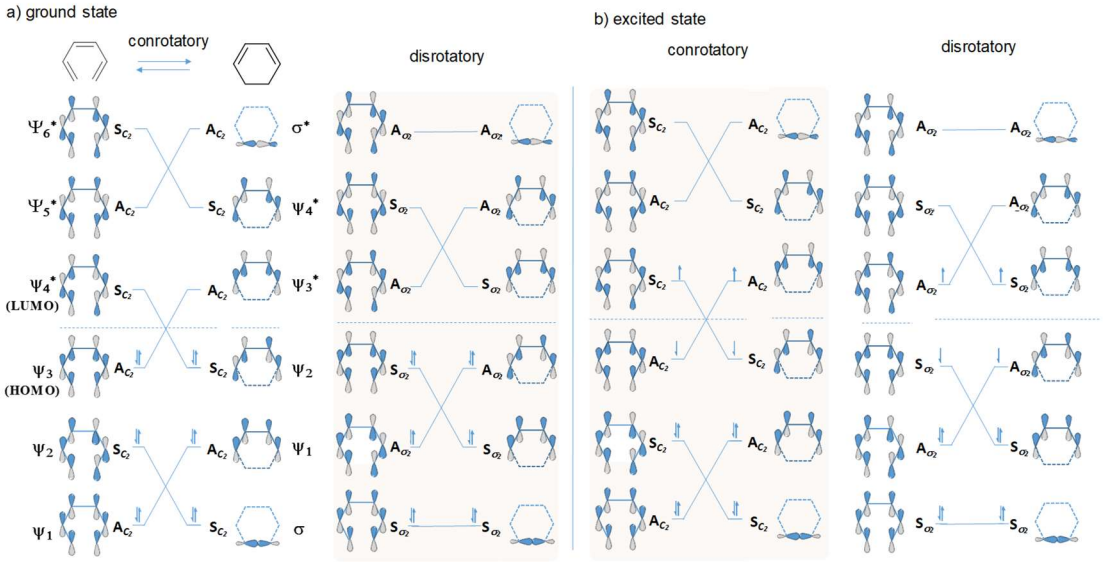

Figure 1-3 Correlation diagrams of electrocyclic reaction or reverse reaction that connect the molecular orbitals of the reactant to those of the product having the same symmetry. It can then be constructed for the two processes either conrotatory or disrotatory in each a) ground state and b) excited state. S_{C_2}: C_2 symmetric to symmetry element, A_{C_2}: C_2 antisymmetric to symmetry element, $S_{\sigma v}$: σ_v symmetric to symmetry element, $A_{\sigma v}$: σ_v antisymmetric to symmetry element

isomerization reaction should proceed through transition state of less symmetry with significantly large activation barrier in the conrotatory reaction. In the photo-excited state, the symmetry conversation role operates oppositely due to the changes in orbital configuration. The photochemical electrocyclic reaction is symmetry allowed through the conrotatory process with the maximum orbital overlap, while the disrotatory process becomes symmetry forbidden. Therefore, the photochemical ring cyclization affords the C_2 symmetric ring-closed form isomer (**c**-form), in which two newly formed sp^3 carbon atoms are anti-configuration.[12] Similarly, the cycloreversion reaction from the C_2 symmetric **c**-form should proceed through the conrotatory process, which should be symmetry allowed in the excited-state but symmetry forbidden in the ground state. The C_2 symmetric **c**-form should thus be thermally stable with an excessively large energy barrier on the ground state cycloreversion reaction.

Although photochromic 1,3,5-hexatriene molecules thus may undergo both conrotatory photochemical- and disrotatory thermal- cyclization reactions, some related substances show isomerization reactions mostly only under the photo-excited state. Such the substances are so-

called as “P-type” photochromic molecules. The several P-type photochromic molecules have been studied actively for exploring future optical data storage material.[5,13] The first well-studied P-type molecule is bismethylene succinic anhydride derivatives, "fulgide"[14,15], which could be colored by both heat and light with an electrocyclic reaction of the triene system (Scheme 1-2). In 1974, Hellar, Paetzold, Ilge, and their coworkers attempted to suppress the disrotatory thermal reaction.[16] They discovered that the disrotatory thermal reaction was suppressed by steric

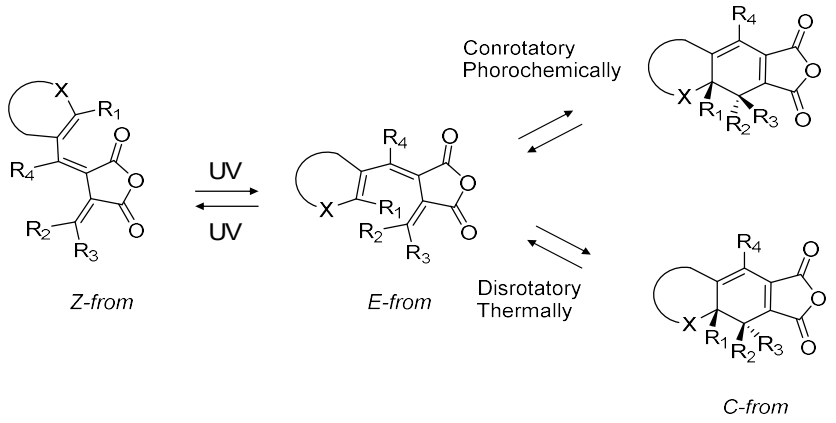

Scheme 1-2 Mechanism of photo- and thermal- isomerization of fulgide.[15]

substituents at R_1, R_2, and R_3, while the photocyclization quantum yields and thermal inactivation were improved by using heterocycles such as furans. In addition, the introduction of a sterically bulky substituent at R_4 suppresses the Z/E isomerization reaction with increasing the quantum yield of the E/C electrocyclic reaction (Scheme 1-2)[15].

Stilbene is also composed of 1,3,5-hexatriene structure and undergoes the cis-trans isomerization and the electrocyclization from the cis-form.[17] Although photo-irradiation to cis-stilbene affords bihydrophenanthrene under degassed conditions via the conrotatory photocyclization, it immediately returns to the cis-stilbene isomer. Whereas this thermal conrotatory ring-opening should be symmetry forbidden[18], bihydrophenanthrene is unstable due to the lack of aromatic stabilization from the two benzene rings compared to cis-stilbene (Figure 1-4a). The transition state in the electronic ground state seems to be stabilized by the partial aromaticity of the two phenyl rings giving a small activation barrier for the ground state thermal isomerization reaction.

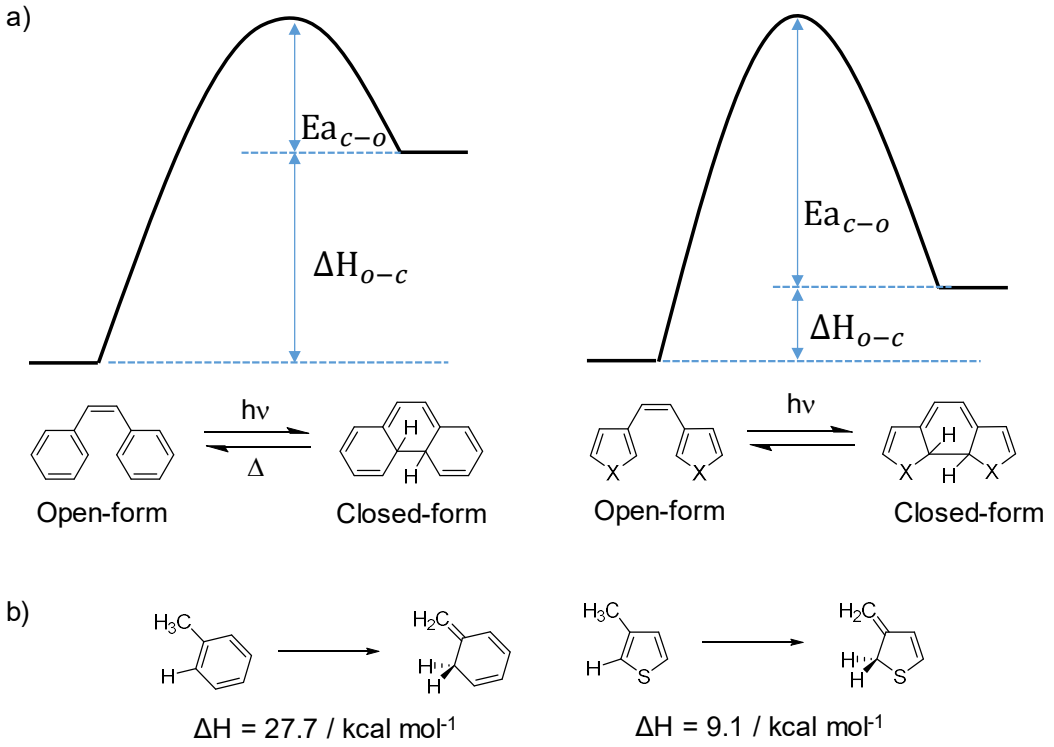

Figure 1-4 a) Mechanism of isomerization reaction and energy diagram for stilbene and diarylethene b) The loss of aromaticity of **one aromatic unit** upon cycloreversion and calculated aromatic stabilization energy difference between two isomers (ΔH_{iso}), by DFT calculation using B3LYP/6-31G(d)

In 1988, Irie and coworkers discovered that 1,2-dithienylethene (DTE) in which both aromatic rings are thiophenes, presenting enough stability in the **c**-form to prevent spontaneous thermal back reaction (Figure 1-4a).[5,19] Molecular orbital calculations suggested that the thermal stability of the conrotatory **c**-form depends on the degree of loss of aromaticity in the aromatic rings on both sides. The aromatic stabilization effect of each aryl group is estimated by density functional theory (DFT) calculation as the difference between the ground state energy of both the isolated benzene and thiophene units in the case of ring-closed and -open reaction (Figure 1-4b). The results indicate that the energy difference between **c**- and **o**-form is larger for the stilbene than for the DTE in the ring-closing reaction. The thiophene ring of DTE has smaller aromaticity than the benzene in stilbene, which must be responsible for the smaller energy difference between the **o**-form and the **c**-form in DTE. The thermal conrotatory ring-opening reaction is therefore

suppressed for DTE, which is rationally understandable regarding the Hammond's postulate (Figure 1-4a).[5,19]

1.2 Terarylene with its thermally stable and excellent photo-switching nature

Diarylethenes, which allow enhanced thermal stability in the **c**-form through choices of aromaticity in the side aryl units, have become a common research topic in molecular photochemistry, and various applications have been proposed, such as a light-induced molecular data storage/memory devices.[13,20,21] To further improve the thermal stability of the c-form, various aryl groups have been investigated.[5,19] Additionally, by introducing cyclic ethenes such as cyclopentene, the cis-trans isomerization reaction was efficiently suppressed, and the ring-cyclization and cycloreversion durability were greatly enhanced. Thermally-stable diarylethenes also show structural changes in response to light with high quantum yield, motivating more detailed optical analysis such as time-resolved transient absorption measurements and multiphoton cycloreversion reactions[22,23,24] Their unique optical properties have recently attracted growing interest for applications in biology-related topics such as super-resolution bio-imaging,[25,26] and enzyme/inhibitor mimicking.[27,28] The structural tunability of diarylethenes encouraged many chemists to combine them with various functional units producing photoswitchable fluorescent, magnetic, catalytic and conducting molecules, polymers and metal complexes.[5,13]

Kawai and coworkers reported triangle terarylene[29,30] which has an additional aromatic aryl unit at the central part of the 1,3,5-hexatriene structure. The chemical structure of terarylenes can be recognized as an extension of diarylethenes modified at the bridging ethene moiety to give extended π-conjugated systems in both isomers. Most changes in the photoswitching effects are thus based on the changes in the extension of the π-conjugation system. In this context, a variety of photoswitching behaviors have been found by taking advantage of the central aryl unit, with four main benefits; **1**) expanding the diversity of structures with combinations of heteroaromatics, **2**) additional possibility to connect them to other units through the central aromatic units preserving the central moieties responsible for photocyclization, **3**) specific stabilization of the **o**-

form due to additional aromatic units, **4**) enhanced redox capability forming stable charged states supported by the extended π-conjugation system.

The structural diversity allows for the control over conformations both in solution and in solid crystals through the molecular design of terarylenes with heteroaromatic rings having specific intramolecular interactions. The intramolecular interactions, such as hydrogen bonding between nitrogens of thiazole units and protons of the other aryl moieties, may specifically stabilize the photo-active C_2 symmetric (antiparallel) conformation, which is preferable for the cyclization in the excited state. The photocyclization quantum yield was found to be close to unity, and photon-quantitative, in hexane (Figure 1-5).[31] Such conformational control in the ground state is also an important approach to extract information about the diversity of excited states.

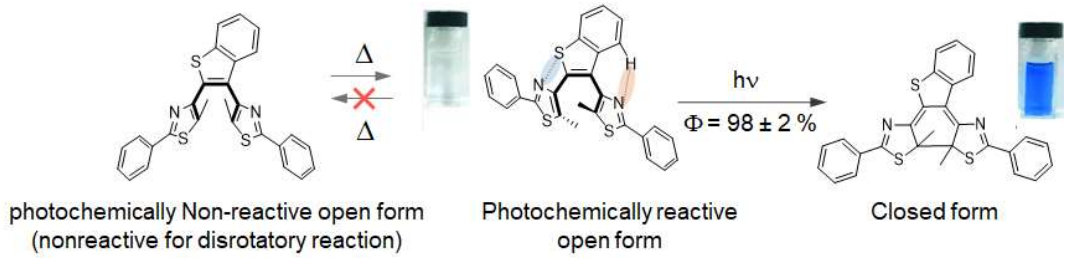

Figure 1-5 Photochromic reaction of the compound in which photocyclization quantum yield was found to be 98 ± 2%[31]

The high photocyclization quantum yields and the high stability of the reaction product have led to the development of terarylenes releasing, hydride, acids and even Lewis acid release (Figure 1-6).[32,33]

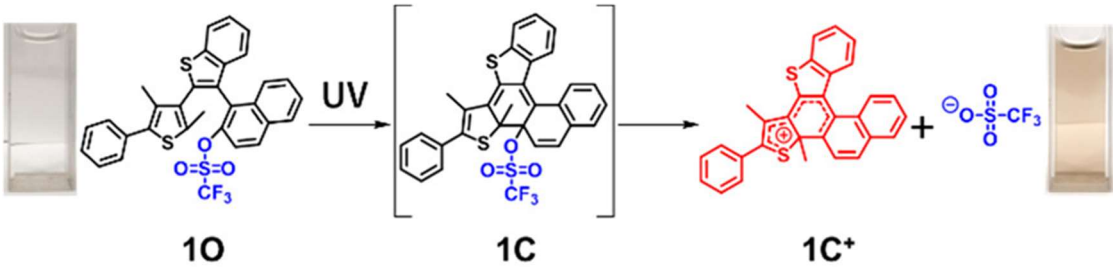

Figure 1-6 Photo-Induced Lewis Acid-Generating Reaction of **1O**[32]

These systems are based on heterolytic elimination of single bond at the reaction center carbon atom of the chemically stable aromatic polycycle. The additional aromatic rings also support specific π-π interactions especially in some extended derivatives containing four or more 2-phenyl-thiazole rings such as in photoswitchable helical oligo-aromatic foldamers.[34] With this, a new dimension in the molecular design, namely chirality, was added so that chiral folding-states were observed[35] and photoswitching of circularly polarized luminescence (CPL) was achieved (Figure 1-7a).[36] Meanwhile, structural tuning of three aryl units has also led to various functional molecules such as photochromic metal complexes for luminescence switching (Figure 1-7b).[37]

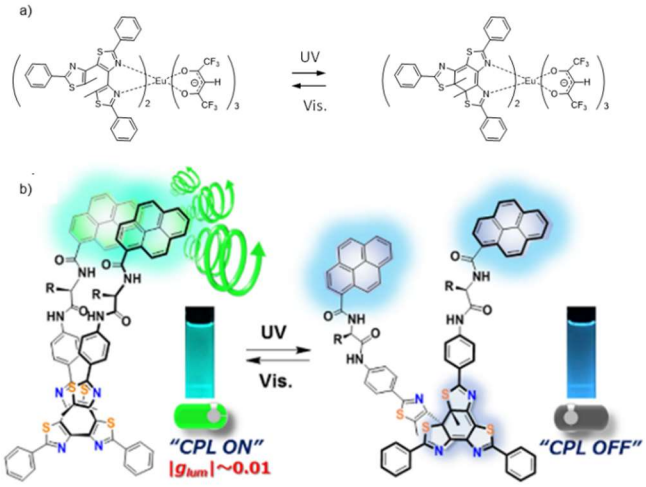

Figure 1-7 a) Photochromic reaction of a terthiazole-Eu(III) complex. The reversible photochromic reaction of terthiazole ligand modulate the emission profile, changing the relative intensity of ED (electric dipole) transition at 614 nm to that of magnetic dipole (MD) transition at 592 nm.[36] b) CPL switching of 2-phenyl-thiazoke derivatives as a photoswitchable helical oligo-aromatic foldamer.[37]

The central aromatic ring also seems to play a major role in reactions of terarylenes in the cationic state. Upon oxidation to the cationic +1 radical state, the **c**-form can spontaneously interconvert to and **o**-form via thermal energy pathways at room temperature, leading to a cascade reaction system.[38] Matsuda and coworkers supposed equilibrium between the **o**-form and the **c**-form at the radical cation state. Their consideration is effectively applicable to some DTE related substances with interconversion highly dependent on the relative stabilities of the two cationic states. Upon addition of aromatic rings to stabilize the charge, the relative stability of the radical

cation of the **o**-form become pronounced so that an efficient oxidative cascade cycloreversion processes was developed for these compounds [39] As a result, he kinetics of oxidative cycloreversion could be improved by 1000-times and the efficiency by 100-times.[40] Using this cascade process, the oxidative cycloreversion of few molecules can be effectively amplified to a macroscopic scale over its surroundings, resulting in a visible color change. These systems create future materials such as highly sensitive photon-detection material. In this thesis, significant X-ray sensing will be demonstrated based upon this principle in Chapter 3.

This additional aromatic central ring additionally grants more sites of substitution and functionalization while preserving the central moieties responsible for photoisomerization. For example, in Figure 1-8, the central moiety can switch between an imidazolium and imidazolinium allowing the ionic charge to move between a delocalized heteroaromatic imidazolium and a localized cationic N-C-N moiety.[41] This essentially uses light to reversibly localize and delocalize charges down to the sub-molecular scale, i.e., inside aromatic rings.

Taking advantage of additional substitution positions, thienothiophene was introduced as an efficient electron-donating unit on the central part, affording a new photoswitchable push-pull (D-

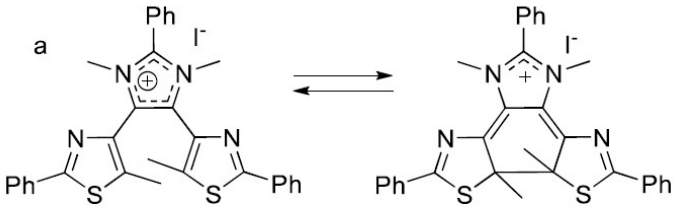

Figure 1-8 Photochromism allowing control of localization of cationic charge.[41]

A) system. A greater level of complexity above that of the classical photoswitching (which was preserved) due to possible protonation, quaternization, and twist-turn switching on the central bridge was achieved (Figure 1-9).[42]

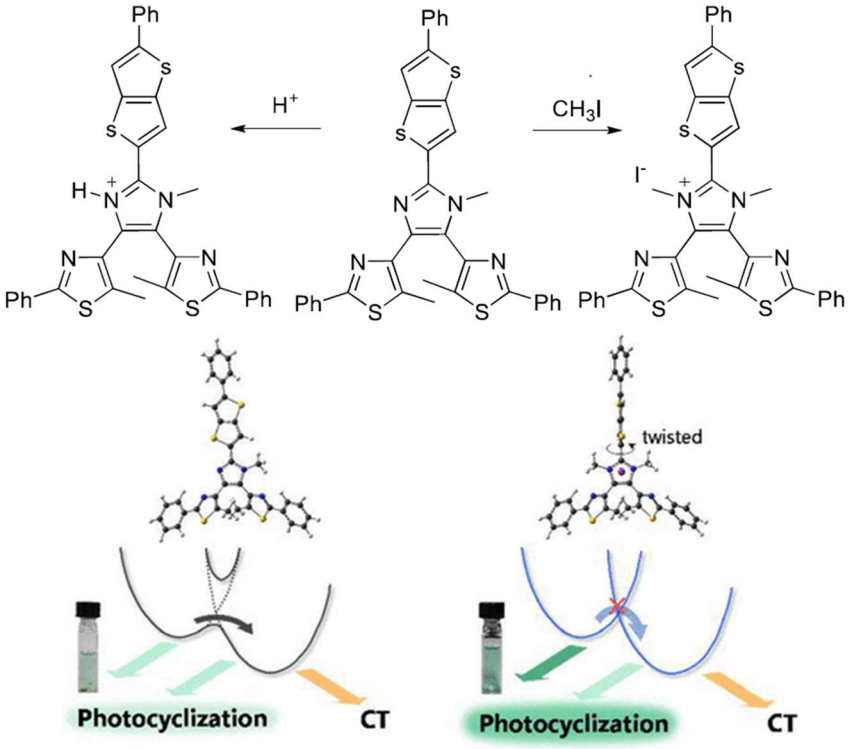

Figure 1-9 functional modification of imidazole ring leading to central moieties whilst keeping the isomerizing unit.[42]

These results also motivated the combination of terarylene with other functional molecular units for advanced photoswitching systems. For instance, the hybridization of terarylene with a rotational molecular motor could achieve photo-control of the rotation by dual external input: the initiation of rotation by electron injection from an STM tip and the locking or unlocking of the rotation by the photo-induced cyclization. This will be discussed in Chapter 2.

The incorporation of central aromatic rings selectively stabilizes the **o**-form due to the aromatic effects more than similar substitutions on the lateral aryl units.[13,19] The careful design in terms of selection and combination of aromatic rings together with substituents can control the thermal stability of the **c**-form with lifetimes ranging from seconds to years.[30,43]

The long lifetime leads to one of the most interesting potential applications of terarylenes in which they are promising candidates for the storage of energy. The long lived **c**-form can be generated and used to store light energy as chemical potential which can later be induced to synergetically release the stored energy thermally. Although a considerable part of the photon energy is converted to heat during the isomerization, a portion is stored as chemical energy in the

c-form which has higher enthalpy than the **o**-form. Such systems have been developed by using various reversible photochromic molecules as MOlecular Solar Thermal storage (MOST) or Solar Thermal Fuel (STF).[44] Even if DTE and related substances have never been studied as MOST materials, terarylene frameworks could fulfill some of the important requirements, such as high ΔH_{iso} for the storage capacity and practical thermal bistability for long term storage of the absorbed energy. This will further be discussed in Chapter 4.

To explore the advantages of terarylene structures and investigate their various promising effects on single and multiple molecular levels such as mechano-, radio- and thermos-chemical responses, this thesis will discuss/focus on the following topics: a molecular motor having photo-brake function, highly sensitive UV and X-ray detection through the oxidative cascade system and possible molecular solar thermal storage and heat release. The background of these topics will be introduced in the subsequent sections.

1.3 Molecular Motor with terarylene unit for on/off switching of rotational motion in single-molecule motors

A molecular-level machine can be defined as a molecule designed to perform a precise function in response to controlled stimulation. This machinery toolkit provides the basis for the future design of bottom-up systems and materials to perform tasks as varied as molecular electronics, information storage, and molecular assembled mechanics. These assembling systems propagate their initial function to adjacent substances or to other part on the same molecule. In the last decade, chemists have created many complex molecular architectures following a monumentalization strategy[45,46]. This approach consists of synthesizing molecules for use as elementary building blocks to later construct more complex systems. Driven by the seminal work of Sauvage, Stoddart, and Feringa, who were awarded the Nobel Prize in Chemistry in 2016, the field of artificial molecular machines[47] has impressively developed over the last decades with many kinds of machines synthesized, revolutionizing the way chemists think about motional molecular systems. Although achieving controlled advanced functions at the molecular level is

still a tremendous challenge, much effort is being spent on building and mastering the different pieces required to realize such integrated molecular devices.

Recently, several examples that may be considered as mechanical molecular devices have been reported, including biomimetic nanomachines[48] such as molecular gears,[49] shuttles (Figure 1-10a),[50] muscles (Figure 1-10b),[51] molecular walkers[52] and technomimetic nanomachines[53] like wheels,[54] nanovehicles,[55] wheelbarrows (Figure 1-10c),[56] molecular scissors,[57] gears,[58] nanowheels,[59] winches,[60] elevators[61] and robotic arms.[62] Although some very elegant examples of molecular rotary motors have already been described, they have been studied as aggregates or generally have many degrees of freedom.[63]

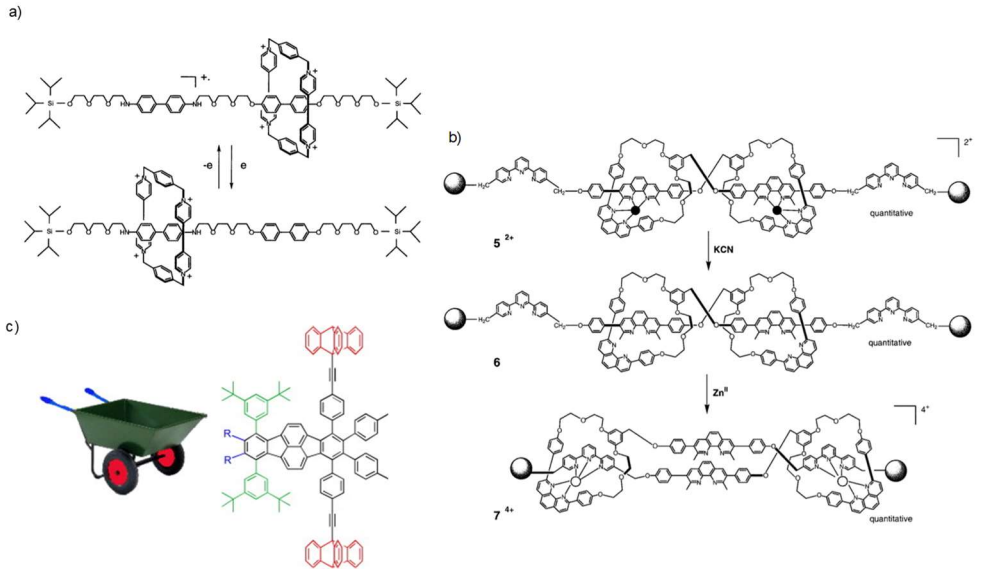

Figure 1-10 a) The molecular "shuttle" is based on electroactive organic functions (aromatic amine) and electron donor and acceptor groups. b) Reversible chemically induced "muscles" motions between extended 5^{2+} and contracted 7^{4+}. The black disk is copper(I); the white circles are zinc(II). c) Macroscopic analog and chemical structure of a molecular "wheelbarrow". R groups allow to vary the 'handles' in order to optimize the interaction of the molecule with the STM tip. Each figures are cited from Ref a)[50], b)[51], c)[56].

A mono-molecular motor is a nanoscale machine which consumes energy to produce work via a unidirectional and controlled movement of one of its parts.[64,65,66] The inspiration of such motors

comes both from nature such as in the fascinating machinery of ATP synthase (Figure 1-11) and from the macroscopic world where rotary motors are very common.

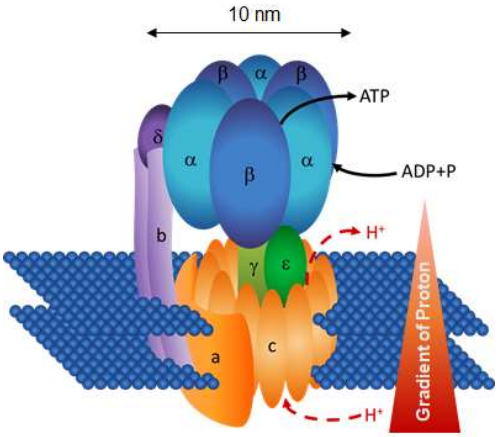

Figure 1-11 One of the inspirations of artificial molecular motors, ATP synthetic scheme.

In such models, it is very important for a multi-component molecular system to have independent inputs controlling their motions. Our laboratory recently achieved triggering and control over the step-by-step rotation of a molecular motor of 2 nm diameter deposited on a metallic surface. Depending on which part of the rotor subunit is approached by the electron injecting STM tip, we can control the rotation with about 80% unidirectionality (Figure 1-12).[66]

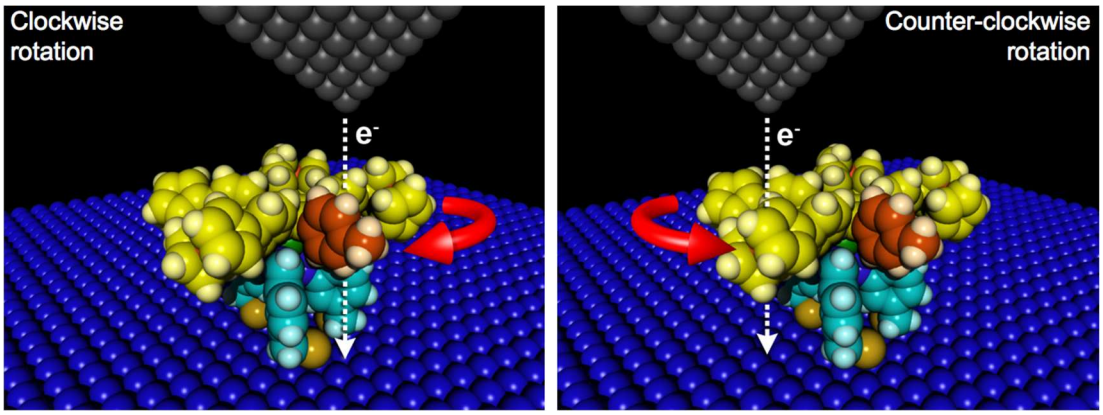

Figure 1-12 a) Structure of the parent ruthenium-based molecular motor adsorbed on a gold surface and related electron-fueled unidirectional rotation. b) Electron injected on one of the four ferrocenes can induce counter-clockwise rotation whereas injection in the tolyl group induce clockwise rotation.[66]

Although this is not sufficient to lead to complete rotational control, it has been observed that chirality also plays a critical role in obtaining unidirectionality.[67] The ruthenium complex used contains two ligands which are not chiral however once deposited on the surface, the trisindazolyl borate and pentaphenylcyclopentadienide ligands are twisted out of the coordination plane[68] with the ruthenium complex becoming chiral.

Aside from the response to electrons, light offers a further interesting independent input to switch on and off the rotation. To achieve this goal, we have designed a dual photo and electro-responsive target motor incorporating a photochromic fragment in the backbone of the rotor. The molecular design and experiment will be shown in Chapter 2.

1.4 Synergetic switching response to photo- and radio-chemical oxidation

One of the most essential demands for stimuli-responsive molecules is sufficient response efficiency, that is, the number of target molecules affected by a single external stimulus. In some biological processes, for example, the initial process of mammalian optical sight is based on retinal-protein hybrids, which regulate the transport of ions through ion-channels in cell membranes.[69] These are capable of amplifying more than a 1 : 1 ratio of transporting ions to absorbed photons, a significant increase in the sensitivity of the system upon activation. Such systems based on similar synergetic responses have been reported in many areas, including biology, catalysis, and polymer development, mainly focusing on photonic applications, including photo-multiplying tube detectors[70], avalanche photodiodes[71]. These systems leverage the output so it can be many orders of magnitude larger than the photonic input and have been known for many years; the exploitation of cascade responses on a molecular level has proved challenging at the moment. Future examples require the development of new molecules responsive to external stimuli such as heat, chemical, or physical stress[30].

Photo-switching has attracted much attention due to the ease with which large packets of energy can be delivered in a non-invasive way, along with how molecular engineering on the design of diarylethene derivatives enables fine-tuning of their optical properties. For instance, our group previously proposed photochromic derivatives harboring atoms at strategic positions to

lock the molecule in its reactive conformation, resulting in a photocyclization quantum yield of almost unity.[31] However, the high photocyclization quantum yield of diarylethenes tends to afford a lower cycloreversion efficiency. This sacrifice has led to the exploitation of alternative ring-opening method such as electro-chemical or chemical oxidative cycloreversion processesand amplified reaction in an autocatalytic manner.[39] Terarylene structures have demonstrated the oxidative cascade cycloreversion with the efficiency beyond unity.[39,40] This proceeds via a cascade resulting from the oxidation of the ring **c**-form to it radical cation (c•+), which spontaneously ring-opens to the cationic radical of the **o**-form (o•+). This immediately reacts with the remaining neutral **c**-form in solution, regenerating the closed radical cation and leading to the formation of multiple **o**-forms from a single oxidation source. Electron efficiencies of up to 900% were reported, implying nine rings open for each single oxidation source,[39] and ring-opening turnover numbers of up to 1000 have been achieved (Scheme 1-3).[40]

On the other hand, a lot of attention has been placed on the use of photo-synergetic systems due to the ease with which they inject large amounts of energy, along with the non-invasive, rapid

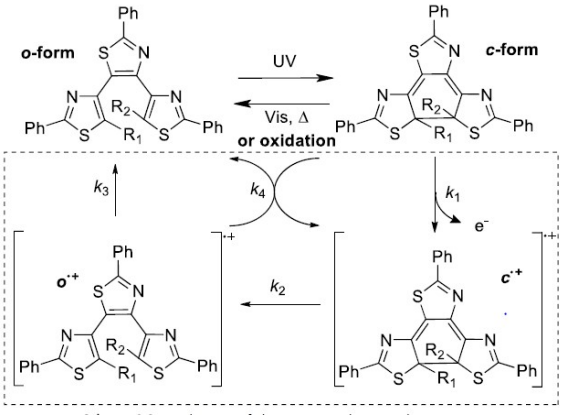

Scheme 1-3 Oxidative cascade reaction mechanism of terthiazole structure R=Me.[39]

way they can be exploited. Demonstration of synergetic response has been reported, including those by Tokumaru and Irie, who have independently studied photoisomerization of ethenes[72] and binaphothylenes, respectively[73] with photoisomerization quantum yields amplified to higher than unity via triplet state energy transfer. Recently Garcia-Garibay reported the specific quantum-chain photodecarbonylation of diarylcyclopropenones in the crystalline state[74]. The photochemical quantum yields are reported to be higher than 300%, resulting from singlet energy migration. The major drawback of these molecules, however, is their irreversibility. To overcome

this, the use of reversibly switchable photochromic molecules, including terarylenes, for photo-induced synergetic electro-chemical cycloreversion and photocyclization, has been investigated.[38] As it has long been known that high energy photons such as X-rays oxidatively-generate radicals in certain halogenated solvents,[75,76,77,78] the use of UV and X-rays to initiate the cascade reaction has been investigated. In addition, this method offers a highly sensitive photoswitching response to low doses of X-rays as a result of the synergetic cascade reaction, allowing for much higher sensitivities than other organic examples already reported.

High-energy photons including X-rays produce major health risks[79,80,81] and as such, there is a growing demand for new highly sensitive detection methods.[82,83] Most existing X-ray sensing compounds are based on expensive and toxic materials, usually including metal-organic frameworks or heavy metals, which are difficult to process into commercial products. As alternatives, a number of organic-based systems have been suggested,[84,85] however, they all suffer from the difficulties of having to be paired with the solid-state electronic detection methods to produce a commercial device. Photochromic organic detectors may then offer a viable alternative as they can make the presence of X-rays detectable by color changes, with recyclability and ease of use as added benefits. Previous X-ray responsive molecules have been typically demonstrated with spiropyrans[86] and diarylethenes.[87] In both cases, however, these organic molecules offered low-level detection limits in the range of 1 - 0.1 Gy even when combined with radio-sensitizers. This motivated the exploration of the possibility of by terarylenes susceptible to cascade reactions for the direct observation of the ring-opening induced using X-Ray radical generation. This method offers a highly sensitive radio-chromic response to low doses of X-Rays, allowing for much higher sensitivities than the previous organic examples so far reported. This study and results will be presented in Chapter 3

1.5 Molecular thermal energy storage fuel and heat release system

Global energy consumption has more than doubled over the past 40 years and will need to roughly triple by 2100 with the growing world population.[88] With the depletion of fossil fuels and emerging environmental problems, the use of natural energy has become essential for the sustainable development of humankind. The use of solar energy, in particular, has been widely considered as the one-hour solar radiation can roughly fill the global annual energy consumption. Schockley and Quiesser calculated the theoretical efficiency limit of a single Si-based p-n junction solar cell to be 33.1%.[89] Although recent technological progress has upgraded the efficiency close to this limit for a single-junction solar cell,[90] the 1.1 eV (1160 nm) bandgap of Si also limits the effective use of solar radiation over a wide spectral range.[91] To overcome this issue, recent developments have involved tandem heterojunctions,[92] multiple exciton generation in quantum dots,[93] and spectral shifting by molecular light-harvesting materials.[94] Since solar radiation is intermittent and fluctuates over time, appropriate energy storage systems are desirable for on-demand use.[95] Secondary batteries such as lithium-ion ones are often combined with solar cells for the practical storage of electric energy.[96] Apart from electricity, solar energy is converted and stored as chemical energy (e.g., as C–H and C–C bonds) as typically represented by photosynthesis.[97] In artificial photosynthesis systems, solar energy is used to produce valuable chemicals and fuels such as methane, hydrogen and so on, through photochemical and photoelectrochemical reactions.[97]

Recently, another system employing photochemical reactions has been attracting attention as solar thermal fuels that convert, store, and release solar energy as heat and also offer increased recycling capability.[98] Photoresponsive molecules display reversible photoisomerization reactions between thermodynamically stable and metastable isomers. The photon-energy propels the molecules into the excited state triggering the isomerization reaction. The photon-energy is initially converted into the electronic-excitation energy at the Franck-Condon state followed by relaxation to certain excited transition states, eventually resulting in the formation of a metastable molecule in the ground state. Upon this isomerization process, the largest part of excitation energy is released to surroundings as heat, while a portion is stored as the excess enthalpy of metastable isomer.[99-103] This enthalpy is released to the surroundings as heat upon switching form the closed

to the **o**-form isomers, which results in the exothermic release of the stored energy. Therefore, the capability of on-demand heat release is highly desired for the MOlecular Solar Thermal storage (MOST).[44a]

The potential for storing solar energy by reversible photo-isomerizations has been recognized from 1909[44a] when the photo-dimerization of anthracene was proposed for this purpose. Since the early 1970's, developments of a closed chemical storage system of solar energy have been based on concerted (electrocyclic) conversion between double C=C and single C–C bonds (Figure 1-13b)[100,102] and E/Z isomerization of azo (N=N) type[101] (Figure 1-15a) and stilbene derivatives (see Figure 1-4). More recently, certain organometallic photochromic compounds[103] (Figure 1-13c) have attracted attention. Inorganic photoreactions were considered in the 1960's but do not appear to be any longer actively pursued. So far the primary focus has been on maximizing the

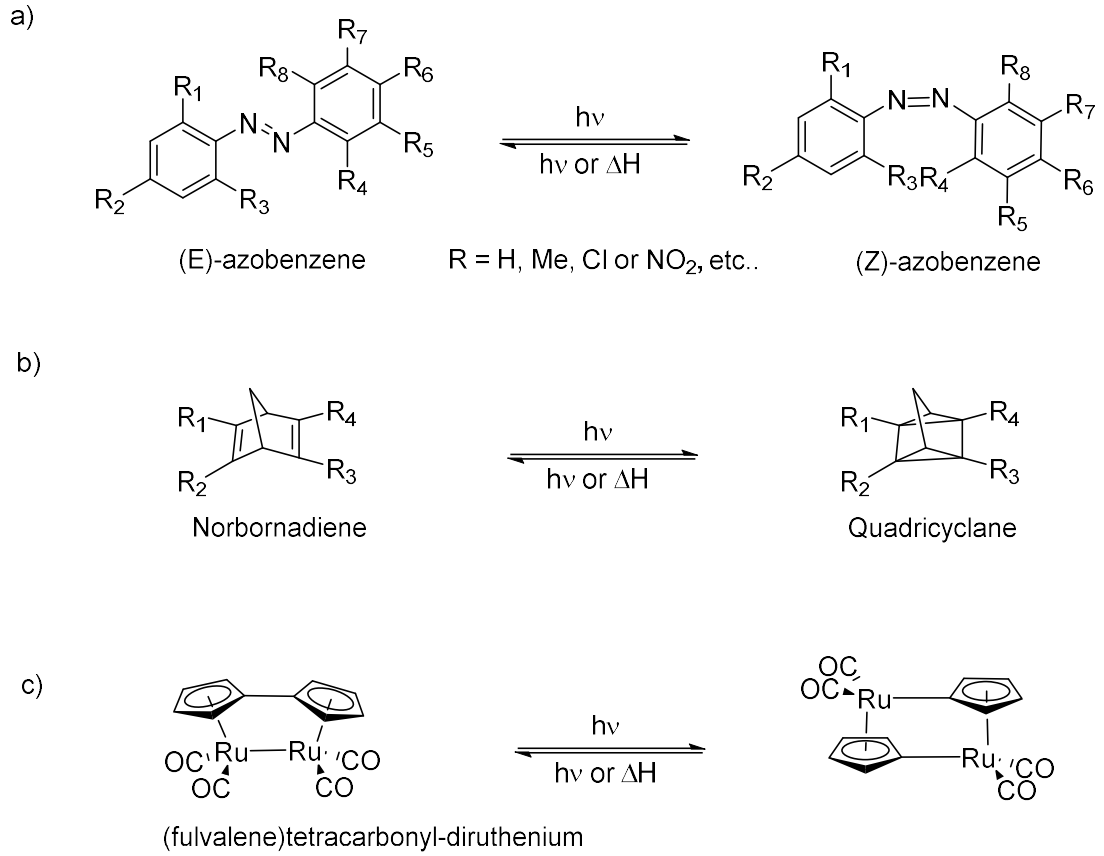

Figure 1-13 Class of chromophores previously studied as potential photothermal solar fuels[44a] : a) E/Z azobenzene, b) norbornadiene /quad- ricyclane c) (fulvalene)tetracarbonyl-diruthenium. The metastable isomers are on the right.

efficiency of energy conversion. As argued above, energy density rather than energy conversion efficiency may be of greater importance in determining the role of chemical solar thermal energy storage schemes.

The MOST efficiency is defined as the ratio of the amount of energy released at use (E_{out}) against the initial energy input (E_{light}). Design of photoresponsive molecules contributes to the efficiency with two factors. One is the quantum yield of photoconversion related to the efficient use of photon energy (E_{light}). The other is an energy difference between the photoisomers (ΔH_{iso}) having a direct correlation with the amount of released energy (E_{out}). A large ΔH_{iso} is also advantageous in view of energy storage density. A number of photoresponsive molecules have been considered as active materials in MOST systems. Azobenzene derivatives (Figure 1-13a) are of great interest for numerous applications due to their low cost and high cyclability.[101] However, single molecules of azobenzene have poor energy storage efficiency due to their short storage lifetimes. Norbornadiene[102](Figure 1-13b) has been shown to suffer from degradation. Fulvalenetetracaronyl-diruthenium[103], which shows less degradation, has significantly lower energy densities and is composed of expensive ruthenium metals (Figure 1-13c). Although the energy storage efficiency of most previous candidates has not been evaluated, they are mostly less than 1%. Azobenzene-CNT hybrid system has shown exceptionally large energy storage efficiency of 14%.[101c] Although CNT should readily suppress the photoisomerization reaction of azobenzene because of their large extinction coefficient and small excited state energy, their evaluation was not clearly described. As the energy storage efficiency should be less than the photochemical quantum yield, photochemical-sensitive molecules are strongly desired. In this regard, diarylethene and related substances are promising due to their relatively large photoisomerization quantum yield. The small energy difference between two photoisomers of diarylethene derivatives[13, 19,31] seems to be a drawback to their potential use in MOST systems.[103a] However, recent developments in molecular engineering on the constituting aryl units and substituents have succeeded in controlling the energy difference between **o**- and **c**-forms ($\Delta H_{c\text{-}o}$). [104,105,106]

In the general physicochemical consideration, the well-known Hammond's postulate [107] implies the trade-off between the activation energy (E_a) and $\Delta H_{c\text{-}o}$. This fact suggests the intrinsic difficulty in simultaneously achieving both large ΔH_{iso} and high thermal stability for

photoresponsive molecules. It is, therefore, a key to consider the photoresponsive scaffold with an optimum correlation between ΔH_{iso} and E_a. Thermal cycloreversion reaction of diarylethenes is symmetry forbidden under the Woodward-Hoffmann rules, which may lead to inherently high E_a values. Kobatake and coworkers suggested three factors which control the thermal stability of diarylethenes:[104a] (i) aromatic stabilization energy of the aryl groups,[19] (ii) electron-withdrawing substituents at the aryl groups,[105] and (iii) steric hindrance of the substituents at the reactive carbon atoms.[104b] The $\Delta H_{c\text{-}o}$ stems from the loss of aromaticity in the aryl units constituting the diarylethene framework upon the photoisomerization from **o**- to **c**-forms.[19a] In the design of diarylethenes with the thermal bistability of both isomers, five-membered rings such as thiophene and thiazole have been employed as the unit of less aromatic stability, promoting smaller enthalpy differences between the two isomers. Therefore, typical DTE are not very promising for MOST materials as a result of their small heat storage capacity, ΔH_{iso}. The central aromatic ring of terarylene frameworks selectively stabilizes the **o**-form and enhance ΔH_{iso}. However, it is needed to make careful designs in terms of framework and combination of aromatic rings together with substituents for simultaneous control of the thermal stability of the **c**-form with lifetimes ranging from seconds to years.[39,43] As discussed above, the thermal stability of the **c**-form is specifically intensified with the symmetry forbidden nature of the cycloreversion reaction at the ground state. This feature of terarylenes seems beneficial to achieve efficient MOST materials. The terarylene framework is thus expected as a promising candidate for the MOST-active molecules to fulfill both the high ΔH_{iso} and practical thermal bistability. Therefore investigation into a series of terarylene molecules as an active material for the MOST applications was carried out. Furthermore, some diarylethenes and terarylenes were reported to undergo oxidative cycloreversion with electro-chemical and chemical oxidation inputs,[38] proceeding in a chain-reaction manner.[39] In particular, a rational design of terarylenes considering the relative stability of transient active species playing an important role in the chain-reaction mechanism boosted the overall reaction efficiency over 100,000%.[40] The addition of only 10^{-4} equivalents of chemical oxidant could trigger the cycloreversion reaction of the entire system. This property should be advantageous from the viewpoint of the on-demand release of stored energy (Figure 1-14).

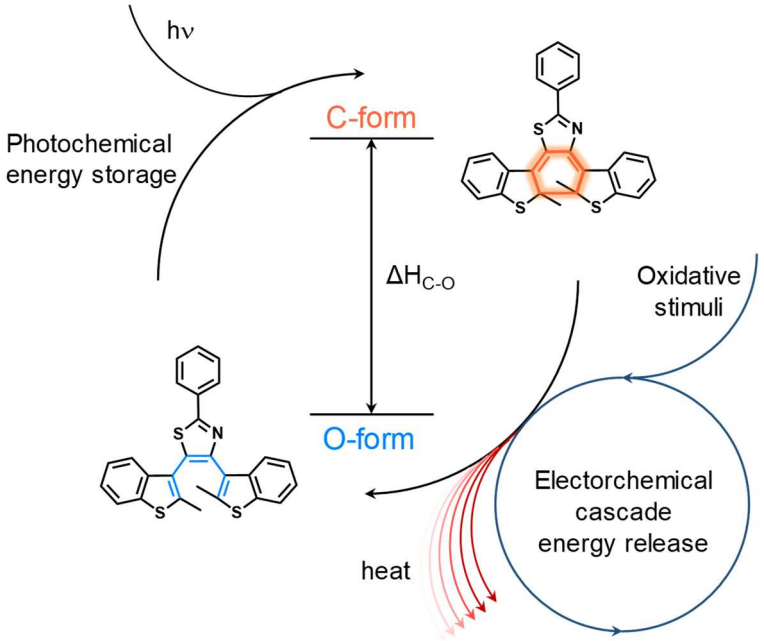

Figure 1-14 The scheme of MOST system. The light energy (hν) is stored as their enthalpy change (ΔH_{c-o}) with photon-induced isomerization. The external energy, oxidative stimuli, trigger the intermolecular cascade system, leading release of the stored energy as heat.

1.6 Summery of Introduction: Objectives and scope

The excellent advantages offered by terarylene allowed us to exploit functional molecular materials controlling the macroscopic functions by analyzing how they operate at the molecular level. In addition, research and development of their unique switching property such as photo-, electro, mechano-, radio- and thermo-chemical responses have the potential to push into new frontiers in various research fields and resolving environmental issues.

To achieve this thesis is composed of three chapters : (1) on/off switching of molecular motors controlled by photoswitchable terarylene unit, (2) synergetic colorchange via cascade reaction system triggered by photo- and radio-chemical oxidation for highly sensitive detection, (3) control of thermochemical properties of terarylene for molecular thermal energy storage.

First, photo- and mechano-chemical responses are developed for the stop/restart of the rotation of a molecular motor. Our laboratory reported a new type of molecular motor activated clockwise or counter-clockwise rotation depending on which part of the rotor subunit receives the electron

injected by the STM tip. In order to control the rotation by an additional light stimulus, a new motor was designed. Light input to switch on and off the rotation and electron to rotate are two orthogonal stimuli which make it highly impactful. The photoswitching subunit thus acting as a light-induced brake. The target terarylene motor unit was chosen using computational methods based on molecular mechanics and DFT calculations in order to visualize the steric interactions. The new synthetic scheme, including the introduction of the photoswitching unit into the motor are presented and the control of the rotation of the synthesized molecular motor discussed using NMR spectral changes under UV light irradiation.

In the second part, photo and radio-chemical synergetic responses are developed for sensitive UV and X-ray detection. Endeavors to enhance the quantum yield of isomerization provides an application of an alternative stimulus to light irradiation. Especially, chemical or electro-chemical oxidation has attracted attention as an alternative route for the ring-opening reaction of diarylethenes because it often proceeds with high efficiency in an (electro)catalytic way involving a cascade reaction mechanism where the apparent reaction efficiency readily exceeds 100,000%. As it has long been known that UV or X-rays oxidatively-generate radicals in certain halogenated solvents those have been employed to help initiate the cascade reaction. This study offered a highly sensitive radio-chromic response to low doses of X-rays, allowing for much higher sensitivities than the other molecular dosimeters so far reported.

In the third part, thermo-chemical response is investigated for thermal storage, and the electro-chemical synergetic response inducing heat release is presented. Terarylene molecules display a reversible photoisomerization reaction between a thermodynamically stable **o**-form and a metastable **c**-form isomer. The photon-energy is eventually converting **o**-form into **c**-form molecules in the ground state and store the thermal energy as the energy difference between them, called as MOlecular Solar Thermal storage system. To enhance the efficiency of this system high photocyclization quantum yield as conversion efficiency is required, the energy difference between the photoisomers, thermal stability of metastable **c**-form for long term storage. In this thesis, photo- and thermo-chemical consideration achieve the highly efficient MOST conversion and guide principle for the molecular design.

2. Development of photoswitchable terarylene unit for on/off switching of molecular motors.

A mono-molecular motor as a machinery toolkit consumes energy to produce work via a unidirectional and controlled movement of one of its parts. In latest molecular motor reported from our group achieved triggering and control over the step-by-step rotation of a molecular motor 2 nm in diameter deposited on a metallic surface.[108] Depending on which part of the rotor subunit is approached by the electron injecting STM tip, they can control the rotation with about 80% unidirectionality achieved (see Chapter 1 Figure 1-12). In such models, it is very important for a multi-component molecular system to have many independent inputs controlling their motion.

I here designed a dual photo and electro-responsive target motor incorporating a photochromic terarylene fragment in the backbone of the rotor. In this system, the photo- and mechano-chemical switching properties of terarylene were applied for light induced brake function. The rotor part having the rigid **c**-form of the selected photochrome lies in the stator part, preventing rotation, while the flexible **o**-form of the photochrome will not interact with the stator, leaving the system free to rotate (Figure 2-1). The motors would then integrate two input signals: electrons as the source of energy to rotate and light which could start or stop the process at will.

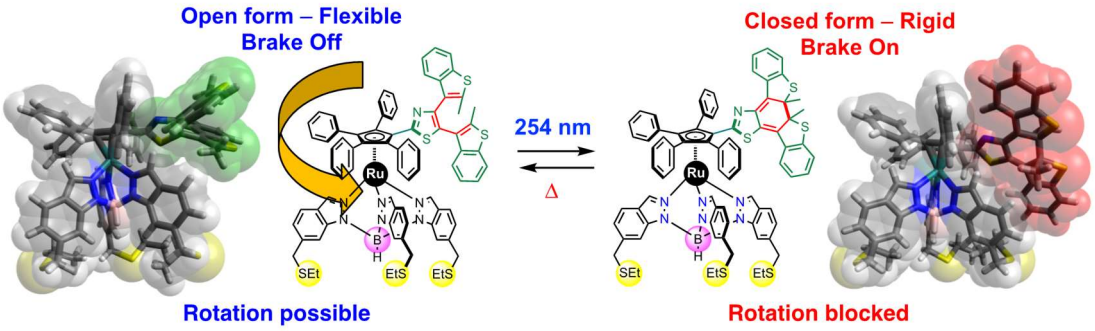

Figure 2-1 Schematic representation of the difference between the **o**- and **c**-forms of the targeted photochrome-substituted molecular motor. Upon application of UV light, the closed-form of the photochrome is obtained preventing the rotation of the rotor part of the motor.

The target photochromic fragment was first designed based on previous examples in the field, using computational estimation of the steric hindrance (Section 2.1), taking advantage of terarylenes nature and the synthetic procedure was newly optimized (Section 2.2). The rotational blocking in the system after the ring closing reaction of the photochromic fragment was demonstrated by NMR (Section 2.3 and 2.4).

2.1 Design of the photochromic molecular motor

To allow for the successful integration of the proposed photochromic brake into the existing motor frameworks I first identified a number of contributing factors that needed to be optimized to allow for its operation. First, the nature of the photochromic moieties, second the linker between the photochrome and the motor which need to be short with a controlled directionality to allow the photochrome (the brake when **c**-form) to block the rotation by interaction with the stator (the tripodal ligand). To design suitable molecular units, Gaussian DFT calculations have been performed-using the hybrid dispersive functional ωB97xD functional[109] to obtain the energy minimized geometries of the **o**- and the **c**-forms of the photochrome-functionalized molecular motor. The optimal target should have the largest steric blocking interactions upon photoisomerism between the flexible **o**-form and the rigid **c**-form.

A number of photochromic moieties with the potential to act as a brake were identified, based upon previous reports of diarylethene and terarylene photochromic properties.[5,13] Each photochrome-substituted molecular motor was modeled and the geometry was optimized in their open and closed photochromic isomers to estimate the changes brought about by ring closure and the resulting effect on rotational motion through steric interactions with the stator part of the molecular motor. These interactions were evaluated qualitatively thanks to the optimized geometries of both isomers in the gas phase which display insightful clues on the ability to rotate and brake of each molecular motor.

The design of the photochromic part was initially considered in terms of the switching efficiency and the geometries of the two isomers. As such, it was decided to use an initial photochromic core framework which is linked to the cyclopentadiene part of the motor (Figure 2-4, middle) at the central ring but not at the peripheral side rings (Figure 2-4, right). A

terarylene core was then chosen rather than a diarylethene because of rigidity of the central aromatic ring of terarylenes and their capability of fine tuning of steric effect. Previous studies on

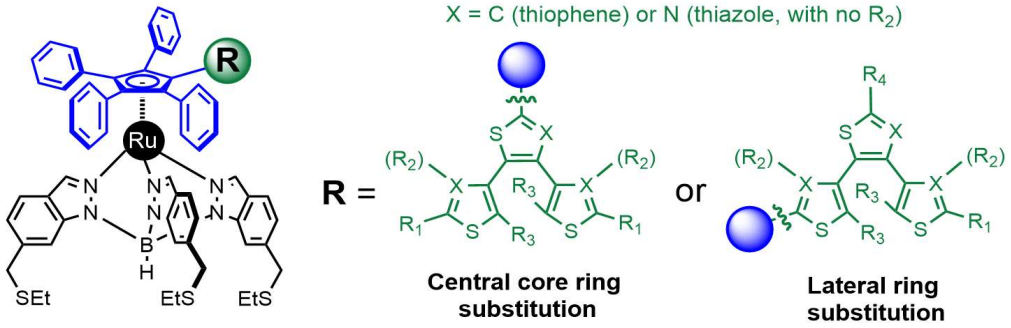

Figure 2-2 Motor (blue) with two possible photochromic terarylene substitution patterns (green).

molecular motors have shown that the aromatic substituents on the cyclopentadiene ring rotate out of the plane.[110] Substitution on the core of the terarylene is thus expected to promote large steric interactions between the photochromic unit and stator parts. Especially, the steric hindrance should consolidate in the c-form isomer blocking the rotation around the Ru-axis of rotation.

Then, I decided to use a combination of thiazole and thiophene rings as the core and peripheral substituents within the photochromic moiety. The presence of both of these substituents is advantageous in terms of conformational preference leading to efficient ring-opening and -closing and higher photochromic quantum yields.[31,30] For the initial braking systems it was decided to use methyl substituents (Figure 2-2, R_3) at the positions of photochromic bond formation as this is known to lead to stable, reversible photochromic switching.

Based on these considerations five target photochromic frameworks **T1** – **T5** (Figure 2-3a) were selected for initial calculations and to screen the effect of substituents present (Figure 2-2, R_1 and R_2) upon their incorporation into the motor frameworks **MM-T1** – **MM-T5**.

Each was modelled computationally using the Material studio Forcite molecular mechanics program operating using Universal force field and the Gaussian 09 DFT program, in collaboration with Yohan Gisbert in CEMES, operating using the ωB97xD functional and the 6-31G(d,p) basis set[109] for all atoms except ruthenium for which LANL2DZ[111] was used.

For the systems containing a thiophene central ring and thiazole peripheral rings (**MM-T1** and **MM-T2**) the absence of a sterically bulky substituent at the thiazole 4-position meant no steric interactions between the photochrome and the stator in either their **o**- or **c**- forms was observed

(Figure 2-3b). **MM-T1** showed no significant steric interaction between the stator and photochromic unit even in the **c**-form.The central thiophene ring of the photochrome is coplanar to the cyclopentadiene ring of the rotor, resulting in the photochrome pointing away from the stator even in the **c**-isomer. For the three systems containing a thiazole central ring and thiophene based peripheral rings (**MM-T3** to **MM-T5**), the increased steric hindrance at the thiophene 4-position led to the prescence of strong steric interactions in the **c**-form which could break the rotation. As such, it was decided to use a thiazole as the central core ring fused to the motor and thiophenes substituted at the 4-position as the peripheral photochrome rings.

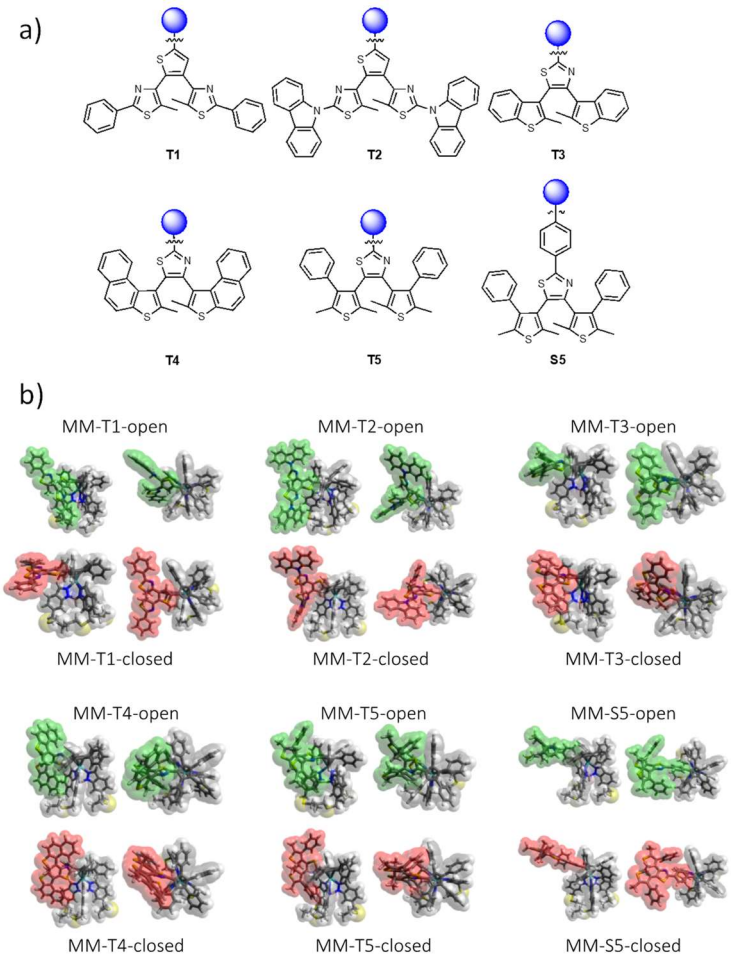

Figure 2-3 a) Preselected photochromic moieties T1-T5 and S4 for incorporation into the motor backbone. The blue spheres represent the motor fragment. b) Optimized geometries of the **o**- and **c**-forms of the molecular motors **MM-T1** to **MM-T5** and **MM-S5** functionalized with photochromic moieties **T1-T5** and **S5**.

In the DFT calculations of these systems (**MM-T3** to **MM-T5**), the **o**-form appears highly flexible and shows no apparent interactions between the photochrome and the stator. However, upon switching to the **c**-form the increased rigidity of the photochrome, in conjunction with the angle between the cyclopentadiene ring and the fused benzothiophene ring of the photochrome (49° for **MM-T3**), leads to the rigid **c**-form taking up a position pointing between two of the three legs of the stator. Such geometries are predicted to result in cessation of the rotation of the molecule as the 'brake' is applied upon switching from the **o**- to **c**-photochromic forms.

To examine the effects of varying the distance between the photochrome and the motor, a phenyl spacer was inserted between them to give **MM-S5**. Both the **o**- and **c**-forms of **MM-S5** showed no clear steric interactions. This leads to the conclusion that the terarylene photochrome should be connected directly to the cyclopentadiene ring.

After consideration of the photochromic units **T3**, **T4** and **T5**, **MM-T3** was chosen as the initial target for several reasons: 1) As it has the lowest steric contact between the photochromic unit in the **o**-form and the stator, the system should be able to freely rotatae prior to application

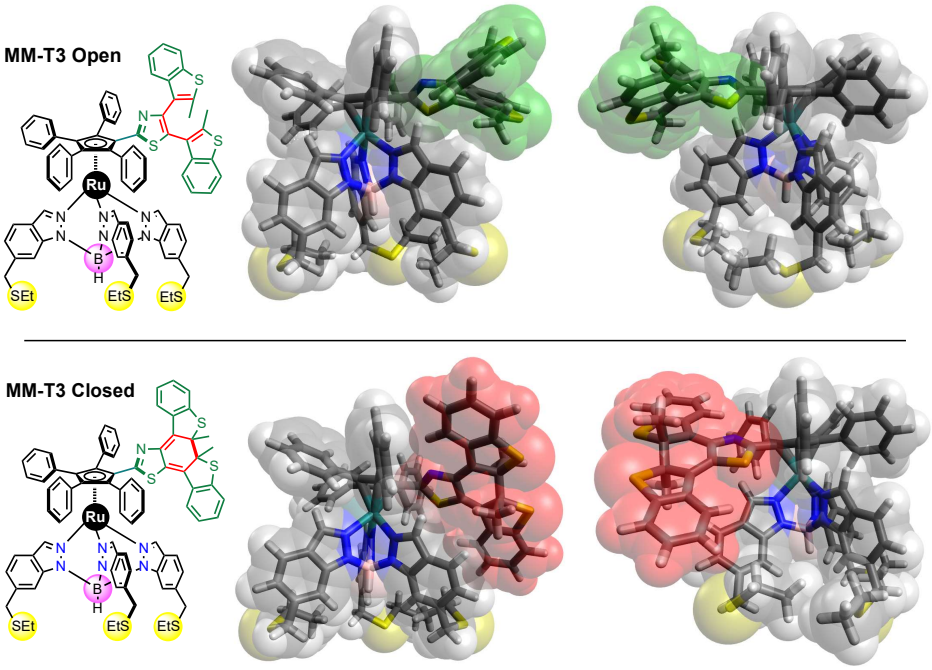

Figure 2-4 **o**- (top) and **c**- (bottom) forms of **MM-T3**, showing the changes in interaction between the stator and the photochromic moiety. The π-system involved in the photochromic isomerization is indicated in red an integration of twenty-eight protons relative to the alcohol OH. A 3D animation movie is available as a supporting information to help to ease

of the light brake. 2) As it also contains the highest levels of hydrogen bonding (CH/S and CH/N) between the constituent aromatic rings in the photochromic moiety, the photoreactive C_2-symmetric conformation should be stable and efficient photoreactivity is expected. 3) As it shows large steric hindrance between the **c**-form isomer and the stator, a significant photo-triggered braking effect is expected. 4) It seems to be relatively simple in the synthesis in comparison with **T4** and **T5**. I decided to incorporate **T3** as the photochromic part of our initial molecular brake motor referred as **MM-T3** (Figure 2-4).

2.2 Synthesis of the photochrome-substituted motor

The synthesis of the photochrome functionalized motor **MM-T3** was obtained in five steps with a global yield of 4.7% (Scheme 2-1 and 2-2) including the synthesis of the required terarylene 4,5-bis(2-methyl-1-benzothiophen-3-yl)-1,3-thiazole (**T3**). To start with, 4,5-dibromo-1,3-thiazole[112] (**1**) was coupled to 4,4,5,5-tetramethyl-2-(2-methyl- 1-benzothiophen-3-yl)-1,3,2-dioxaborolane[30] (**2**) through Suzuki-Miyaura coupling to give terarylene **T3** in a 74% yield after

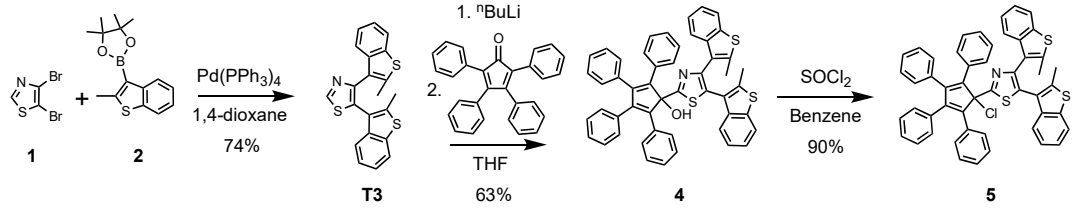

Scheme 2-1 Synthesis of the cyclopentadiene rotor functionalized with a terarylene fragment (**5**).

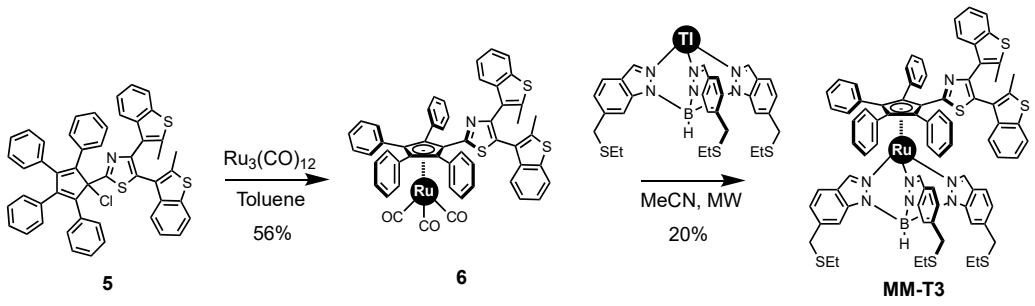

Scheme 2-2 Synthesis of the photochromic motor **MM-T3** incorporating a terarylene brake.

purification by column chromatography. **T3** was then lithiated at the 2-position of the thiazole ring using *n*-butyllithium and reacted with 2,3,4,5-tetraphenylcyclopentadienone to give the tetraphenylcyclopentadienol **4** in 63% yield. **4** was then converted to its chloride analog **5** by reaction with thionyl chloride in benzene in a yield of 90%. The presence of this chlorine center allowed us to coordinate the cyclopentadiene ring to the ruthenium atom by oxidative addition of the triruthenium dodecacarbonyl cluster through the carbon-chlorine bond of **5**. The ruthenium cyclopentadienyl complex **6** was obtained as a bright yellow solid in 45% yield.

Finally, coordination of the tris[(ethylsulfanyl)methyl]indazolylborate ligand was performed by reaction of the ruthenium cyclopentadienyl complex **6** with two equivalents of the thallium salt of the hydrotris(indazolyl)borate derivative[113] by microwave heating in acetonitrile at 100 °C (Scheme 2-2). Due to the evolution of carbon monoxide during the reaction, the pressure was released every 10 min and the conversion followed by TLC of the crude mixture. The target photochromic motor **MM-T3** was obtained in 20% after 1 hour. Each compound was characterized using NMR and mass spectral data, however the presence of multiple conformational and rotational is

omers made complete assignment of the NMR spectroscopic data difficult due to significant broadening of signals.

2.3 Photoswitching of the precursor ligand

To examine the effect of illumination upon the motor structure, a ^{1}H NMR study was carried out. Initially the photochromic switching of the precursors was examined; due to the relative stabilities of the molecules it was decided to look at the alcohol **4** as a representative example. To allow for comparison with **MM-T3**, this was done in deuterated dichloromethane. Here, sharp signals are observed at 7.68, 7.64 and 6.83 ppm for three of the four photochrome benzothiophene protons, along with a large broadened region between 7.45 and 6.90 ppm masking the fourth benzothiophene signal (Figure 2-5 top). This broadening of the aromatic region is consistent with what is seen for the photochromic precursor T3 along with observations of similar non-photochromic cyclopentadienyl systems. Due to this broadness a precise integration is not possible, however approximate value of ratio of the reactive anti-parallel to the non-reactive parallel conformations show an integration of a proton relative to the alcohol OH singlet at 4.71 ppm. Along with this, broad signals for the methyl substituents on the photochrome, integrating for six protons, are observed between 1.98 and 1.75 ppm. The sample was then dissolved in hexane and illuminated for 30 minutes at 254 nm, solvent removed, and the solution redissolved in deuterated dichloromethane to examine the spectrum of the photostationary state containing a

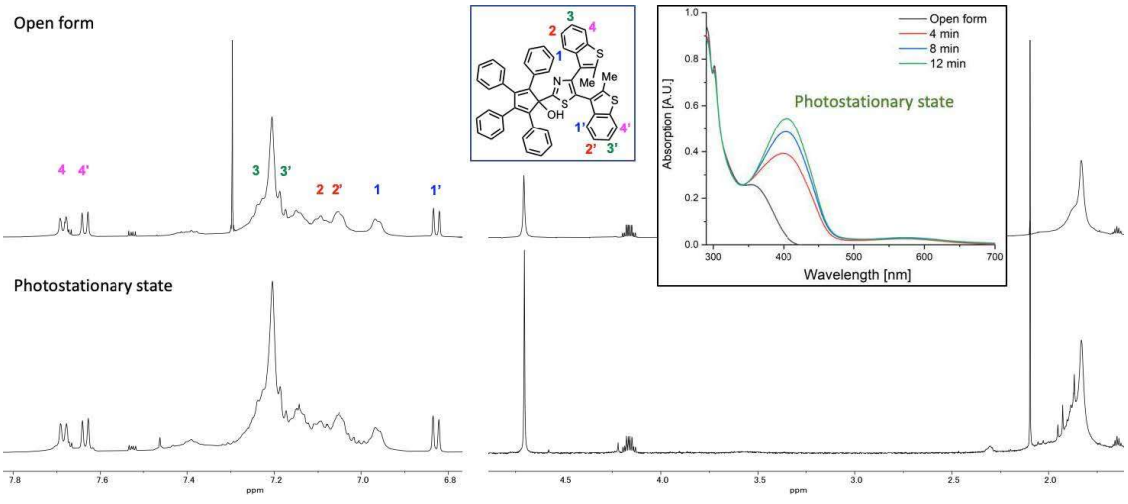

Figure 2-5 Photoswitching of the precursor ligand (**4**) by illumination at 254 nm followed by UV-Vis. spectroscopy (Insert) and by ^{1}H-NMR (600 MHz) in CD_2Cl_2.

mixture of **o**- and **c**-forms (Figure 2-5, bottom). It can be seen that some changes occur in the aromatic peaks, however more significantly there are shifts seen in the methyl peaks between 1.98 and 1.75 ppm, indicating that photochromic ring closure has taken place with the appearance of structural isomers in both the **o**- and **c**-forms. This is consistent with the absorption spectra of **4** where new peaks showing the formation of a photostationary state (Figure 2-5, insert) including **c**-form are observed. The band around 400 nm is reasonably corresponding the TD-DFT calculation value of **c**-form of compound **4**. This new band returns to the absorption profile of the **o**-form upon application of light above 400 nm.

2.4 Photoswitching of the photochromic ruthenium complex (MM-T3)

Next, the ^{1}H-NMR of **MM-T3** was run in dichloromethane. Broad aromatic peaks are again seen between 7.80 and 6.80 ppm, indicating the presence of the cyclopentadiene rotor. Four further aromatic peaks are seen, each integrating for three protons (with two overlapping), for the protons located on the tripodal stator legs. These can be assigned based on previous reports with H^{1} and H^{6} (Figure 2-6, top) appearing downfield at 8.32 and 7.83 ppm and H^{3} and H^{4} overlapping for a total integration of six protons between 6.96-6.92 ppm. The signals for the aliphatic stator chains can also be observed with H^{7} appearing as a singlet at 3.87 ppm, a quartet for H^{8} at 2.44 ppm and H^{9} appearing as a triplet at 1.26 ppm. Also very broad signals indicating the presence of multiple conformational and rotational isomers are seen between 2.0 and 1.7 ppm for the photochrome methyl substituents. Despite the apparent broadness the expected signals for the

cyclopentadienyl rotor, the photochromic brake and the indazolylborate stator can be seen in the ^{1}H-NMR of **MM-T3**.

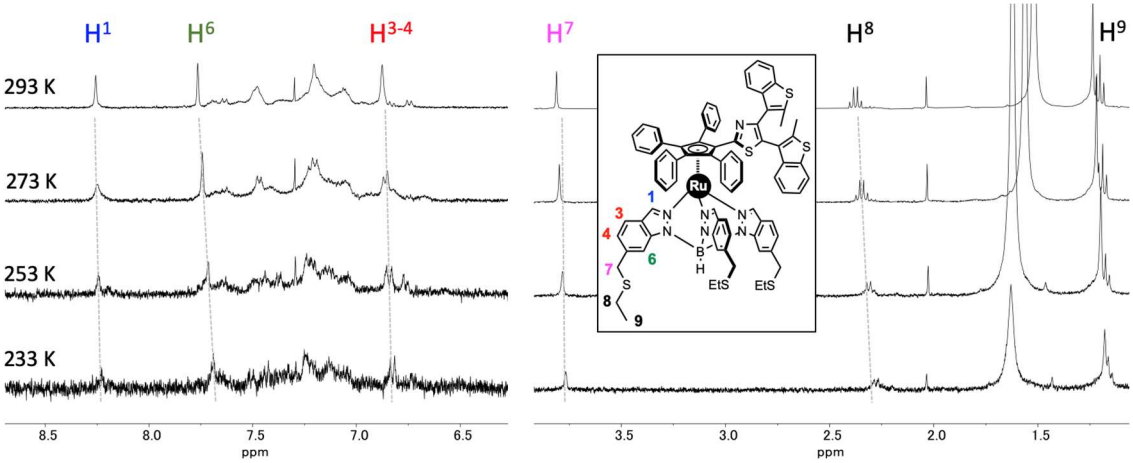

Figure 2-6 ^{1}H-NMR of **MM-T3** (Open form) at 293, 273, 253 and 233K in CD_2Cl_2 (400 MHz).

To resolve the broad peaks and to observe the effect of thermal cooling on the rotation, the ^{1}H NMR of **MM-T3** was run at 10 K increments between 293 K and 233 K (Figure 2-6). The two overlapping stator peaks between 6.96 and 6.92 ppm begin to separate at 273 K. Upon further cooling to 253 K all four of the aromatic stator peaks split into two resulting from the rotation slowing as the solution cools. Upon rotational "breaking", a 2:1 splitting of these peaks is expected, with two of the stator legs remaining equivalent and the other becoming independent. Indeed, it is stator proton H^1 that points towards the rotor that shows the largest thermal splitting. Upon further cooling to 233 K a further increase in resolution of the aromatic signals is observed, however this is not enough to allow for their further characterization. Such splitting of the stator protons offers a clear measure of the changes in the rotational environment of **MM-T3**. To examine the effect of illumination on **MM-T3**, it was next exposed to UV light (254 nm, 6W, 265 mW/cm^2) for 15 minutes and the ^{1}H-NMR before and after compared (Figure 2-7, top and middle).

Illumination results in a rapid broadening of the aromatic stator signals along with the formation of some new peaks in the broadened cyclopentadienyl region. This rapid broadening is indicative of a significant change in the molecules rotational ability upon ring closure, resulting from the now closed bulky photochrome. Upon ring closure the rotation of the molecule becomes hindered by the **c**-form photochrome, with the rotation becoming more difficult due to the

increasing rotational energy barriers. It is important to note however that unlike in the case of temperature decrease this does not lead to a splitting of the stator peaks. Thus, it can be assumed that while the rotation of the motor may be greatly hindered, it is not completely stopped at room temperature. However, the observation of this broadening even under room temperature NMR conditions, indicates the possibility of obtaining complete light induced rotational `breaking` under different conditions, including those employed for STM analysis. Next the sample was then illuminated using orange (above 550 nm) light in an attempt to return the closed photochrome to its **o**-form, however NMR showed that the sample remained in the **c**-form even after illumination for 15 min. This can be attributed to a combination of the competition in absorption between the photochrome and the ruthenium center at these frequencies and energy quenching of the ligand-centered excited state by the ruthenium center. Instead the system was left in the dark for seven days to allow the ring-opening to occur thermally. NMR analysis after this time showed the successful reversion to the **o**-form, indicating full thermodynamic release of the `brake` over time (Figure 2-7, bottom).

To further examine the change in **MM-T3** with light, its absorption profile before and after illumination was observed and compared with calculated DFT values. In dichloromethane (Figure

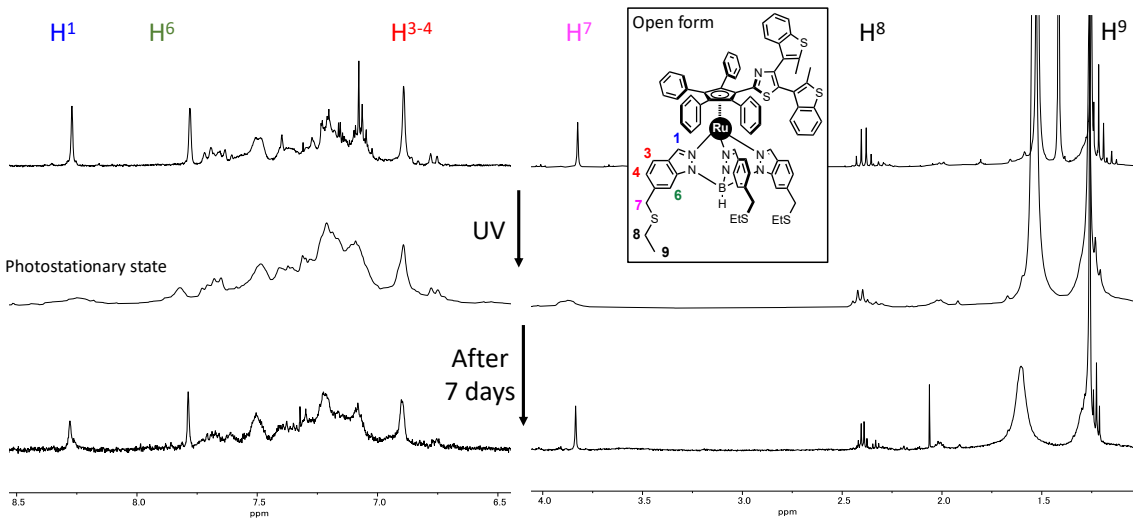

Figure 2-7 ^{1}H-NMR of **MM-T3** before (top) and after (middle) illumination along with after seven days (bottom) in CD_2Cl_2 (600 MHz).

2-10, left, black line) the **o**-form of **MM-T3** shows absorption bands between 400 and 600 nm

similar to those reported for similar non-photochromic motors.[113] TD-DFT calculations show these absorptions as ruthenium centered coming mainly from the metal dominated HOMO-1 orbital level. Upon formation of the photostationary state only small changes are seen, indicating absorption by the ruthenium center is not significantly affected by photochromic ring closure. To monitor these changes, the difference in absorption between the PSS and the **o**-form was calculated (Figure 2-8 left, inset). This shows a decrease in absorption around 275 nm along with two broad areas of increased absorption about 344 and 529 nm. This was compared to the changes predicted between the **c**-and **o**-forms by DFT (Figure 2-8, right) which showed a decrease at 276 nm and increases around 334 and 471 nm. Both experimental and DFT absorptions in the region expected to induce ring-opening of the photochromic unit (400-600 nm) appear overlapped with the ruthenium centered absorptions. This further explains the lack of photoreversion to the **o**-form upon illumination above 550 nm despite **MM-T3**'s ability to ring open thermodynamically over time.

2.5 Conclusion

In this chapter, a molecular motor functionalized with a terarylene photochromic fragment was designed for developing photo-triggered breaking on the molecular rotator, taking into account a

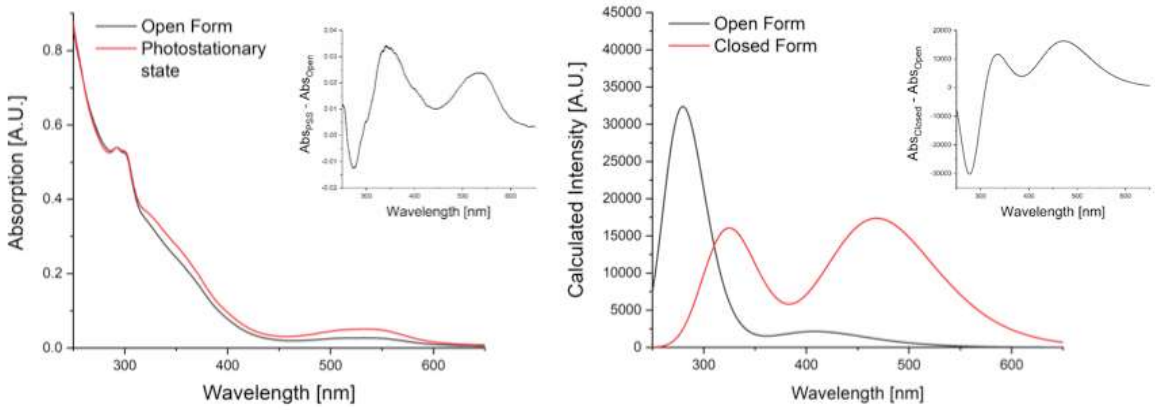

Figure 2-8 Comparison of the measured (left) and DFT calculated (right) absorptions of **MM-T3** in CD_2Cl_2. Insets show the difference between the **c**-and photostationary states (red) from the **o**-form (black).

computational estimation and the inherent properties of terarylene. The terarylene photochromic core frameworks that can be conjugated to the cyclopentadiene rotor part of the motor through

the linkage at the central aromatic units but not one of the peripheral side rings, in which terarylene structure is advantageous to control precisely the steric interactions with the stator part. After the computational study, the terarylene fragment was designed, synthesized, and fully characterized. The NMR study showed that the rotation of the functionalized cyclopentadienyl ligand becomes slowly restrained when the **c**-form is generated by light irradiation, suggesting their photocyclization acted as a brake. Afterward, the system was left in the dark for seven days to allow the ring-opening to occur thermally. Work should be extended to investigate by STM the complementary functionality of the light to block electron-induced rotation of our motor on surfaces.

2.6 Experimental

General

All commercially available chemicals were of reagent grade and were used without further purification. Anhydrous tetrahydrofuran, anhydrous toluene, anhydrous diethyl ether, magnesium sulfate, HCl, ammonium chloride, *n*-butyllithium (2.5M in hexanes), 5-bromopyrimidine and

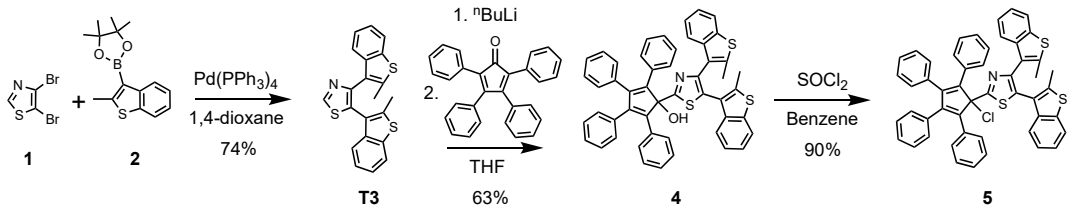

Scheme 2-1 Synthesis of the cyclopentadiene rotor functionalized with a terarylene fragment (**5**).

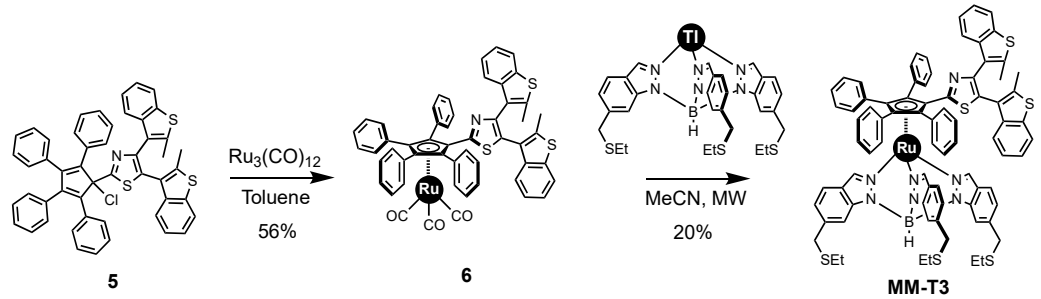

Scheme 2-2 Synthesis of the photochromic motor **MM-T3** incorporating a terarylene brake.

2,3,4,5-tetraphenylcyclopenta-2,4-dienone were purchased from Aldrich. Triruthenium dodecacarbonyl was purchased from Acros or Fluorochem. Benzene was purchased from Fluka. Thionyl chloride and thionyl bromide were purchased from Wako or Aldrich. CpOHAr1,[16b] CpBrAr1,[16b] CpOHAr3,[7d] CpBrAr3,[7d] CpOHAr4,[15] CpClAr4,[15] RuCpClAr4[15] were prepared according to the corresponding published procedures. Reactions were carried out using standard Schlenk techniques under an argon atmosphere. Thin layer chromatography (TLC) was performed on pre-coated aluminium-backed silica gel 60 UV_{254} plates (Macherey-Nagel) with visualisation effected with ultraviolet irradiation (λ = 254, 366 nm). Flash column chromatography was carried out on 230-400 mesh silica gel (Aldrich) unless otherwise stated.

NMR spectra were recorded with a Bruker Avance 300, a Bruker Avance 500 or a JEOL JNM-ECA600 spectrometer and assignments were made with the assistance of COSY, HMBC and HSQC spectra when necessary. ^{1}H and ^{13}C NMR chemical shifts (δ) are reported in ppm relative to the signal of tetramethylsilane (TMS). Residual solvent signals were used as an internal reference. Coupling constants (J) are given in Hz and the following abbreviations have been used to describe the signals: singlet (s); doublet (d); triplet (t); multiplet (m). The numbering system used for the assignment of signals in some compounds is provided in the supporting information document, along with the spectra of new compounds. IR spectra were recorded with a Jasco 4200 FTIR-ATR. Only selected characteristic peaks are listed. High-resolution mass spectra (HRMS) were performed with a Waters GCT Premier spectrometer (DCI), with a Waters Xevo G2 QTof spectrometer (ESI) and a JEOL JMS-Q1000TD spectrometer with JMS-700 Mstation (MALDI). Elemental analyses have been measured on a Perkin Elmer 2400 Series II CHNS/O system. Melting points were measured using a Krüss M5000 melting point meter or a MEL-TEMP capillary melting point apparatus. Melting points were not reported for compounds obtained as a mixture of regioisomers.

Synthesis

The synthesis of the photochrome functionalized motor **MM-T3** was obtained in five steps with a global yield of 4.7% (Scheme 2-1, 2-2) including the synthesis of the required terarylene 4,5-bis(2-methyl-1-benzothiophen-3-yl)-1,3-thiazole (**T3**). Compound **1** エラー! ブックマークが定義されていません。 and **2**[114] was synthesized as previously reported.

4,5-bis(2-methylbenzo[b]thiophen-3-yl)thiazole (T3)

4,5-Dibromo-1,3-thiazole (**1**) (1 eq., 1.00 g), 4.12 mmol) and 4,4,5,5-tetramethyl-2-(2-methyl-1-benzothiophen-3-yl)-1,3,2-dioxaborolane (**2**) (2.3 eq., 2.60 g, 9.47 mmol) were dissolved in 1,4-dioxane (15 mL) and aqueous tripotassium phosphate (2 M, 15 mL) was added dropwise. The solution was bubbled with nitrogen for 15 min. Then, tetrakis(triphenylphosphine)palladium (5 mol%, 0.230 g, 0.206 mmol) was added and the solution stirred at 105°C for 36 hours. After cooling down to room temperature, the solution was extracted by ethyl acetate and washed with water and saturated aqueous solution of sodium chloride. The organic layer was dried with anhydrous sodium sulfate, filtered, and concentrated. Silica gel column chromatography (9:1

hexane:ethyl acetate) gave a white solid (1.1 g, 74%). ^{1}H-NMR (500 MHz, CD_2Cl_2, 25ºC, TMS) δ (ppm) 2.02 (m, 6H), 7.20-7.29 (m, 4H), 7.56 (s 2H), 7.72-7.74 (m, 2H), 9.14 (s, 1H), NMR consistent with previous report.[114]

1-(4,5-bis(2-methylbenzo[b]thiophen-3-yl)thiazol-2-yl)-2,3,4,5-tetraphenylcyclopenta-2,4-dien-1-ol (4)

4,5-Bis(2-methyl-1-benzothiophen-3-yl)-1,3-thiazole (**T3**) (1 eq., 0.70 g, 1.85 mmol) was dissolved in 50 mL of degassed anhydrous tetrahydrofuran and cooled down to -78 °C. *n*-Butyllithium (1.6 eq., 2.3 M, 1.29 mL, 2.97 mmol) was added dropwise while keeping at this temperature. The solution turned brown-red, and was stirred for 2 hours at this temperature. Then, 2,3,4,5-tetraphenylcyclopentadienone (2.36 eq., 1.68 g, 4.37 mmol) was dissolved in 50 mL degassed anhydrous tetrahydrofuran and cannulated dropwise into the solution. The resulting solution was stirred for 1 hour at -78°C and allowed to warm to room temperature and stirred for 1 hour. Finally, 5 mL of saturated aqueous ammonium chloride was added slowly. The solution was extracted by ethyl acetate and washed with water and a saturated aqueous solution of sodium chloride. The organic layer was dried with anhydrous sodium sulfate, filtered, and concentrated. Silica gel column chromatography (2:1 dichloromethane:hexane) gave a white solid (0.89 g, 63%). ^{1}H-NMR (600 MHz, CD_2Cl_2, 25ºC) see Figure 2-11 δ (ppm) 1.86-1.90 (m, 6H), 4.75 (s, 1H), 6.86 (d, ^{3}J = 7.8 Hz, 1H), 7.00-7.46 (m, 22H), 7.66 (d, ^{3}J=8.4 Hz, 1H), 7.71 (d, ^{3}J=7.8 Hz, 1H). ^{13}C NMR (151 MHz, CD_2Cl_2, 25ºC) δ (ppm) 14.8, 14.9, 90.1(>C*OH*), 121.9, 122.1, 122.3, 122.9, 123.1, 124.1, 124.5, 124.6, 124.9, 126.8, 127.7, 127.9, 128.1 ,128.4, 129.4, 129.9, 130.0, 134.0, 134.2, 134.9, 135.1, 138.1, 138.2, 139.6, 139.7, 140.2, 141.1, 146.5, 171.8 (-C*SN*). HRMS (DCI/CH_4) (*m/z*): $[M]^+$ calcd. for $C_{50}H_{35}NOS_3$ 761.1881; found 761.1882. Assignments were made with the assistance of COSY, NOESY, HMQC and HMBC.

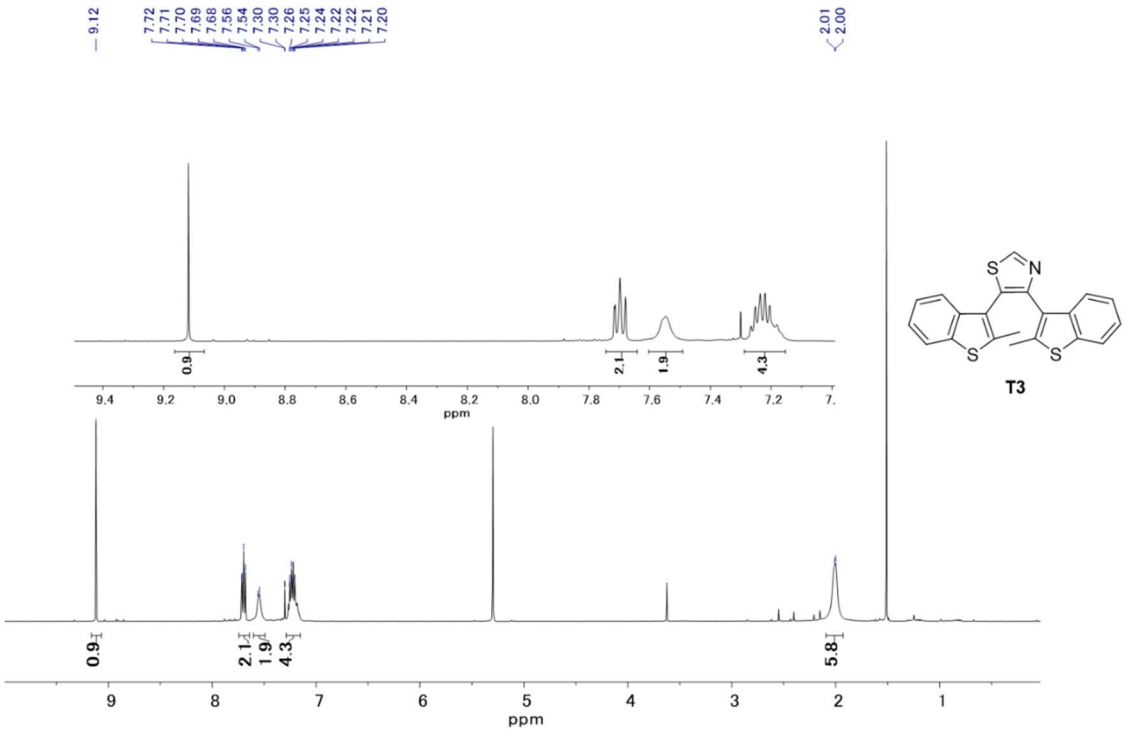

Figure 2-11 ^{1}H NMR spectrum of **T3** (500 MHz, 25°C, CD_2Cl_2).

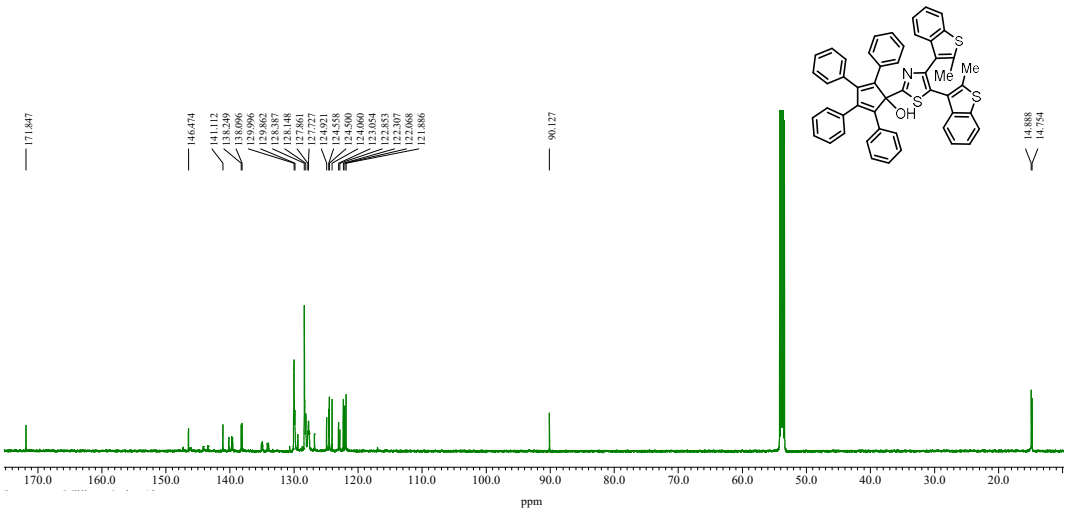

Figure 2-12 ^{13}C NMR spectrum of 4 (151 MHz, CD_2Cl_2, 25ºC)

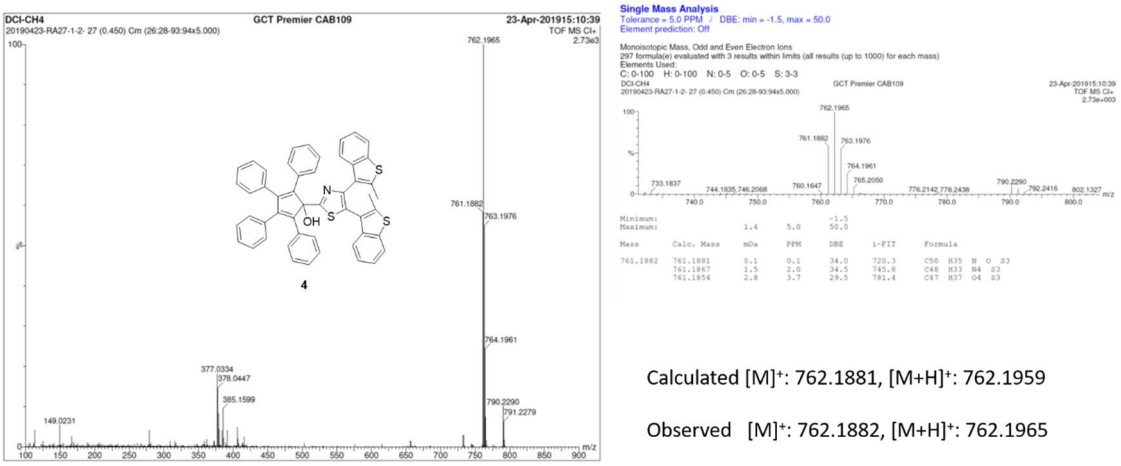

Figure 2-13 HR-MS spectrum of **4**.

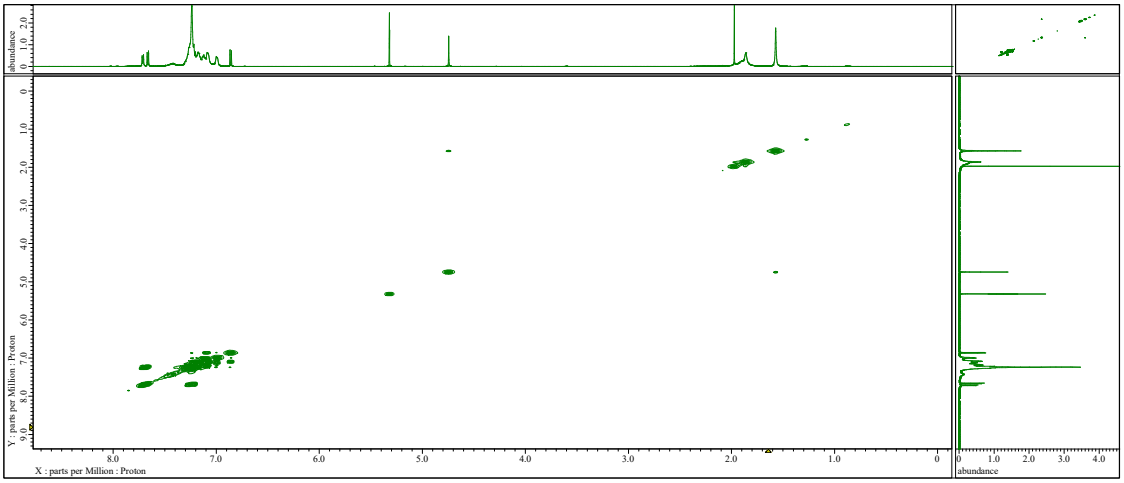

Figure 2-14 ^{1}H-^{1}H COSY of **4** (600 MHz, 25°C, CD_2Cl_2).

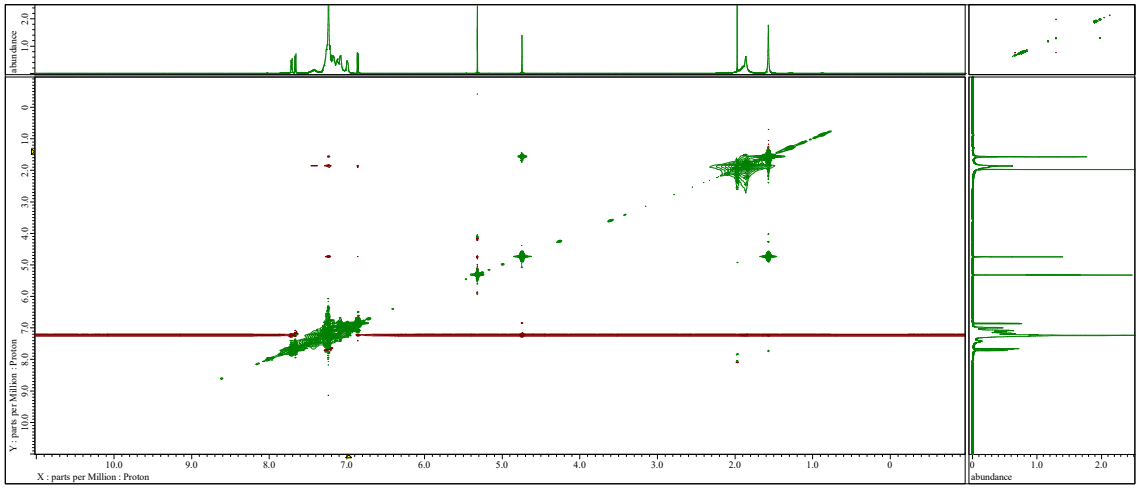

Figure 2-15 NOESY of **4** (600 MHz, 25°C, CD_2Cl_2).

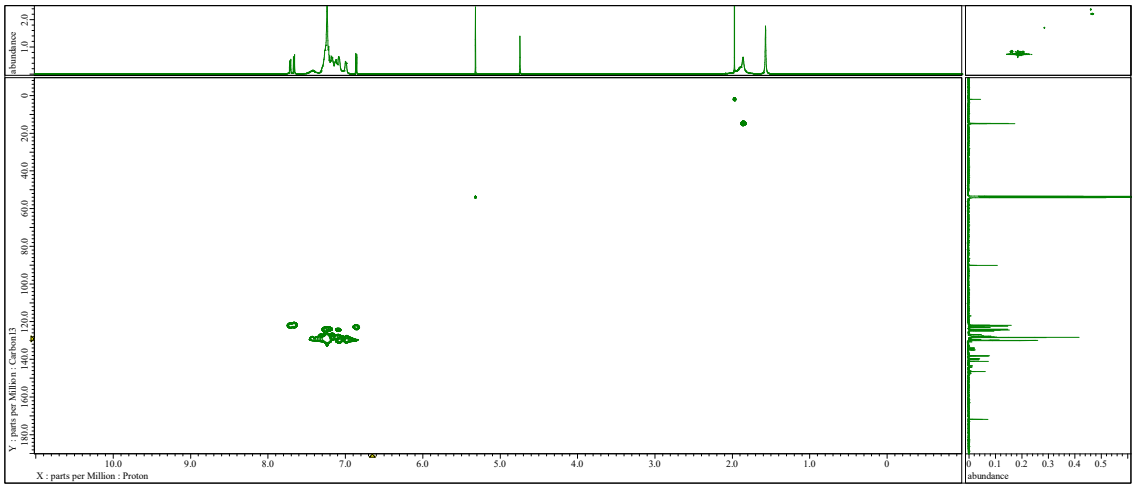

Figure 2-16 HMQC of **4** (600 MHz, 25°C, CD_2Cl_2).

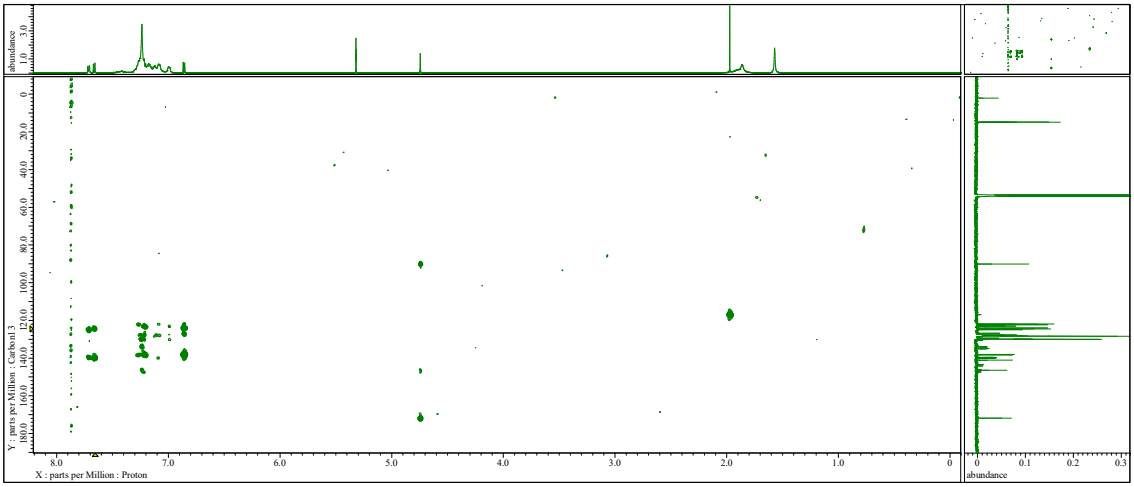

Figure 2-17 HMBC of **4** (600 MHz, 25°C, CD_2Cl_2).

2-(1-chloro-2,3,4,5-tetraphenylcyclopenta-2,4-dien-1-yl)-4,5-bis(2-methylbenzo[b]thiophen-3-yl)thiazole (5)

1-[4,5-Bis(2-methyl-1-benzothiophen-3-yl)-1,3-thiazol-2-yl]-2,3,4,5-tetraphenylcyclopenta-2,4-dien-1-ol (**4**) (1 eq., 50 mg, 0.066 mmol) was dissolved in 2 mL of benzene. Thionyl chloride (6 eq., 69 mg, 0.042 mL, 0.58 mmol) was slowly added, and the solution heated to reflux. After heating for 30 min, the solution was allowed to cool down to room temperature. An orange solution was purified by silica gel column chromatography (1:1 dichloromethane:hexane) to give compound **5** as yellowish orange powder. (45 mg, 87%). ^{1}H-NMR (500MHz, CD_2Cl_2, 25ºC) shows broad signals in the aromatic region due to conformational isomers, see Figure 2-18, for the full spectrum δ (ppm) 1.51-2.03 (6H, CH_3 peaks), 6.62-7.45 (24H, aromatic signals), 7.57-7.74 (4H, aromatic signals). ^{13}C-NMR (125 MHz, CD_2Cl_2, 25ºC) shows broad signals due to conformational isomers, see Figure 2-19 for the full spectrum δ (ppm) 14.5, 14.6, 15.2, 58.4 (>C*Cl*), 121.3, 121.4, 121.8, 121.9, 123.5, 123.6, 124.1, 124.6, 126.5, 127.5, 127.6, 127.7, 127.8, 128.0, 128.3, 128.5, 128.8, 129.0, 129.2, 129.5, 130.0, 130.3, 133.4, 134.2, 134.6, 137.8, 137.9, 140.4, 147.9, 159.2 (-C*SN*). HRMS (ESI) (*m/z*): $[M+H]^+$ calcd. for $C_{50}H_{35}ClNS_3$ 780.162; found 780.167.

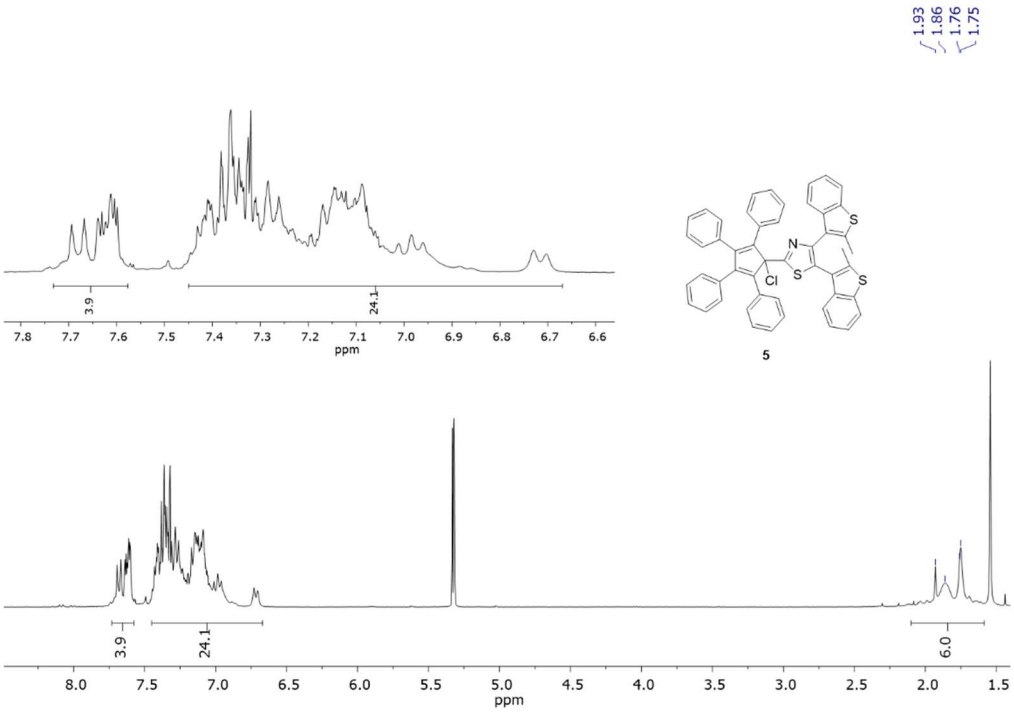

Figure 2-18 ^{1}H NMR spectrum of **5** (600 MHz, 25°C, CD_2Cl_2).

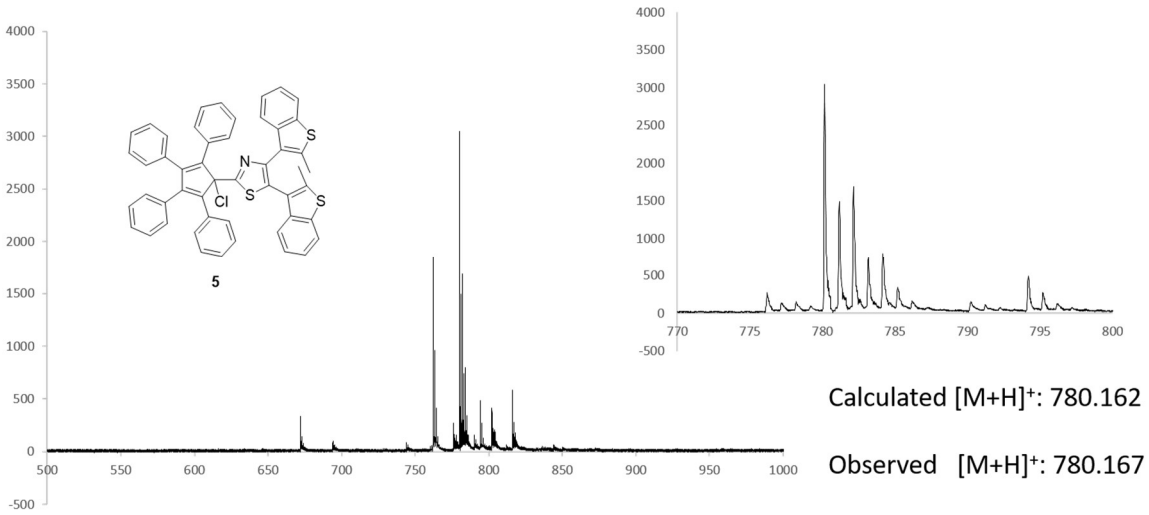

Figure 2-20 HR-MS spectrum of **5**.

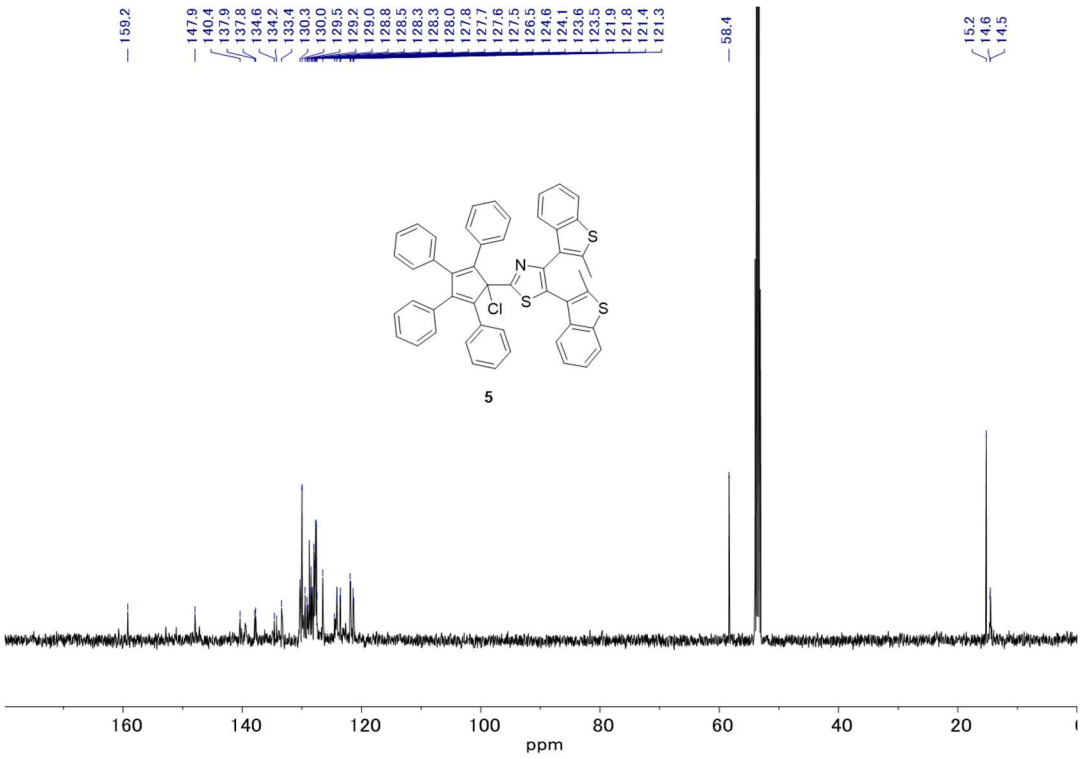

Figure 2-19 ^{13}C NMR spectrum of **5** (150 MHz, 25°C, CD_2Cl_2).

Chlorodicarbonylη^5-1-(4,5-bis(2-methylbenzo[b]thiophen-3-yl)thiazol-2-yl)-2,3,4,5-tetraphenylcyclopentadienyl]ruthenium(II) (6)

2-(1-Chloro-2,3,4,5-tetraphenylcyclopenta-2,4-dien-1-yl)-4,5-bis(2-methyl-1-benzothiophen-3-yl)-1,3-thiazole (**5**) (1 eq., 50 mg, 0.0564 mmol) and triruthenium dodecacarbonyl cluster (0.6 eq., 21.6 mg, 0.0338 mmol) were introduced. Anhydrous and degassed toluene (2 mL) was then added. The mixture was heated to reflux for 2 hours under argon. Then the solution was allowed to cool down to room temperature, the organic layer concentrated and purified by column chromatography (1:1 dichloromethane:hexane) to give compound **6** as bright yellow solid (30 mg, 56%). ^{1}H-NMR (600MHz, CD_2Cl_2, 25ºC) shows broad signals in the aromatic region due to conformational isomers, see Figure 2-21, for the full spectrum δ (ppm) 1.63 (s, 1H, CH_3 peak), 1.80 (s, 1H, CH_3 peak), 2.06 1.80 (s, 2H, CH_3 peak), 2.34 1.80 (s, 2H, CH_3 peak), 6.37-7.84 (28 H, aromatic signals). ^{13}C NMR (151 MHz, CD_2Cl_2, 25ºC) shows broad signals due to conformational isomers, see Figure 2-22 for the full spectrum δ (ppm) 14.6 (-C*H*$_3$), 14.8 (-C*H*$_3$), 77.6 (>C*Cl*), 113.0, 115.4, 121.6, 122.1, 124.4, 124.6, 124.9, 127.6, 127.7, 128.0, 128.2, 128.4, 131.7, 133.7, 138.1, 139.1, 142.1, 144.0, 205.0 (CO), 205.8(CO). IR (ATR, solid): cm^{-1} 2360 (CO), 2342 (CO).

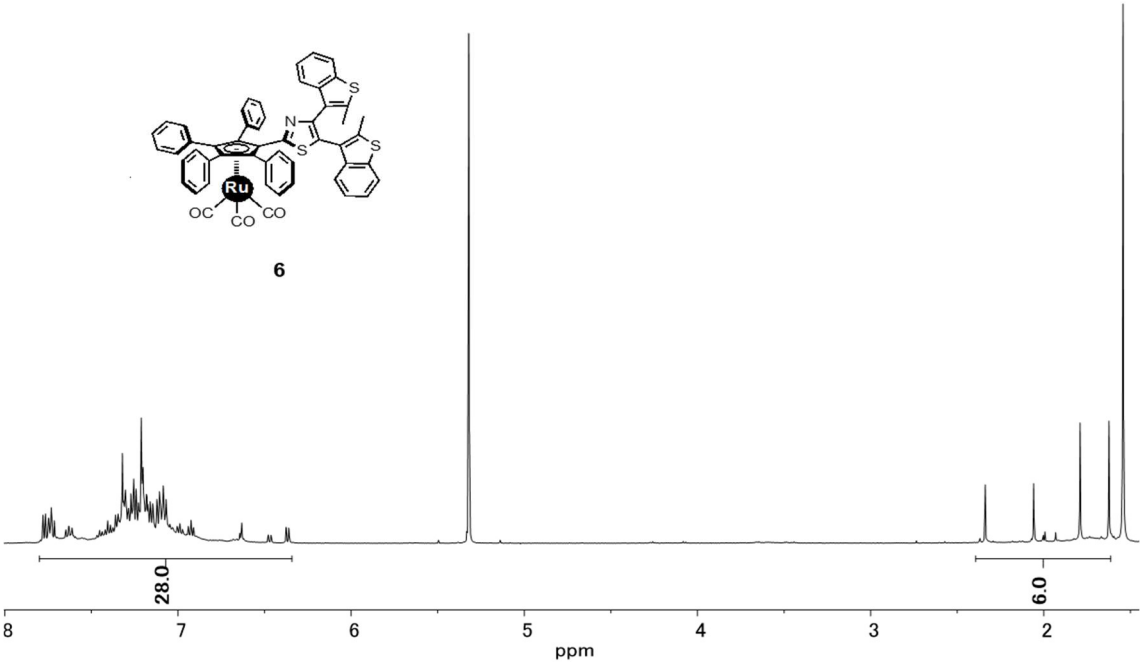

Figure 2-21 ^{1}H NMR spectrum of 6 (600 MHz, 25°C, CD_2Cl_2).

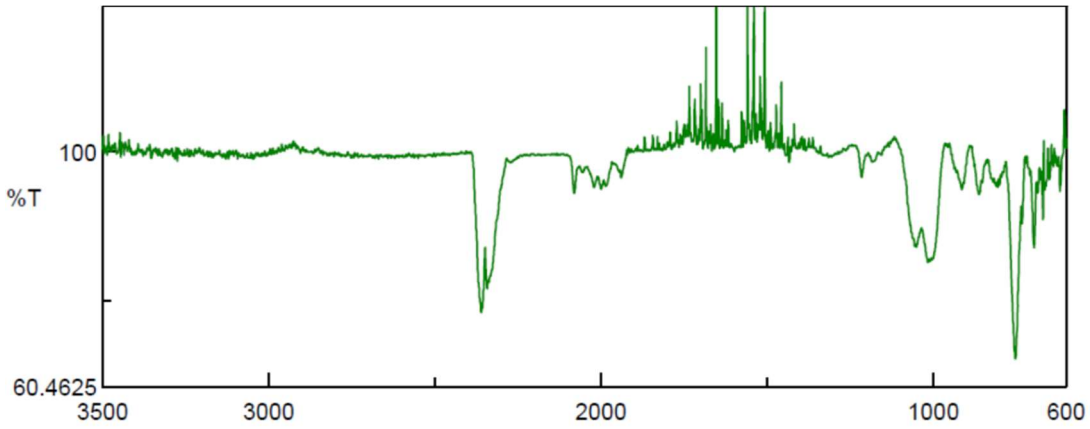

Figure 2-23 IR spectrum of **6**.

η^5-1-(4,5-bis(2-methylbenzo[b]thiophen-3-yl)thiazol-2-yl)-2,3,4,5-tetraphenylcyclopentadienylhydrotris{6-[(ethylsulfanyl)methyl]indazol-1-yl}borateruthenium(II) (MM-T3)

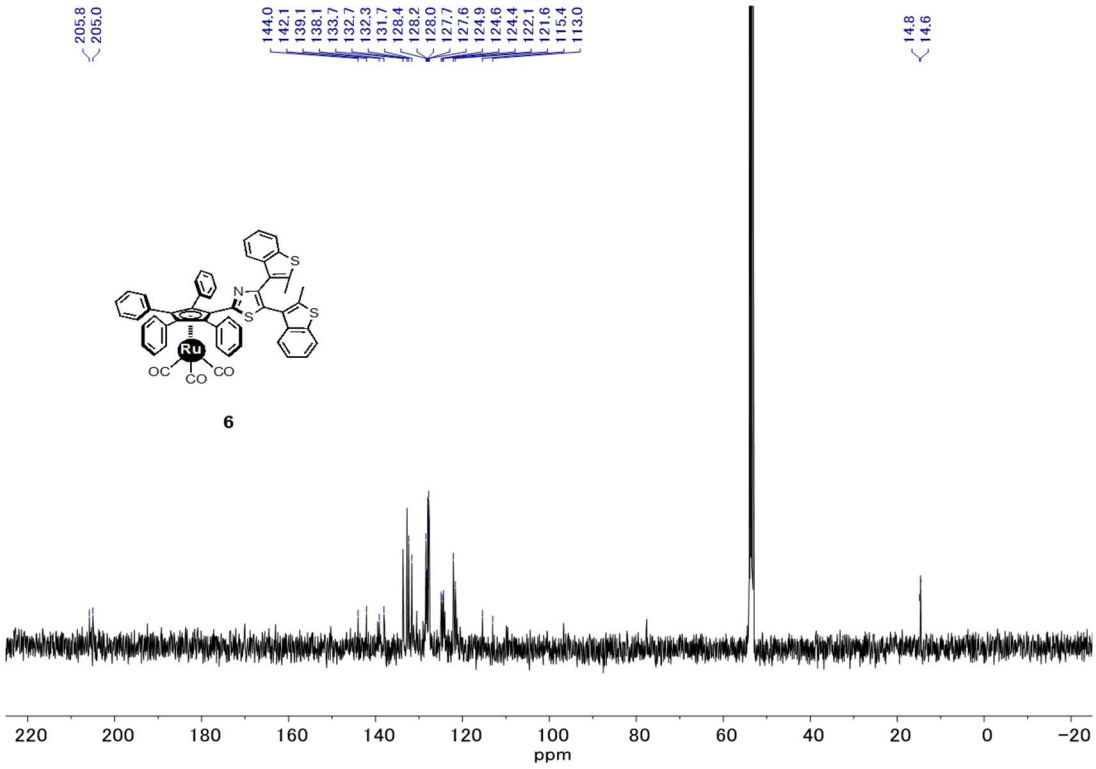

Figure 2-22 ^{13}C NMR spectrum of **6** (151 MHz, 25°C, CD_2Cl_2).

In a glove box, in a dried reactor specifically designed for microwave irradiation under argon were successively added a magnetic stirrer bar, chlorodicarbonyl[(1,2,3,4,5-η)-1-(4,5-bis(2-methylbenzo[b]thiophen-3-yl)thiazol)-2,3,4,5-tetraphenyl-2,4-cyclopentadien-1-yl]ruthenium(II) (**6**) (1 eq., 32 mg, 0.0341 mmol), thallium hydrotris{6-[(ethylsulfanyl)methyl]indazol-1-yl}borate (2.5 eq., 64.4 mg, 0.0815 mmol) and degassed acetonitrile (8.38 mL). The reaction mixture was heated to 100°C six times for 10 min in each heating cycle. A pressure of 5 bar was achieved and it was released between heating cycles. The completion of the reaction was monitored by TLC. The resulting mixture was diluted with dichloromethane and filtered through silica gel. The solvents were removed under reduced pressure and the residue was purified by column chromatography (2:1 dichloromethane:hexane) to afford compound **MM-T3** (9.8 mg, 20%) as a brown solid. ^{1}H-NMR (400MHz, CD_2Cl_2, 25ºC, TMS) δ (ppm) 1.30 (t, ^{3}J=7.4 Hz, 9H), 2.47 (q, ^{3}J=7.3 Hz, 6H), 3.87 (s, 6H), 6.92-6.96 (m, 6H), 6.99-7.69 (m, broad signals due to conformational and rotational isomers, accurate integration is not possible), 7.83 (s, 3H), 8.32 (s, 3H) (Figure 2-8 top). ^{13}C-NMR (151 MHz, CD_2Cl_2, 25ºC, TMS) shows broad signals due to conformational isomers see Figure 2-24 for spectra. δ (ppm) 1.3, 14.5, 14.9, 23.3, 25.7, 27.7, 29.9, 30.2, 30.3, 32.5, 33.7, 37.0, 47.0, 47.1, 111.4, 120.5, 122.4, 122.6, 124.5, 128.1, 128.5, 129.3, 130.5, 132.7, 138.5, 140.4, 144.0. MS (ESI) (*m/z*): $[M]^+$ calcd. for $C_{80}H_{68}BN_7RuS_6$ 1431.3; found 1431.3.

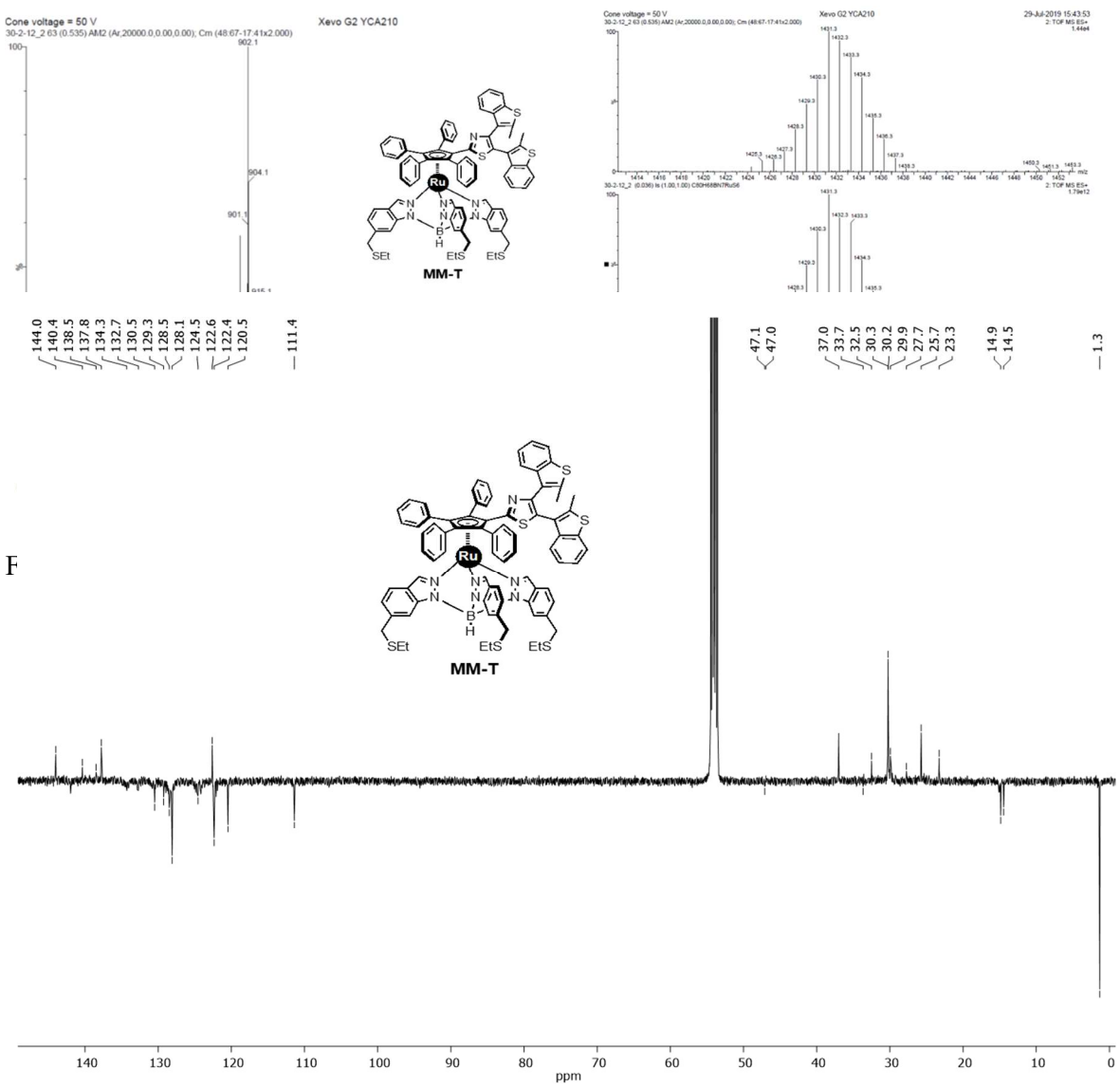

Figure 2-24 ^{13}C NMR spectrum of **MM-T3** (600 MHz, 25°C, CD_2Cl_2).

3. Synergetic photoswitching: cascade reaction triggered by photo- and radio-chemical oxidation for highly sensitive detection.

A successful molecular switching material requires precise performance on a single molecular level along with large scale propagation on multiple molecular levels to amplify the effect on property being changed. This chapter focuses on synergetic electro-chemical molecular switching via charge transfer from an initial catalytic amount of oxidized molecules. In chapter 1, I introduced some of this class including terarylene, which undergo a color changing reaction with external stimuli, including not only heat or light but also oxidative input. The discussion is then developed into synergetic phenomena which is the foundation of a cascade cycloreversion reaction with terarylene, induced by an oxidative input (see Chapter 1.4). Following this result, Section 3.1 provides new designs of molecules to enhance the oxidative cascade reaction yield. In addition, some of the structures showed a radiation induced oxidative reaction in halogenated solvent. The amplified response is also observed after irradiation with high energy photons such

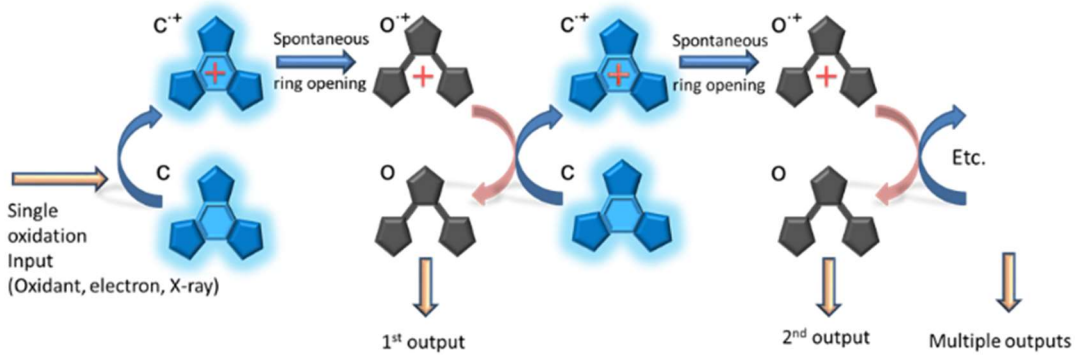

Scheme 3-1 Oxidative cascade reaction mechanism for cycloreversion.

as X-rays and the detection limit was dramatically enhanced compared to previous reports due to synergetic reaction (Section 3.2 and Section 3.4).

3.1 Molecular design for the highly efficiency, synthesis and characterization.

3.1.1 Molecular design

Compound **TA1o** was taken from a class of triangle terarylenes reported to have a higher photo-cyclisation quantum yield (0.6) than dithiazolylthiazole based ones (0.4).[115] **TA2o** was designed as a target containing phenyl rings on both photochemically reactive carbon atoms, as these rings were shown to accelerate the rate-limiting step of the oxidative cycloreversion (Scheme 3-1) and increase the efficiency of amplification by three orders of magnitude or more.[40] However, such phenyl rings were also known to increase the steric hindrance on the **c**-forms which suppress the thermal stability and lower photocyclisation quantum yields. For these reasons, two new compounds **TA3o** and **TA4o** were prepared, each having only one phenyl ring on the reactive carbons via consecutive coupling reactions, as inspired by previous works.[116] Compound **TA5o**[114] containing benzothiophene moieties instead of phenylthiophene groups, in which the capability of the aforementioned cycloreversion cascade process does not take place, was also employed as a reference (Figure 3-1).

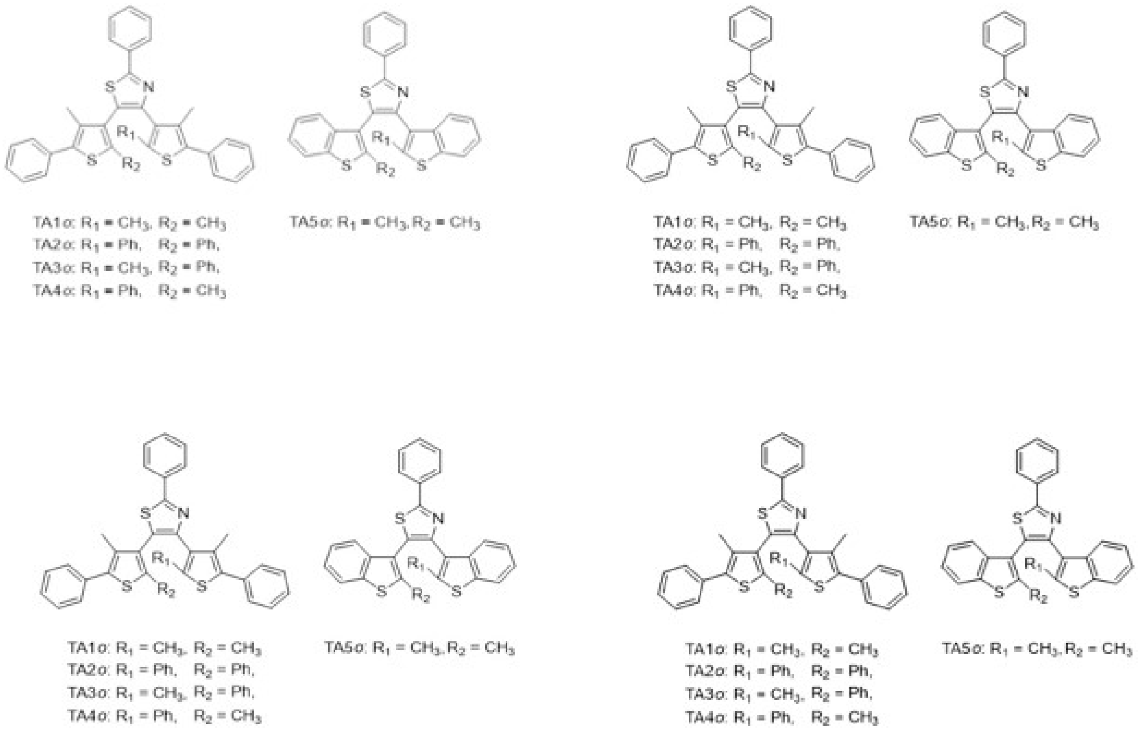

Figure 3-1 targeted terarylene structures for cascade reaction.

3.1.2 Synthesis

TA1o[30] and **TA5o**[114] were synthesized as previously reported. **TA2o**, **TA3o** and **TA4o** were prepared according to the routes depicted in Schemes 3-2, 3-3 and 3-3 from starting materials prepared with methods similar to those of **TA1o** and **TA5o**. The structures have all been successfully characterized using NMR and MS. The experimental details and all NMR and MS spectra are in section 3.7.

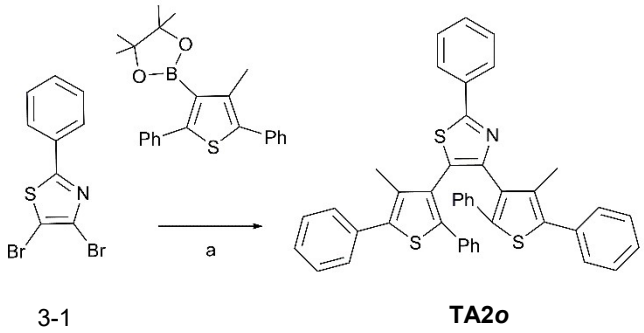

Scheme 3-2: Synthesis of **TA2o**: a) [$Pd(PPh_3)_4$], PPh_3, 2 M Na_2CO_3, K_3PO_4 Water/1,4-dioxane.

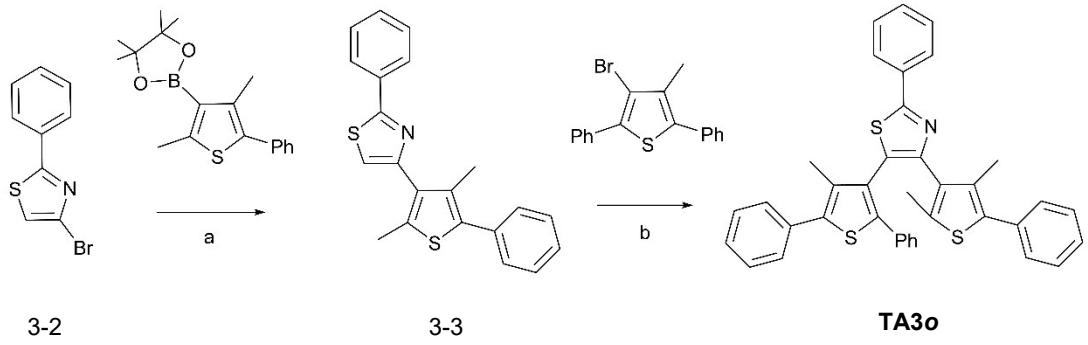

Scheme 3-3: Synthesis of **TA3o**: a) [$Pd(PPh_3)_4$], PPh_3, 2 M K_3PO_4, Water / 1,4 -dioxane, b) [$Pd(OAc)_2$], pivalic acid, di‐*tert*‐butylmethylphosphine tetrafluoroborate, mesitylene.

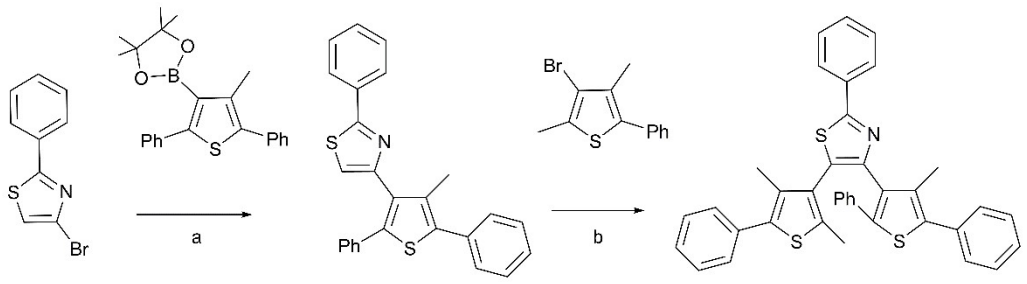

3-2 3-3 **TA4*o***

Scheme 3-4: Synthesis of **TA4o**: a) [$Pd(PPh_3)_4$], PPh_3, 2 M K_3PO_4, Water / 1,4-dioxane; b) $Pd(OAc)_2$, pivalic acid, di‐*tert*‐butylmethylphosphine tetrafluoroborate, mesitylene.

3.2.3 Optical properties

First the photoswitching properties of these compounds was examined in acetonitrile, under UV irradiation (λ= 365 nm), which resulted in the typical coloration of diarylethenes and terarylenes in all cases (Figure 3-2). Compounds **TA1–4** share a π-conjugated system with a similar geometry in their closed-ring forms, leading to an almost identical absorption peak at around 600 nm with photo-cyclisation quantum yields >50%, typical of terarylenes. The molar absorption coefficients of **TA3c** and **TA4c** (ε) were determined based on the ^{1}H NMR and absorption spectra after UV irradiation (Figure 3-3). The conversion ratios of the **c**-forms in the photostationary state (PSS) were estimated based on the obtained ε values. The optical properties estimated by NMR and reported, including the conversion ratio of the **c**-forms at the PSS are

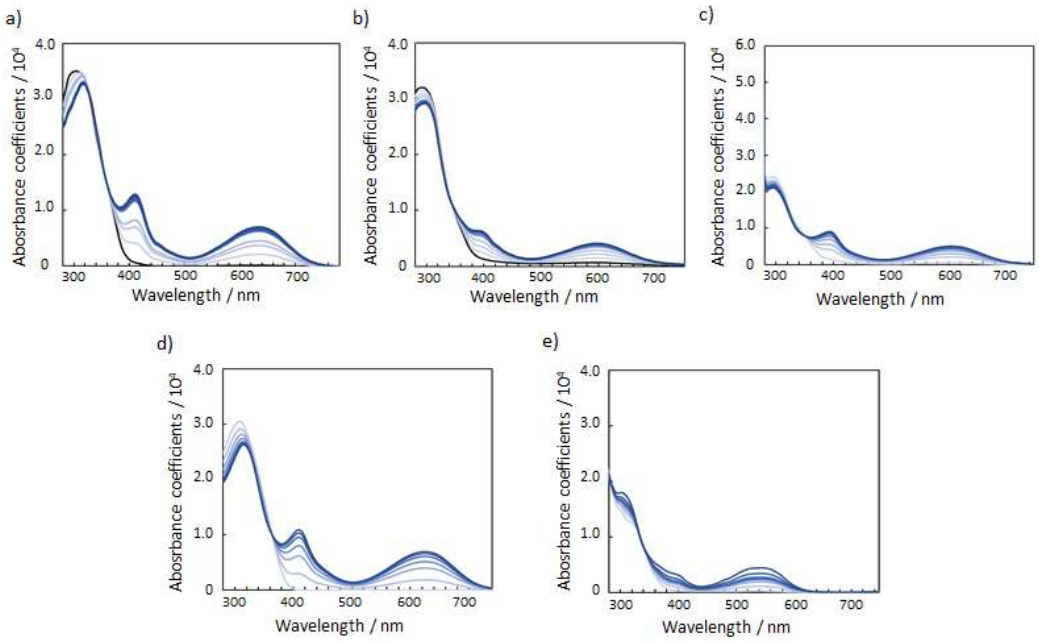

Figure 3-2 New absorption bands in the visible region appear for compounds a) **TA1**; b) **TA2**; c) **TA3**; d) **TA4**; and e) **TA5** upon irradiation with UV light at 365 nm in acetonitrile with abs coefficients based on the **o**-forms. Each spectrum was taken every after irradiation for 30 s. Visible light irradiation turns them back to the **o** form. Concentration of **o**-forms = a) 3.0 x 10^{-5} M; b) 3.7 x 10^{-5} M; c) 1.5 x 10^{-5} M; d) 5.2 x 10^{-5} M; e) 4.0 x 10^{-5} M.

summarized in the Table 3-1.

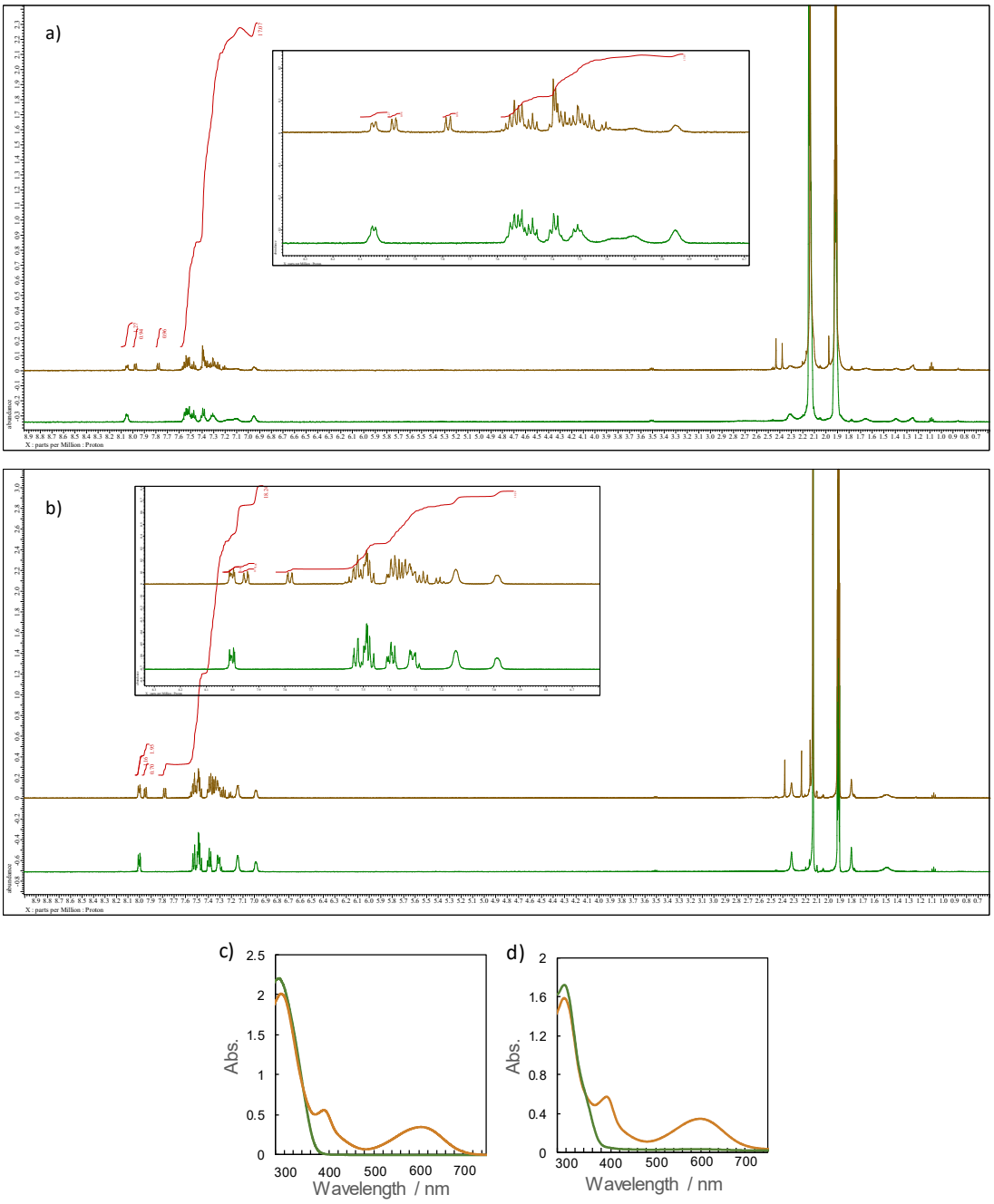

Figure 3-3 ^{1}H-NMR spectra of a) **TA3o**; b) **TA4o** before (green) and after UV light irradiation for 3 min (brown) (400 MHz, CD_3CN, 25 °C). The conversion of c form after UV light irradiation was a) 36%, b) 38%. Absorption spectra of c) **TA3o/c**; d) **TA4o/c** solution (brown) and **o**-form (green). The ^{1}H-NMR sample solution was diluted and the absorbance was measured. After visible light irradiation, the absorbance of **o**-form was measured. Concentration of **c**-forms in **o**/**c** solution are b) 3.0 x 10^{-5} M; d) 2.7 x 10^{-5} M which is determined from conversion of **c**-form in ^{1}H NMR.

Table 3-1. Optical and photochemical properties of **TA1-5** in acetonitrile.

	λ_O / nm ($\varepsilon \times 10^{-4}$ $M^{-1}cm^{-1}$)	$\lambda_{max,\ C}$ / nm ($\varepsilon \times 10^{-4}$ $M^{-1}cm^{-1}$)	Conversion ratio of **c**-form at PSS
TA1o	290 (2.20)	613 (1.10)	0.61
TA2o	294 (3.12)	610	-
TA3o	299 (2.4)	614 (1.1)	0.52
TA4o	299 (2.4)	613 (1.2)	0.54
TA5o	273(2.21)	539(1.20)	0.76

Visible light irradiation (λ > 480 nm) of the colored acetonitrile solutions induced the cycloreversion reaction to afford colorless solutions with the original absorption profiles of the **o**-forms. The **c**-form of compound **TA2** exhibited spontaneous bleaching at room temperature within minutes, probably due to the steric interactions destabilizing isomer **TA2c**. Photocyclisation-cycloreversion cycles were repeated several times showing the same isosbestic point, indicating typical two-metastable reversible isomerizations. No significant solvatochromism was reported with **TA1o/1c** displaying the same spectra in hexane.[117] Thermal stability of the closed-ring forms for **TA1c** was investigated in the dark and the half-lifetime at room temperature were estimated to be fourteen days; the half-lifetime of both **TA3c** and **TA4c** are estimated at six hours, a relatively short time. The half-lifetime of **TA5c** is previously reported to be 500 days in toluene.[114]

3.2 Cascade reaction of new target molecules

Although the spontaneous bleaching of **TA2c** to **TA2o** within minutes prevented their further characterization, the half-lifetimes of **TA1c**, **TA3c** and **TA4c** being more than six hours allowed the evaluation of the oxidative cycloreversion reaction cascade, most of which was complete within an hour. First, the oxidative chain cycloreversion for these compounds was tested using tris(bromophenyl)ammoniumyl hexachloroantimonate (TBPA) as a one-electron oxidant initiator in acetonitrile. As in previous reports,[39,40] complete cycloreversion could be accomplished even with catalytic amounts of TBPA, indicating the chain reaction process. A minimum amount of 2% equivalents of TBPA was necessary to induce the complete cycloreversion of **TA1c** (Figure 3-4a), an estimated turnover number of 200 for each initial trigger molecule (5,000% oxidant-based yield).

For the **TA3c** and **TA4c**, oxidant equivalents as low as 0.1% was found to lead to complete decoloration, resulting in a turnover number of over 1,000 for each initial trigger molecule, i.e. 100,000% oxidant-based yield (Figure 3-4b). This value was comparable to that of terthiazole-based compounds having two phenyl moieties on the reactive carbons[40] One phenyl ring on the

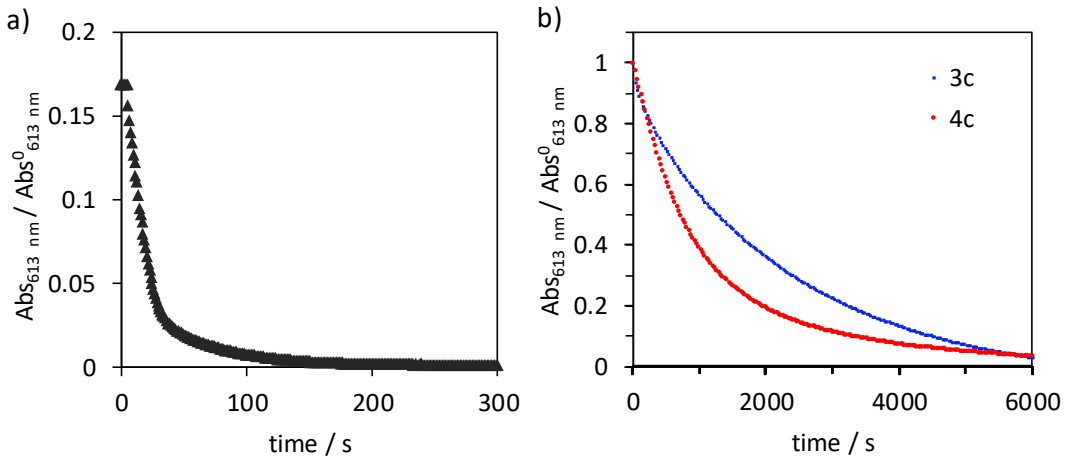

Figure 3-4 a) Decay in absorbance of TA**1*c*** at 613nm after adding 0.02 eq. TBPA in acetonitrile (0.05 mL) into acetonitrile solution (1.5 x 10^{-5} M, 3 mL). b) Decay in absorbance of **TA3c** and **TA4c** after adding 0.001 eq. TBPA in acetonitrile (0.05 mL) into acetonitrile solution (3 mL). Concentration of **c-**forms = ca. 2.0 x 10^{-5} M.

reactive carbon atoms appears enough to make oxidative cycloreversion faster and more efficient in the present compounds. Contrarily, the complete bleaching of **TA5c** required an equimolar amount of TBPA, confirming the absence of a chain reaction mechanism in this case (Figure 3-5).

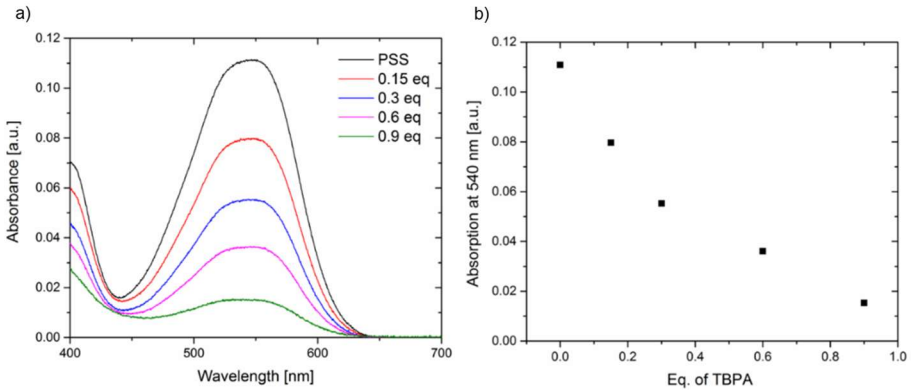

Figure 3-5 a) Absorption spectra after adding TBPA in acetonitrile (0.05 mL) into acetonitrile solution of **TA5c** (3 mL). Concentration of c forms = 1.0 x 10^{-5} M; b) Absorbance after addition of TBPA in acetonitrile (0.05 mL) into acetonitrile solutions of **TA5c** (1.0 x 10^{-5} M, 3mL). As **TA5c** showed no cascade reaction, the absorbance reached to a steady state immediately after addition of TBPA.

3.3 UV and X-ray induced cycloreversion.

The oxidative cycloreversion reaction was examined by irradiation with UV in chloroform. The **c** forms of compounds were produced by illuminating 0.3 mL solutions in toluene under UV (365 nm) until the amount of the **c**-form reached 9.0×10^{-8} mol. Then, the solution was diluted with 2.7 mL of chloroform to generate the **c**-form solution of concentration of 3.0×10^{-5} M which was irradiated with a controlled number of photons at 313 nm using absorbed photon counting system. Figure 3-6 monitors the peak absorbance at 610 nm for **TA1**, **TA3** and **TA4** following the initial UV irradiation at 313 nm for 30 s. After stopping the light irradiation, the continuous decrease in the closed-ring concentration of **TA1c**, **TA3c** and **TA4c**, indicates that cycloreversion takes place, with absorptions typical of the **o**-forms recovered. It can be seen that cycloreversion of **TA1c** took around 30 min in an almost linear fashion, similar to previous results.[39] Meanwhile, cycloreversions of **TA3c** and **TA4c** were completed within half an hour in a quasi-zero order fashion, in accordance with the results of oxidative cycloreversion of derivatives having aromatic rings on the reactive carbons. The half-lives of **TA3c** and **TA4c** were found to be six hours, thus the effect of thermal cycloreversion on this experiment is ignorable. In addition, in acetonitrile and toluene, only the photocyclization (coloration) reaction is induced by UV irradiation (either

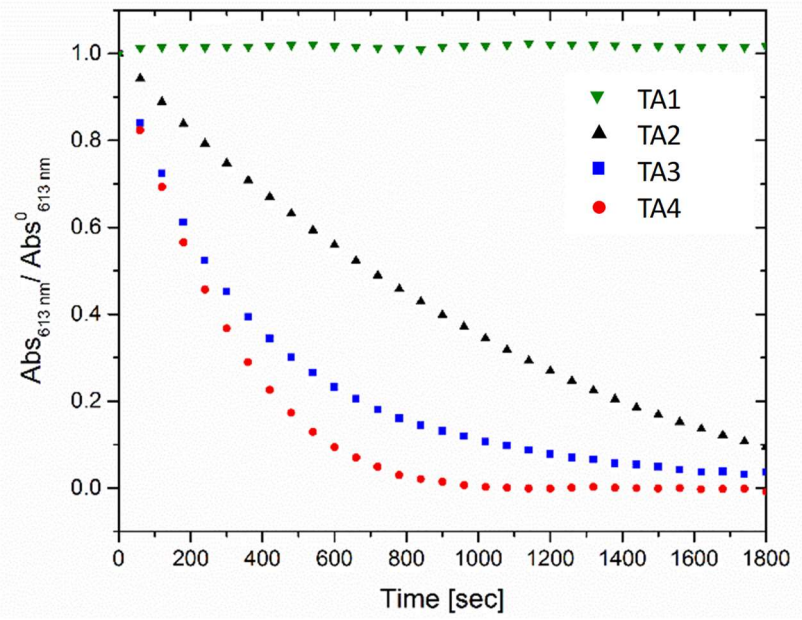

Figure 3-6 Decay in absorbance at λ_{max} after UV irradiation (313 nm), of toluene: chloroform (1: 9) solutions of the **c**-forms of each compound. Concentration of c forms = 3.0×10^{-5} M.

at 313 or 365 nm). The spontaneous bleaching of **o**-forms was not observed upon irradiation in the visible region (610 nm). Therefore, the cation radical species triggering the oxidative-cycloreversion cascade was generated upon UV irradiation in chloroform. This can be the result of either photo-induced charge transfer between the higher excited state of the **c**-forms and chloroform molecules[77] or the excitation of a charge-transfer state.[78] Meanwhile, a decrease was not observed for **TA5c**, again indicating the importance of the cascade reaction capability.

Furthermore, photocyclization and cycloreversion cycles were also performed showing the repeatability (Figure 3-7). After the first cycloreversion and recovering of a clear solution of the **o**-form by UV irradiation (1), another cycle was restarted by evaporating the chloroform (2), then the dried product was dissolved in toluene. UV irradiation reproduced a stable blue solution, without evidence of spontaneous cycloreversion. Addition of chloroform and subsequent UV irradiation restarted bleaching of the color again. This was cycled several times with no evidence of degradation from ^{1}H-NMR (Figure 3-8).

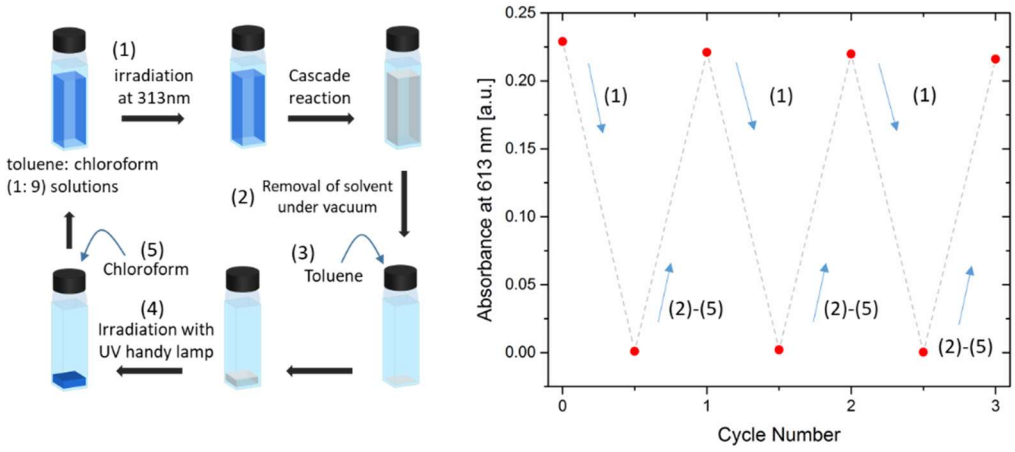

Fig. 3-7 UV-induced bleaching–coloration cycles by irradiation with UV for **TA4**. Experimental procedure: (1) Toluene-chloroform (v/v = 1/9) solutions of **TA4o/4c** (concentration of the **c**-forms = 2.0 x 10^{-5} M, 3 mL) were irradiated with UV (313 nm) for 60 sec. After the cascade bleaching reaction finished in 10 min, the absorbance of fully bleached solution was measured confirming Abs 613nm < 0.01; (2) The solution was removed under vacuum; (3) Toluene (0.3 mL) was added into the cuvette; (4) The toluene solution was irradiated with UV (365 nm) for 300 sec; (5) the irradiated toluene solution was diluted by chloroform (2.7 mL) and the absorbance was measured observing Abs 613nm > 0.20.

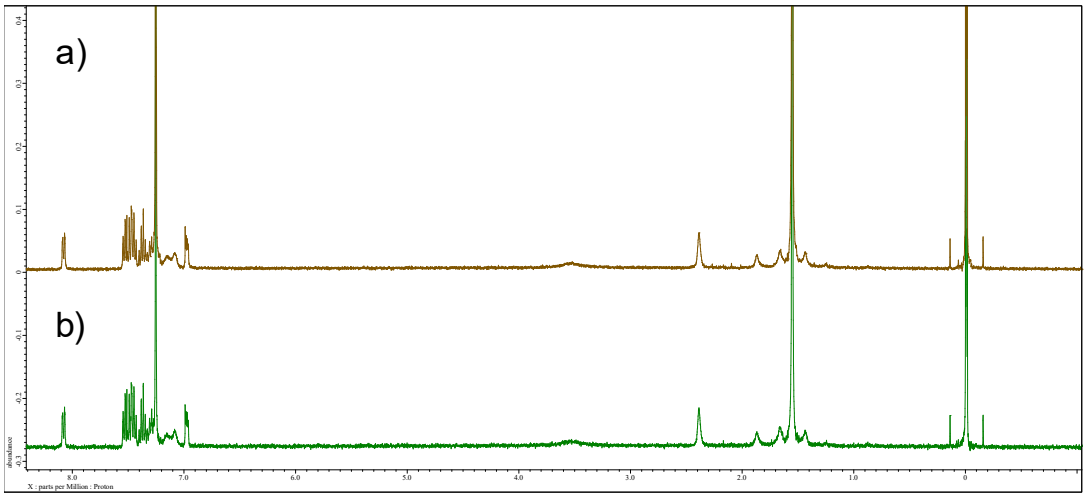

Figure 3-8 ^{1}H-NMR spectra of (a) **TA4o**, (b) after UV induced fading reaction of **TA4o** (400 MHz, $CDCl_3$, 25 °C, TMS); In this experiment, after measurement of **TA4o**/$CDCl_3$ solution (a), solvent was removed under vacuum and toluene was added followed by UV light irradiation (365nm) for 60 sec. Toluene was then removed under vacuum and $CDCl_3$ was introduced. The **TA4o/4c** sample in the ^{1}H-NMR tube was irradiated with UV (313 nm) and ^{1}H-NMR spectrum (b) was obtained at the fully bleached steady state, about 20 min later. No significant changing of ^{1}H-NMR spectra was observed.

The absorbed photon numbers at 313 nm were then counted using an absolute photoreaction quantum yield evaluation system for estimation of an apparent cycloreversion quantum yield.[118] For **TA3c** and **TA4c**, the maximum turnover number of the chain reaction process was found to be 33 to 1; that is, for every absorbed photon induced oxidation, an average of 33 molecules undergo cycloreversion, resulting in a quantum yield up to 3,300%. Moreover the solution being irradiated with UV may contain some neutral, not photoconverted **o**-forms that can also absorb photons at 313 nm inducing the opposite cyclization to the cycloreversion.

Finally, to test for X-ray irradiation induction of the cascade cycloreversion, I again prepared the **c**-form solution in toluene/chloroform mixture in a similar manner to the UV-induced cycloreversion experiment described above (see Figure 3-7). The solutions were then exposed for 6 s under 100 mGy overall X-ray dose using a conventional X-ray tube (40keV, Cu-target). Under continued stirring after X-ray irradiation, absorbance at 613 nm continuously decreased for **TA1c**, **TA3c**, and **TA4c**, indicating conversion to their respective **o**-forms (Figure 3-9).

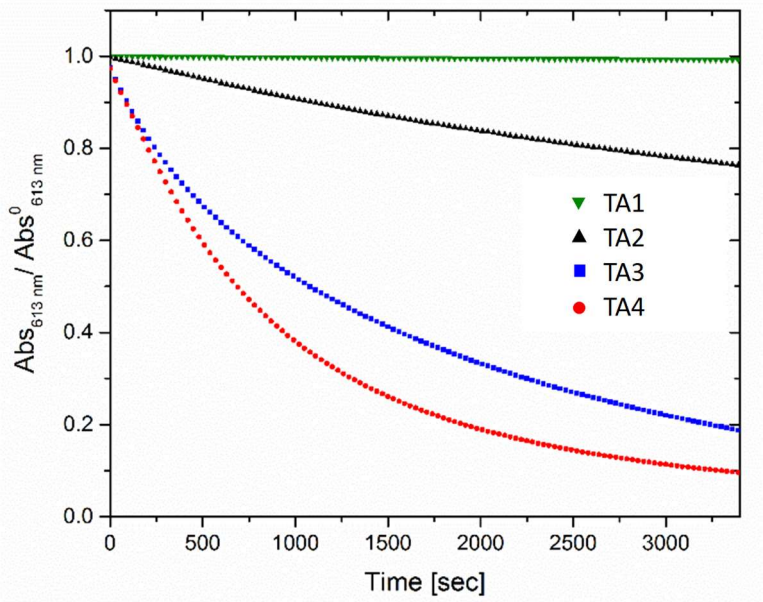

Figure 3-9 Decay in absorbance at $\lambda_{max, vis}$ after irradiation of 100 mGy of X-rays in toluene: chloroform (1: 9) solutions of the **c**-forms of each compounds. Concentration of **c**-forms = 3.0 x 10^{-5} M.

The decay in absorbance of **TA1c** was not completed within two hours while those of **TA3c** and **TA4c** were almost complete within an hour. The effect of cycloreversion due to thermal processes is limited since the thermal half-lives of the **c**-forms are considerably longer than the timescales for this X-ray induced reversion. To ensure that no significant degradation was caused by X-rays, the **o**-form was also reproduced completely after the removal of chloroform following the same system in the UV-irradiated cycloreversion (see Figure 3-7), which is confirmed by the unchanged ^{1}H-NMR spectrum (Figure 3-10).

As no oxidant was used, a simpler recovery method can be employed where the mixture was heated to 60°C under reduced pressure leaving chloroform in toluene. Subsequent exposure of this solution to UV light recovered the absorbance of the **c**-form, confirming the reversibility of the process. To the best of our knowledge, this is the first X-ray-induced cycloreversion for diarylethenes or terarylenes. More importantly, the dose amount of 100 mGy is one of the most radio-sensitive value for the organic color changing materials. Thus, maximum sensitivity will be discussed in the following section in detail.

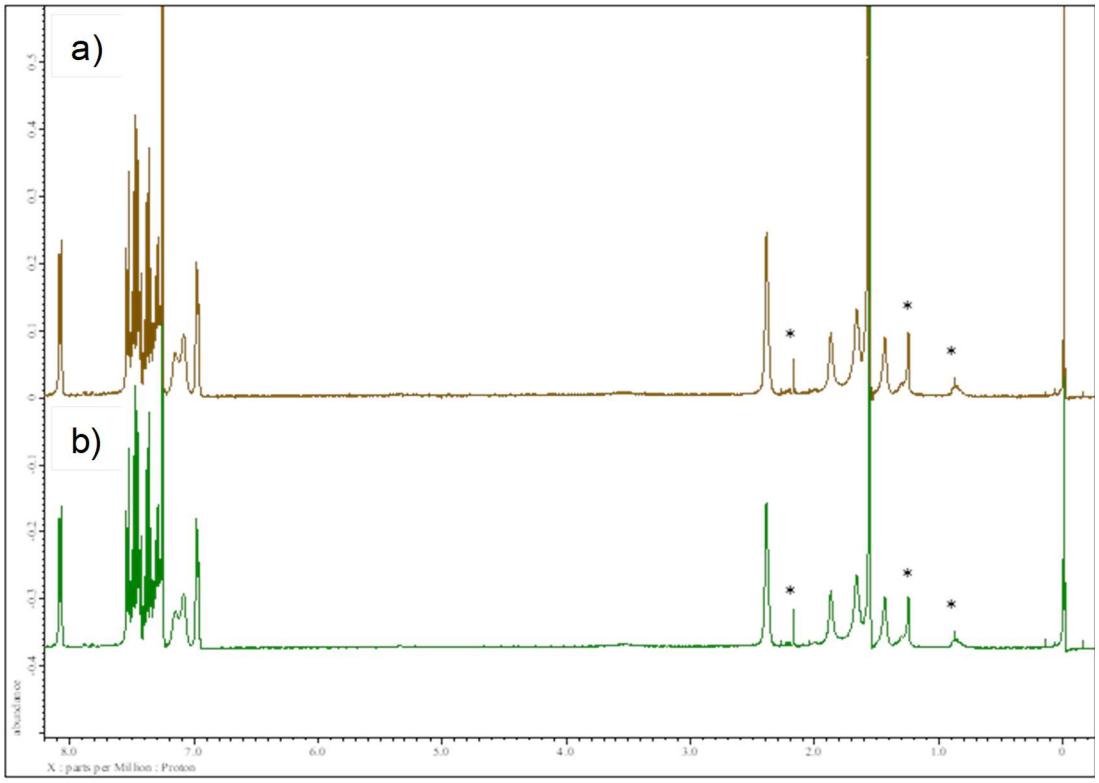

Figure 3-10 ^{1}H-NMR spectra of (a) **TA4o**, (b) after X-ray induced fading reaction (400 MHz, $CDCl_3$, 25 °C, TMS) Experimental procedure: after ^{1}H-NMR measurement of **TA4o**/$CDCl_3$ solution (a), solvent was removed under vacuum and toluene was added followed by UV light irradiation (365nm) for 60 sec. Toluene was then removed under vacuum and $CDCl_3$ was introduced again. The **TA4o**+**TA4c**/$CDCl_3$ solution in the NMR tube was irradiated with X-ray (100 mGy). ^{1}H-NMR spectrum (b) was obtained at the fully bleached steady state, about 20 min later. No significant changing of ^{1}H-NMR spectra was observed. As marked with *, the solution indicated small amount of acetone (δ = 2.17 ppm) and hexane (δ = 0.87, 1.26 ppm).

3.4 A highly sensitive photoswitching response to low doses of X-Rays

The minimum amount of X-ray radiation dosage for complete cycloreversion reaction was then estimated for **TA4c** in order to estimate radio-chromic sensitivity. Almost complete bleaching was observed with X-ray irradiation of 100 mGy within 30 min, 10 mGy irradiation led to discoloration to 30% after one hour, and 80% remained after one hour with 1 mGy dosage (Figure 3-11).

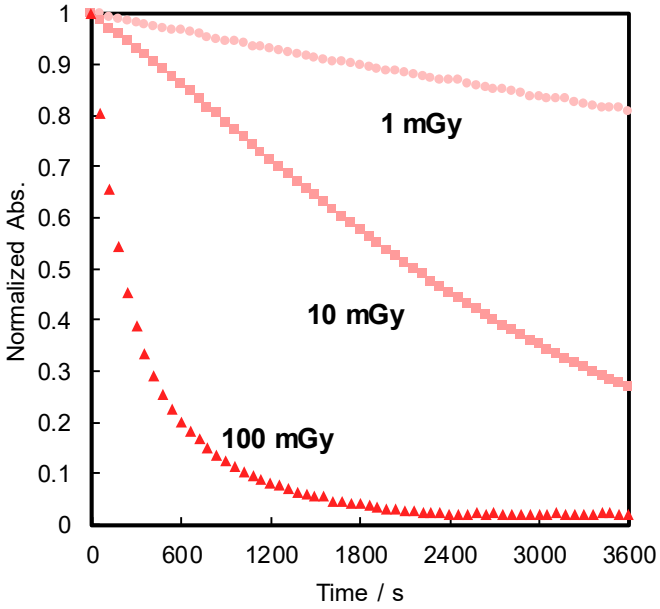

Figure 3-11 Decay in absorbance upon irradiation with varying doses of X-ray for **TA4c**

X-ray irradiation to the halogenated alkanes is expected to generate radical cation species,[76] which can further oxidize the neutral **c**-forms triggering the oxidative cycloreversion. Even with the low efficiency in the charge transfer reaction between the radical cation species generated from chloroform and the neutral **c**-forms, the subsequent oxidative cycloreversion cascade could amplify the imitated reaction, resulting in the highly sensitive detection of X-rays. The rate of cycloreversion can be controlled depending on the amount of radical species initially oxidatively generated, which is directly related to the X-ray dosage, since the electron transfer process propagates in a chain like manner of quasi-zero order. In order to apply the discoloration process as an analytical tool, I here define X_{cyclo} as the "% decay in absorbance ten minutes after X-ray exposure" to be used as an analytical index for X-rays (eq. 1):

$$X_{cyclo} = \frac{Abs_0 - Ab_t}{Abs_0} \times 100\ \% \qquad \text{eq.1}$$

where Abs_0 is the initial absorbance at $\lambda_{max,\ vis}$ of toluene: chloroform (1: 9) solutions of the **c**-forms. Abs_t is the absorbance at $\lambda_{max,\ vis}$ of toluene: chloroform (1: 9) solutions of the **c**-forms after ten minutes without irradiation. A solution of the **c**-form of **TA4** was exposed to X-rays of varying doses and the absorbance decay monitored for ten minutes. A plot of X_{cyclo} as a function of X-ray dosage in the mGy range showed a linear response (Fig. 3-11) and X_{cyclo} was proportional to X-ray dosage in the range of 1-10 mGy (Fig. 3-12), indicating the amount of cations generated by X-rays is proportional to the rate of cycloreversion and the reaction proceeds in the zero-order kinetics. Furthermore, X-ray dosage in the range of 1-10 mGy led to X_{cyclo} with only a slight deviation of linearity, which leads to a proposed analytical dynamic range of X-ray detection of at least one order of magnitude. This result therefore provides a method not only for X-ray detection but also for quantification of X-ray dosage; as measurement/calculation of cycloreversion rate can be correlated with any X-ray dosage in the range of 1-10 mGy. Then, the limit of detection (LOD) was evaluated following the general equation:

$$LOD = \frac{3\sigma_{blank}}{m} \qquad \text{eq. 2}$$

Here σ_{blank} is the standard deviation of X_{cyclo} for multiple (15) blank measurements (no X-ray irradiation), this is a measure of the % decrease in absorbance due to spontaneous cycloreversion by mainly thermal effects (Table 3-2), and *m* is the slope of the graph on Fig. 3-12. It was determined for **TA4c** that the LOD is 0.3 mGy, which is two orders of magnitude lower than the record set by Han and co-workers using small organic molecules[75] and similar to that of Xie and co-workers for uranyl-based frameworks.[119]

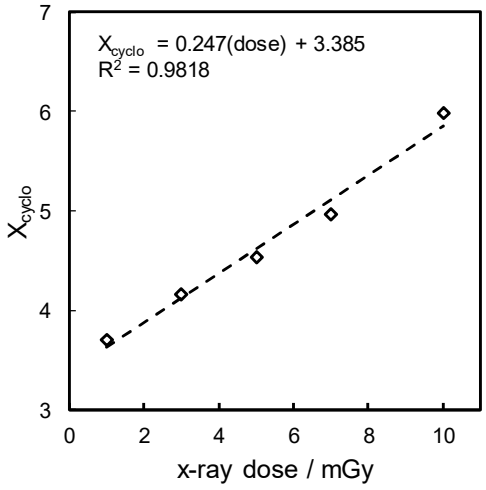

Figure 3-12 Linear relationship between X_{cyclo} and X-ray dose for **TA4**.

Table 3-2. Blank experiment to measure σ_{blank} of TA4c

run#	Abs^0_{613nm} [a]	Abs_{613nm} [a],[b]	X_{cyclo} (%) [c]
1	0.37645	0.36884	2.023
2	0.39380	0.38592	2.001
3	0.43275	0.42389	2.048
4	0.30769	0.30143	2.034
5	0.45280	0.44364	2.022
6	0.40266	0.39467	1.986
7	0.32215	0.31559	2.036
8	0.57182	0.55977	2.107
9	0.46331	0.45391	2.029
10	0.42328	0.41458	2.056
11	0.38512	0.37729	2.033
12	0.36817	0.36065	2.045
13	0.31491	0.30840	2.067
14	0.44276	0.43375	2.035
15	0.31945	0.31290	2.052
		σ_{blank} (%)[4]	*0.028*
		LOD	*0.34*

a) Absorbance was measured with a UV-vis spectrometer in 6 digits after the decimal point.
b) Abs^0_{613nm} and Abs_{613nm} are absorbance of TA4o/4c (concentration of TA4c= 2.7-5.1 x 10^{-5} M in toluene) solution measured before and after an interval of 600 sec at dark condition without X-ray irradiation.
c) X_{cyclo} (%) denotes decrease in absorbance due to the spontaneous cycloreversion, Xcyclo (%) = Abs^0_{613nm} - $Abst_{613nm}$*/ Abs^0_{613nm} x 100
d) Standard division of X_{cyclo}

3.5 Conclusion

Five photoswitching terarylenes including three new compounds, showing cyclization and cycloreversion with high quantum yield and complete recyclability have been prepared. Three of them showed highly efficient cyclization reactions using the electron transfer cascade process. The introduction of a single phenyl unit on a carbon atom at the photocyclization reaction center significantly enhanced the amplification efficiency. UV irradiation in a non-halogenated solvent allows induction of coloration forming the thermally stable **c**-form, while UV irradiation in the presence of chloroform induce a highly efficient bleaching reaction from the **c**-form to the **o**-form. This reaction kinetics represents a chain reaction process. Estimation of this UV-induced quantum chain reaction showed it to be significantly higher than unity (3,300%), even with the UV-induced coloration occurring at the same time. Similar amplified photochemical reactivity can be expected when other haloalkanes such as dichloromethane, dichloroethane, bromoethane, and iodomethane are used. The phenyl thiophene or diphenyl thiophene units composing the present compounds would support the photo-oxidation capacity by stabilizing the cationic radical intermediates, resulting in the UV-induced cascade reaction observed. Indeed, light-triggered cascade reactions were not observed for conventional terthiazole derivatives with low oxidation activity and the other terarylene, which shows electro-chemical oxidative cycloreversion. The fading reaction was also observed even with very low doses (mGy level) of X-rays, indicating a returning to a colorless **o**-form. These new compounds provide a new approach to the development of visually detectable dosimeters that could signal the presence of low-level radiation through color fading by forming quasi-solids using a gel support. The Limit of detection (LOD) of 0.3 mGy is the highest sensitivity among organic X-ray color-changing materials.

This low LOD is attributed to a very small change in the linear sensitivity to X-ray irradiation, thus the large change in absorbance with X-ray irradiation is mainly due to a very efficient charge transfer cascade reaction mechanism for cyclization. This demonstrates the high utility of efficient photosynergetic reactions for highly sensitive detection or accuracy of absorbance measurements. Furthermore, σ_{blank} is minimized by the reasonable thermal stability of the c-form and would be further improved by the structural considerations. There is immense anticipation to actualize a practical X-ray sensing material of higher sensitivity.

3.6 Experimental

General

^{1}H and ^{13}C NMR (300, 400, and 600 MHz) spectra were recorded on JEOL JNM-AL300, JEOL JNM-ECP400, and JEOL JNMECA600 spectrometers, respectively. Reversed-phase HPLC separation was performed with a LaChrom Elite apparatus (Hitachi). Mass spectrometry and high-resolution mass spectrometry were performed on JEOL JMS-Q1000TD and JMS-700 MStation JMS-S3000 spectrometers, respectively. UV/Vis spectra, quantum yields of photochromic reactions (ϕc-o and ϕo-c) and photo-induced fading reaction were measured using a JASCO V-660, V-760 spectrophotometer and a Shimadzu QYM-01 set-up, respectively. For kinetic thermal analyses, the temperature was controlled by a JASCO ETC 505 T temperature controller. Stopped-flow measurements were conducted with a rapid-scan stopped-flow spectroscopic system (Unisoku).

Oxidative cycloreversion experiments

Oxidative cycloreversion experiments were performed by mixing the requisite amounts of the oxidising agent tris(4-bromophenyl)ammonium hexachloroantimonate with the closed forms of 1, 3, 4 and 5 in acetonitrile and monitoring the evolution of absorbance at λmax, with constant stirring to avoid the effect of diffusion on the electron transfer.

UV-induced cycloreversion experiments

UV-induced cycloreversion experiments were performed on the closed forms of 1, 3, 4 and 5 in chloroform solution by monitoring the evolution of absorbance at λmax, with constant stirring to avoid the effect of diffusion on the electron transfer. Chloroform solution of closed from was prepared by diluting the 0.3 mL solutions of the compounds in toluene which was irradiated with LED-UV light at 313 nm until a photostationary state was achieved. Then the solution irradiated with a controlled number of photons in a QYM machine (SHIMADZU QYM-01) and absorption changes ware monitored using the QYM machine.

X-ray induced cycloreversion experiments

X-ray induced cycloreversion experiments were performed the closed forms of 1, 2, 4 and 5 in chloroform solution which was prepared in the same method as UV induced cycloreversion experiments monitoring the evolution of absorbance at λ_{max} after X-ray irradiation for six

seconds, with constant stirring to avoid the effect of diffusion on the electron transfer. The irradiation source of X-ray (XRB80, Spellman) was a conventional X-ray tube equipped with a tungsten anode target and beryllium window. The applied tube Electronic Supplementary Material (ESI) for Chemical Science. This journal is © The Royal Society of Chemistry 2020 S2 voltage and current were 40 kV and 0.052 -5.2 mA, respectively.

Synthesis

TA1o エラー! ブックマークが定義されていません。 and **TA5o**[30] were synthesized as previously reported. **TA2o**, **TA3o** and **TA4o** were prepared according to the routes depicted in Schemes 3-2, 3-3 and 3-3 from starting materials prepared with methods similar to those of **TA1o** and **TA5o**. The structures have all been successfully characterized using NMR and MS. The experimental details and all NMR and MS spectra are in section 3.7.

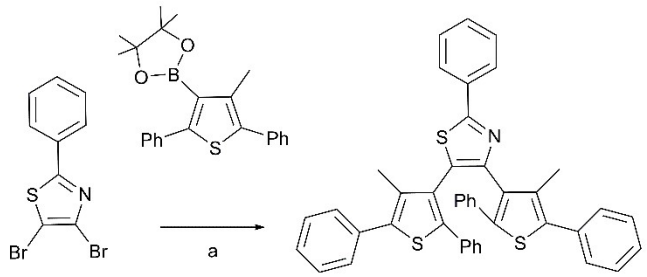

3-1 **TA2o**

Scheme 3-3: Synthesis of **TA2o**: a) $[Pd(PPh_3)_4]$, PPh_3, 2 M Na_2CO_3, K_3PO_4 Water/1,4-dioxane

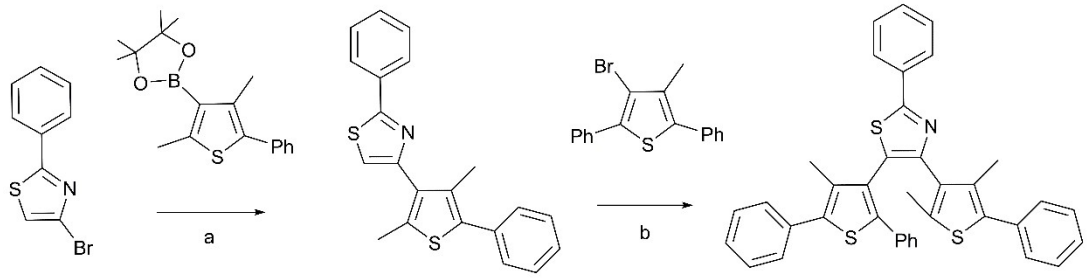

3-2 3-3 **TA3o**

Scheme 3-4: Synthesis of **TA3o**: a) $[Pd(PPh_3)_4]$, PPh_3, 2 M K_3PO_4, Water / 1,4 -dioxane, b) $[Pd(OAc)_2]$, pivalic acid, di‐*tert*‐butylmethylphosphine tetrafluoroborate, mesitylene.

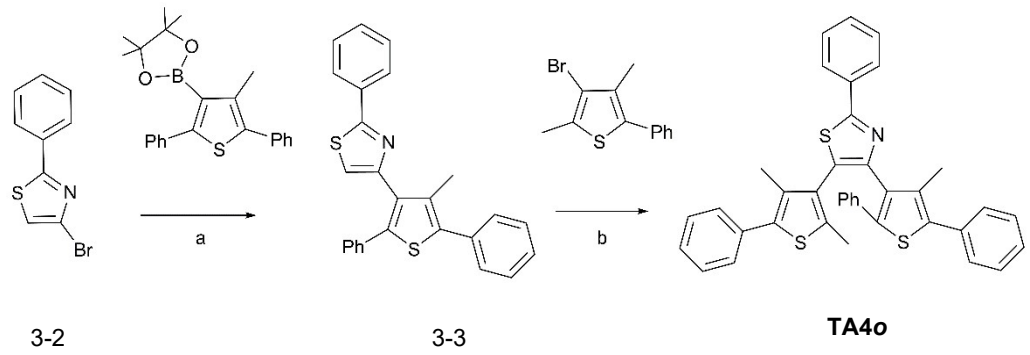

3-2 3-3 **TA4o**

Scheme 3-5: Synthesis of **TA4o**: a) $[Pd(PPh_3)_4]$, PPh_3, 2 M K_3PO_4, Water / 1,4-dioxane; b) $Pd(OAc)_2$, pivalic acid, di‐*tert*‐butylmethylphosphine tetrafluoroborate, mesitylene.

4,5-bis(4-methyl-2,5-diphenylthiophen-3-yl)-2-phenylthiazole (TA2o):

4,5-dibromo-2-phenylthiazole (322 mg, 0.85 mmol.), 4,4,5,5-tetramethyl-2-(4-methyl-2,5-diphenylthiophen-3-yl)-1,3,2-dioxaborolane (751 mg, 2.35 mmol.), PPh_3 (162 mg, 0.43 mmol.) and 2 M aqueous K_3PO_4 (15 mL) were dissolved in 1,4-dioxane (15 mL). After 15 minutes stirring under N_2 atmosphere, $Pd(PPh_3)_4$ (352 mg, 30 mol%) was added and the mixture refluxed under N_2 atmosphere at 110 °C for 72 h. Thereafter, the organic layer was extracted with chloroform, and the combined extracts were washed with water and dried over anhydrous Na_2SO_4. The sample was then filtered and the filtrate was concentrated in vacuo. Silica gel column chromatography (hexane:ethyl acetate, 40:1) of the residue and Reversed-Phase HPLC (acetonitrile) afforded 4,5-bis(4-methyl-2,5-diphenylthiophen-3-yl)-2-phenylthiazole (0.12 g, 19% yield) as a white solid. ^{1}H NMR (500 MHz, $CDCl_3$, 25 °C, TMS): δ = 8.26-8.25 (m, 4H), 8.19-8.17 (m, 2H), 7.70-7.61 (m, 8H), 7.56-7.48 (m, 9H), 7.46-7.42 (m, 2H) 1.57 (s, 6H); ^{13}C NMR (151 MHz, CD_3CN, 25 °C, TMS): δ = 166.0, 150.0, 129.2, 128.5, 128.4, 128.3, 128.2, 127.3, 126.4, 116.2, 94.4, 83.9, 77.3, 77.1, 76.9, 56.4, 40.3, 38.6, 34.7, 33.3, 28.8, 25.0, 24.5, 15.0, 14.5, 13.0 ppm; HRMS (MALDI SpiralTOF): *m*/*z* calcd. for $C_{43}H_{31}NS_3$ $[M]^+$: 657.16131; found 657.16125.

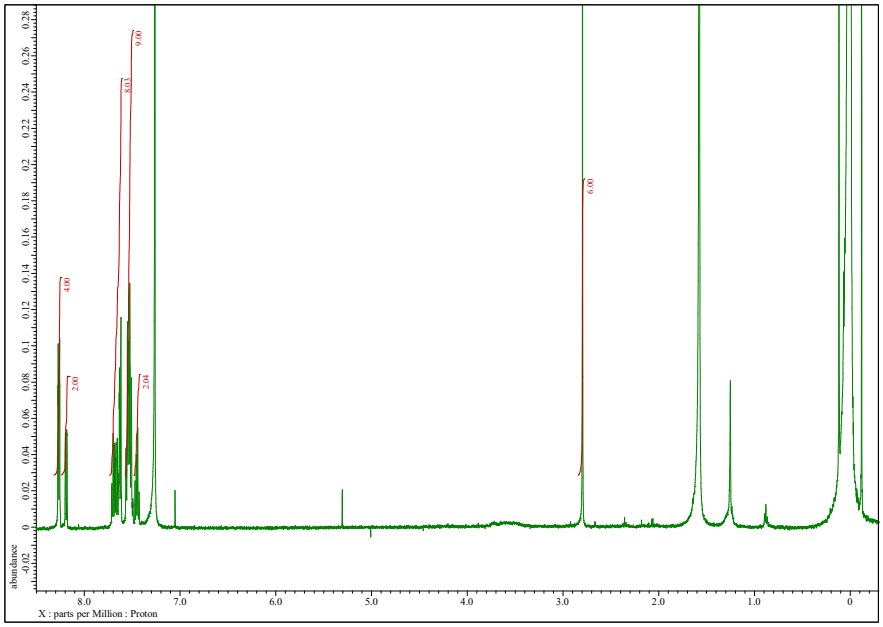

Figure 3-12 ^{1}H-NMR spectrum of **TA2o** (500 MHz, $CDCl_3$/TMS, 25 °C).

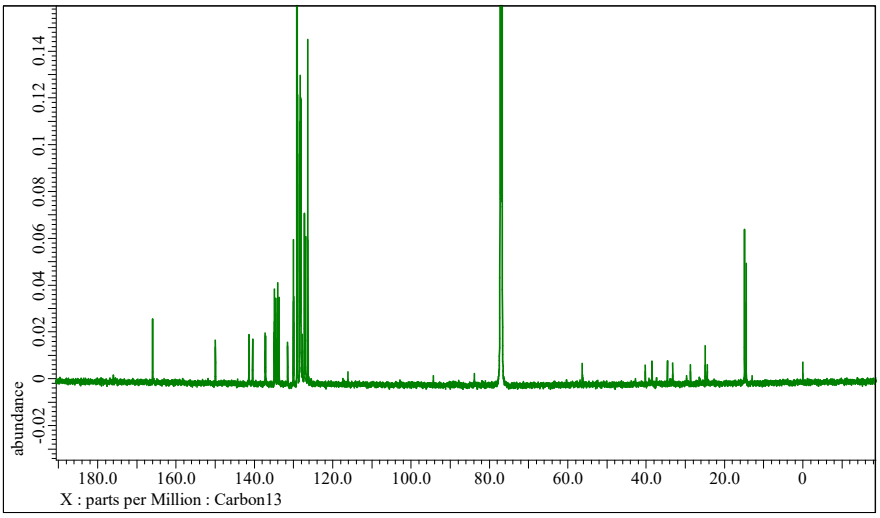

Figure 3-13 ^{13}C-NMR spectrum of **TA2o** (151 MHz, CD_3CN, 25 °C, TMS).

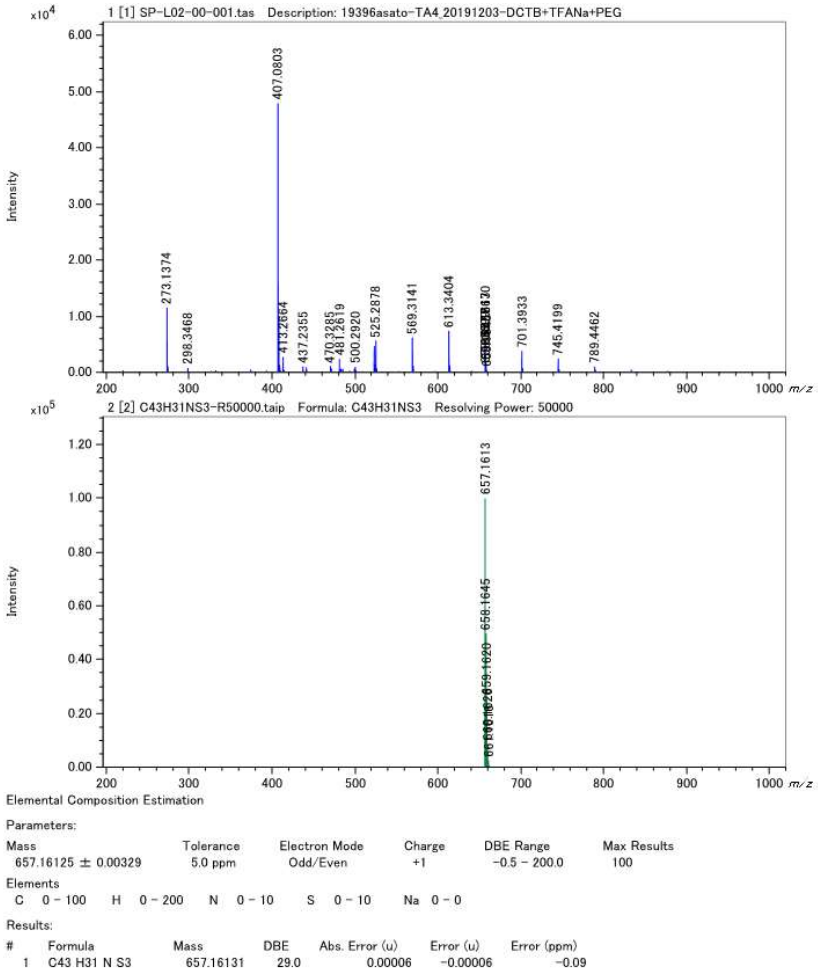

Figure 3-14 HR-MS data of **TA2o**. A MALDI Spiral TOF system (JEOL, JMS-S3000) was used with polyethylene glycol asinternal standard.

2-(2,4-dimethyl-5-phenylthiophen-3-yl)-4,4,5,5-tetramethyl-1,3,2-dioxaborolane (1):

4-bromo-2-phenylthiazole (694 mg, 2.9 mmol), 4,4,5,5-tetramethyl-2-(3,5-dimethyl-2-phenylthiophen-3-yl)-1,3,2-dioxaborolane (1.20 g, 3.2 mmol), PPh_3 (379 mg, 1.4 mmol.) and 2 M aqueous K_3PO_4 (10 mL) were dissolved in 1,4-dioxane (10 mL). After 15 minutes stirring under N_2 atmosphere, $Pd(PPh_3)_4$ (369 mg, 0.32 mmol.) was added and stirred under N_2 atmosphere at 110 °C for 72 h. Thereafter, the organic layer was extracted with chloroform, and the combined extracts were washed with water and dried over anhydrous Na_2SO_4. The sample was then filtered and the solution was concentrated in vacuo. Silica gel column chromatography (hexane:ethyl

acetate, 10:1) of the residue afforded **1** (582 mg, 58% yield) as a white solid. ^{1}H NMR (300 MHz, $CDCl_3$, 25 °C, TMS): δ = 8.07-7.92 (m, 3H), 7.49-7.27 (m, 7H), 7.19 (s, 1 H), 2.52 (s, 3H), 2.26 (s, 3H).

4-(2,4-dimethyl-5-phenylthiophen-3-yl)-5-(4-methyl-2,5-diphenylthiophen-3-yl)-2-phenylthiazole (TA3o)

1 (0.58 g, 1.6 mmol.), 3-bromo-4,5-dimethyl-2-phenylthiophene (593 mg, 1.8 mmol.), di‐*tert*‐butylmethylphosphine tetrafluoroborate (40 mg, 0.16 mmol.), Cs_2CO_3 (1.08 g, 3.3 mmol.), $Pd(OAc)_2$ (18 mg, 0.08 mmol.), and pivalic acid (51 mg, 0.5 mmol.) were dissolved in mesitylene (6 mL). The mixture was heated under reflux at 150 °C overnight. Thereafter, it was filtered through celite, extracted with ethyl acetate, and the combined extracts were washed with water and dried over anhydrous Na_2SO_4. Silica gel column chromatography (hexane:ethyl acetate, 9:1) and gel permeation chromatography afforded **TA3o** (98 mg, 10% yield) as a colorless powder. ^{1}H NMR (600 MHz, $CDCl_3$, 25 °C, TMS): δ = 8.04 (dd, J = 2.4 Hz, 8.0 Hz, 2 H), 7.54-7.45 (m, 7H), 7.40-7.28 (m, 6 H), 7.19-7.11 (m, 3H), 7.03-6.98 (m, 2H), 2.36 (s, 3 H), 1.84 (s, 3H), 1.59 (br-s, 1 H), 1.29 (br-s, 1 H) 0.87 (br-s, 1 H); ^{13}C NMR (151 MHz, $CDCl_3$, 25 °C, TMS): δ = 166.5, 150.4, 142.3, 138.5, 135.6, 134.8, 134.5, 134.2, 134.1, 130.4, 129.6, 129.5, 129.4, 129.3, 128.9, 128.8, 128.7, 128.0, 127.9, 127.2, 126.6, 31.0, 30.1, 15.6, 14.4, 14.1 ppm; HRMS (MALDI SpiralTOF): *m*/*z* calcd. for $C_{38}H_{29}NS_3^+$: 595.14566 [M^+]; found: 595.14529.

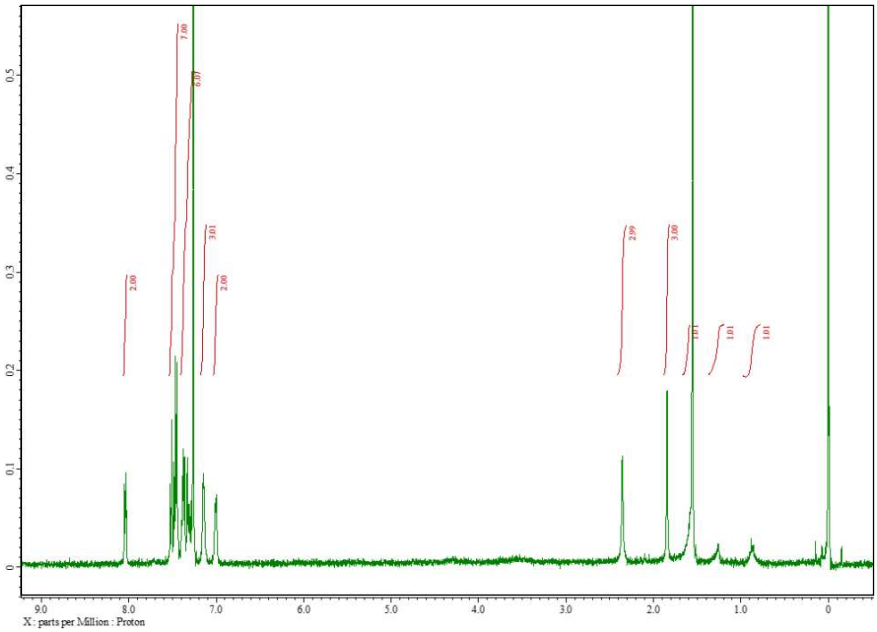

Figure 3-15 ^{1}H-NMR spectrum of **TA3o** (600 MHz, $CDCl_3$/TMS, 25 °C).

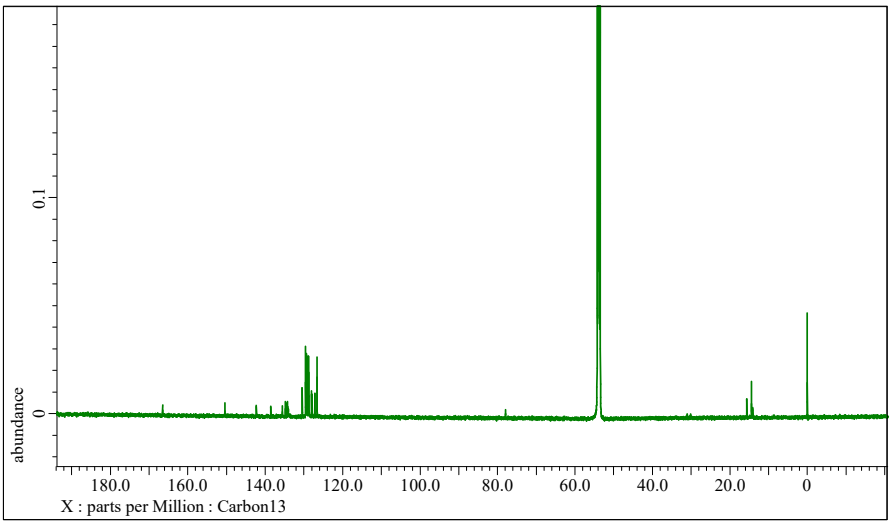

Figure 3-16 ^{13}C-NMR spectrum of **TA3o** (151 MHz, $CDCl_3$, 25 °C, TMS).

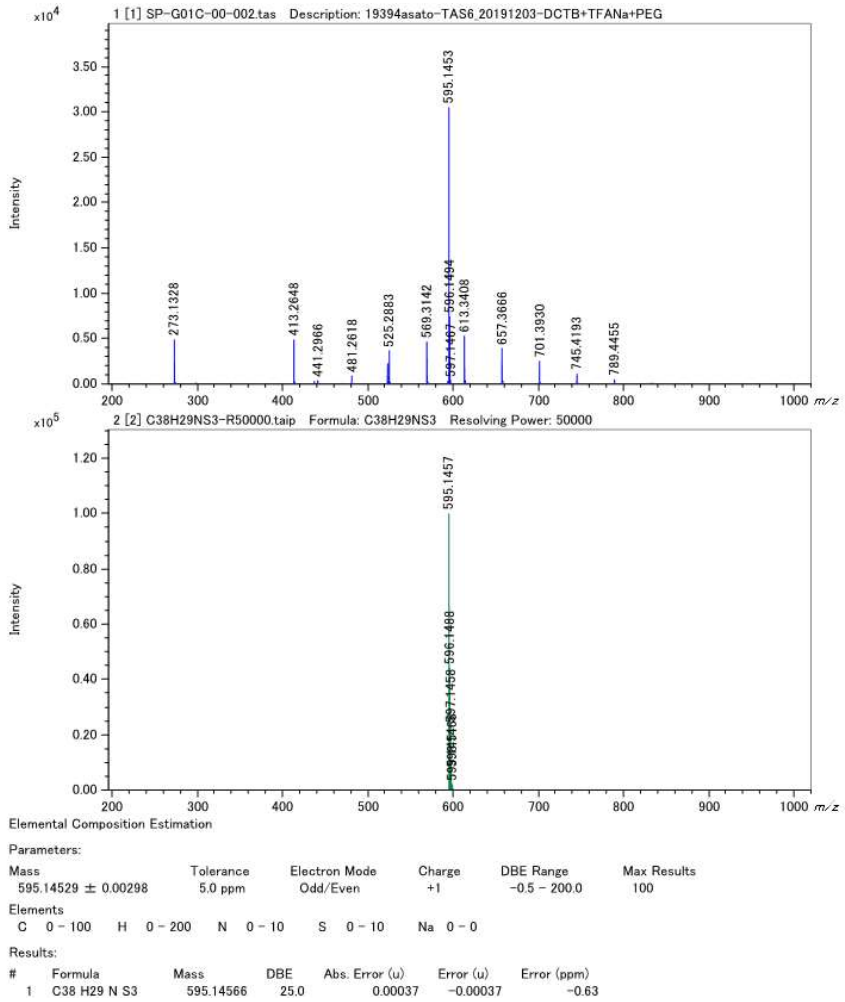

Figure 3-17 HR-MS data of **TA3o.** A MALDI Spiral TOF system (JEOL, JMS-S3000) was used with polyethylene glycol as an internal standard.

4-(4-methyl-2,5-diphenylthiophen-3-yl)-2-phenylthiazole (3-3):

4-bromo-2-phenylthiazole (1.07 g, 3.7 mmol), 4,4,5,5-tetramethyl-2-(4-methyl-2,5-diphenylthiophen-3-yl)-1,3,2-dioxaborolane (972 mg, 4.1 mmol), PPh_3 (547 mg, 1.9 mmol.) and 2 M aqueous K_3PO_4 (15 mL) were dissolved in 1,4-dioxane (15 mL). After 15 minutes stirring under N_2 atmosphere, $Pd(PPh_3)_4$ (427 mg, 0.37 mmol.) was added and the solution refluxed under N_2 atmosphere at 110 °C for 36 h. Thereafter, the organic layer was extracted with chloroform, and the combined extracts were washed with water and dried over anhydrous Na_2SO_4. The sample was then filtered and the filtrate concentrated in vacuo. Silica gel column chromatography (hexane:ethyl acetate, 20:1) of the residue afforded **3-3** (0.18 g, 23% yield) as a white solid. ^1H NMR (300 MHz, $CDCl_3$, 25 °C, TMS): δ= 8.07-8.02 (m, 3H), 7.49-7.30 (m, 12H), 7.18 (s, 1 H), 2.52 (s, 3H).

5-(2,4-dimethyl-5-phenylthiophen-3-yl)-4-(4-methyl-2,5-diphenylthiophen-3-yl)-2-phenylthiazole (TA4o):

2 (180 mg, 0.44 mmol), 3-bromo-2,4-dimethyl-5-phenylthiophene (141 mg, 0.53 mmol.), di‐*tert*‐butylmethylphosphine tetrafluoroborate (11 mg, 0.044 mmol.), Cs_2CO_3 (220 mg, 0.88 mmol), pivalic acid (14 mg, 0.13 mmol.) and $Pd(OAc)_2$ (4.9 mg, 0.022 mmol.) were dissolved in mesitylene (6 mL). The mixture was heated under reflux at 150 °C overnight. Thereafter, it was filtered through celite, extracted with ethyl acetate, and the combined extracts washed with water and dried over anhydrous Na_2SO_4. Silica gel column chromatography (hexane: ethyl acetate, 9:1) and gel permeation chromatography afforded TA4o (89.3 mg, 34% yield) as a white solid. ^1H NMR (400 MHz, $CDCl_3$, 25 °C, TMS): δ = 8.08 (d, J = 8.0 Hz, 2 H), 7.58-7.35 (m, 7 H), 7.21-7.03 (m, 6H) 7.00-6.95 (m, 3H), 6.99-6.26 (m, 2H), 2.39 (s, 3H), 1.87 (s, 1H), 1.66 (s, 1H), 1.54 (s, 3H), 1.44 (s, 1H); ^{13}C NMR (151 MHz, $CDCl_3$, 25 °C, TMS): δ = 134.9, 133.8, 133.1, 132.7, 130.1, 129.4, 128.7, 128.6, 128.5, 127.4, 127.3, 127.1, 126.5, 29.8, 15.2, 14.9, 14.7, 14.6, 14.1, 14.0 ppm; HRMS (MALDI SpiralTOF): *m/z* calcd. for $C_{38}H_{29}NS_3$: 595.14566 [M^+]; found:595.14511.

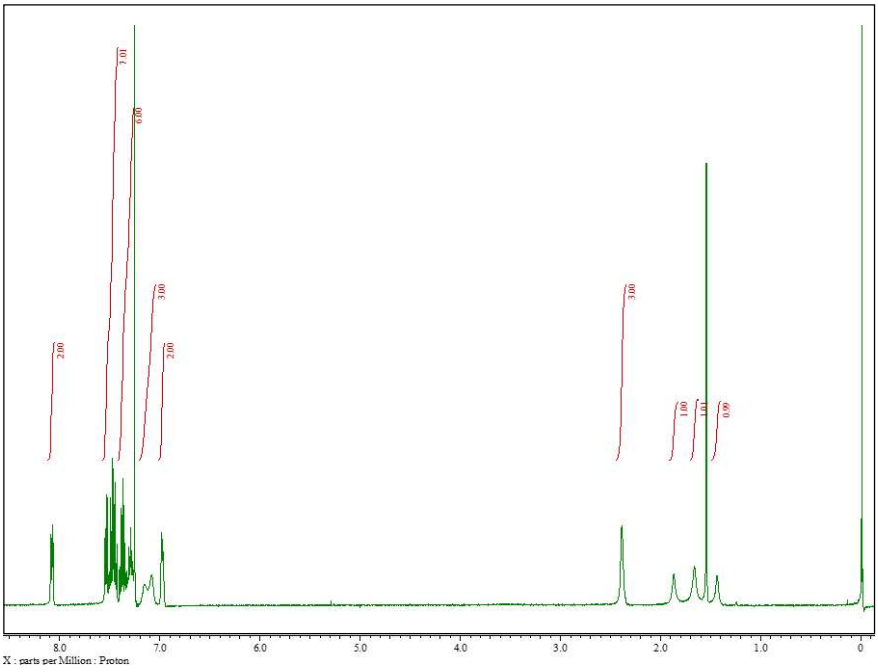

Figure 3-18 ^{1}H-NMR spectrum of **TA4o** (400 MHz, $CDCl_3$/TMS, 25 °C).

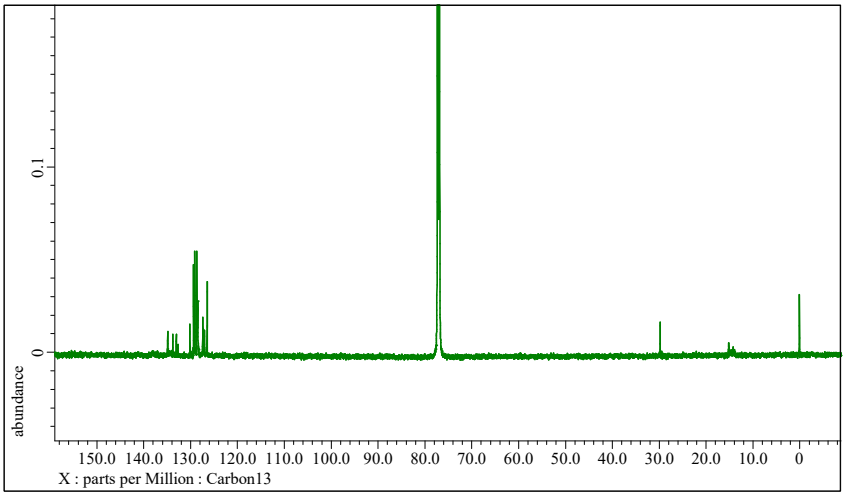

Figure 3-19 ^{13}C-NMR spectrum of **TA4o** (151 MHz, $CDCl_3$, 25 °C, TMS).

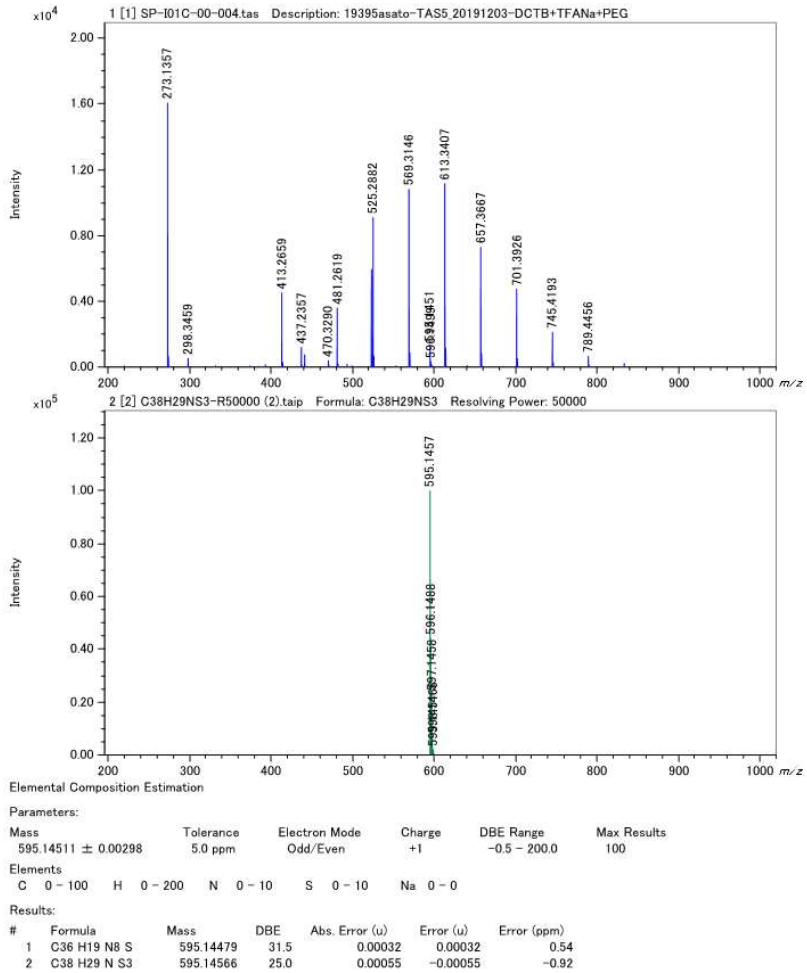

Figure 3-20 HR-MS data of **TA4o.** A MALDI Spiral TOF system (JEOL, JMS-S3000) was used with polyethylene glycol as an internal standard.

4. Control of Thermochemical properties of terarylene for molecular thermal energy storage

In this chapter, the study of thermo-chemical response with terarylene is reported. The results of an experimental and numerical study on terarylenes are presented as a new candidate as a molecular solar thermal (MOST) fuel, in which the previously reported synergetic cascade reaction further highlights their advantage for stimulated heat release. Especially the consideration of the relation between the activation energy (E_a) and energy difference between the photoisomers (ΔH_{iso}) provided knowledge about the thermo-chemical properties of terarylene and projection for the design of efficient MOST molecules. Besides, the high energy density of MOST fuel offers the potential for massive heat release, through the cycloreversion reaction via synergetic cascade reaction. Firstly, the critical factors for MOST efficiency estimation will be introduced in Section 4.1. Then, section 4.2 will present molecular design. Following the synthesis and characterization of the target molecule, the MOST efficiency is estimated in Session 4.3. The discussion was expanded to the relationship of activation energy for thermal stability and energy difference between the **c**- and **o**- forms (section 4.4). The heat release is finally demonstrated with the cascade reaction (section 4.5).

4.1 MOST efficiency

Previous works[120a-j] have proposed several requirements for efficient MOST materials, taking into consideration comparability with photovoltaics (see Chapter 1). Figure 4-1 illustrates an energy diagram typical of the MOST systems.

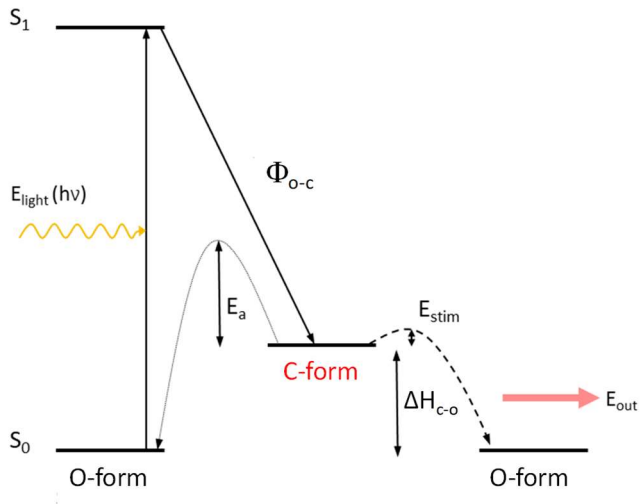

Figure 4-1 energy diagram in a MOST system.

To achieve high MOST efficiency, a number of parameters are optimized for photoresponsive fuel molecules as mentioned briefly. The MOST efficiency (η) can be estimated on the basis of the following equation:

$$\eta = \frac{E_{out}}{E_{in}} = \frac{\phi_{o-c}\Delta H_{c-o}}{E_{light} + E_{stim}} \quad (1)$$

where E_{out} and E_{in} are the output and sum of input energies respectively. The numerator is expressed by the product of ring-cyclization quantum yield (ϕ_{o-c}) and the enthalpy difference between the **o**- and **c**-form (ΔH_{c-o}). The denominator is then obtained as the sum of light radiation energy (E_{light}) and the energy for external stimulus (E_{stim}) to trigger the cycloreversion reaction for the release of stored energy (Figure 4-1).

The terarylenes, as described previously, exhibited a highly efficient cycloreversion reaction in a chain reaction manner through oxidation of metastable **c**-form. In other words, chemical potential of a single oxidant molecule is able to lead to the cycloreversion reaction of one thousand

molecules in the **c**-form. Therefore, the E_{stim} could be almost zero for the on-demand energy release through the oxidation, giving the following approximate expression.

$$\eta \approx \frac{\phi_{O-C}\Delta H_{c-o}}{E_{light}} \quad (2)$$

4.2 Molecular design of terarylene, Synthesis and Optical Properties

The **o**-form isomerizes to the **c**-form as they are exposed to UV light with a ring cyclization reaction in high quantum yield. They lose aromaticity on the side aromatic rings during the cyclization to the **c**-form. The aromatic stabilization operates selectively on the **o**-form, resulting in relatively large $\Delta H_{c\text{-}o}$.[19,104] That is, the $\Delta H_{c\text{-}o}$ is predominantly controlled and even tuned by the molecular design on the aromatic rings. The larger difference in the aromaticity of their **c** and **o** forms should enhance the $\Delta H_{c\text{-}o}$. Although the aromatic stability in five or six-membered rings has long been discussed, reported typical calculation method for the aromatic stabilization energy (ASE)[121,122] are summarized in table 4-1. On the other hand, Irie and co-workers estimated aromatic stabilization energy in the **o**-form against the **c**-form to investigate the effect on the thermal cycloreversion reactivity of diarylethene derivatives[13,19] (Figure 4-2).

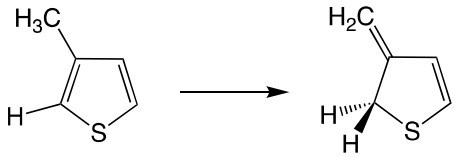

Figure 4-2 The loss of aromaticity of 3-methylthiophene The half-lifetimes of **TA2** upon cycloreversion.

Table 4-1 the aromatic stabilization energy[121,122]

Aromatic moiety	ASE / kcalmol^{-1}
fruran	12.3
thiazole	14.5
thiophene	15.6
pyridine	19.8
Benzene	21.5

naphthalene	47.3

This aromaticity consideration could be expanded further for terarylenes, which have an additional aromatic ring on the central bridge, making the $\Delta H_{c\text{-}o}$ larger and more tunable. In addition to these effects of aromatic rings, substituent groups at the reaction center carbon atoms such as isopropyl, phenyl, and cyclohexane groups enhances $\Delta H_{c\text{-}o}$ due to their steric effect, which destabilizes the **c**-form selectively.[104]

A series of terarylene derivatives with various combinations of substituted aromatic units were investigated as possible candidates for MOST applications (Figure 4-3). **TA1o** and **TA5o, TA7o** exhibited relatively high photocyclization quantum yields ($\phi_{o\text{-}c}$) over 58% in hexane. Intramolecular non-covalent interactions such as N-H, S-H and S-N interactions operating between the central and side aromatic units were considered to selectively stabilize the photochromic active conformation around the 6π-system, achieving the photon-quantitative cyclization reactivity for **TA7o**.[30,31,114] Phenyl groups were then introduced at the reactive carbon atoms to form **TA2o, TA4o, TA6o** and **TA8o**, enhancing $\Delta H_{c\text{-}o}$ by decreasing the relative stability of **c**-form with the steric effect of the bulky substituents.

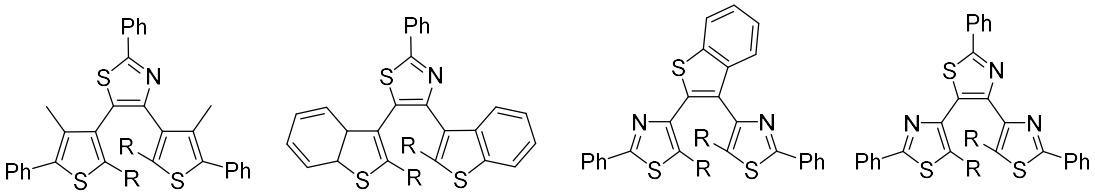

Figure 4-3 Target molecules for enhancement of MOST efficiency.

4.2.1 Synthesis

TA6o and **TA8o** were prepared according to the route depicted in Scheme **4-1** and Scheme **4-2**. Compounds **3-1** and **3-2** were prepared in Chapter 3 and compound **4-1** was commercially available. Compound **4-3** was synthesized as previously reported.[31] The structures have all been successfully characterized using NMR and MS spectral methods. The experimental detail and all NMR and MS spectral are in experimental section 4.7.

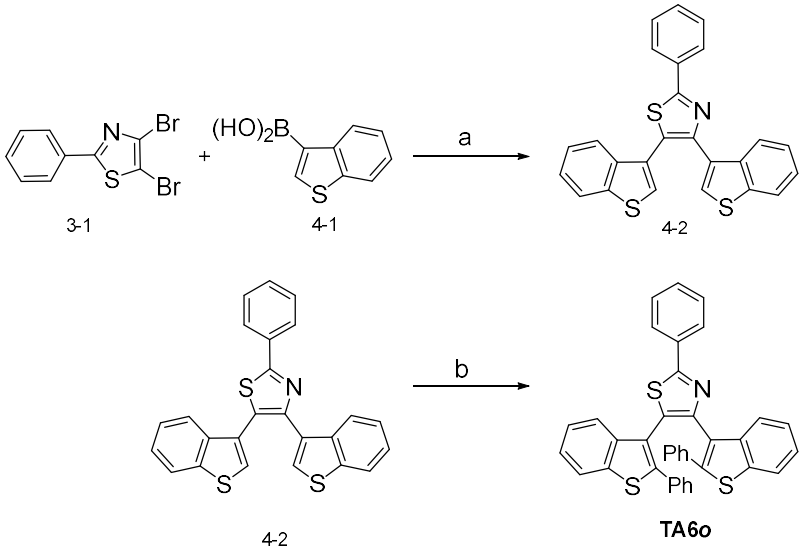

Scheme 4-1. Synthesis of **TA6*o***: a) $[Pd(PPh_3)_4]$, PPh_3, 2 M K_3PO_4, water/1,4-dioxane, THF; b) Phenylboronic acid, $(^tBu)_2PMeHBF_4$, pivalic acid, Cs_2CO_3, $Pd(OAc)_2$.

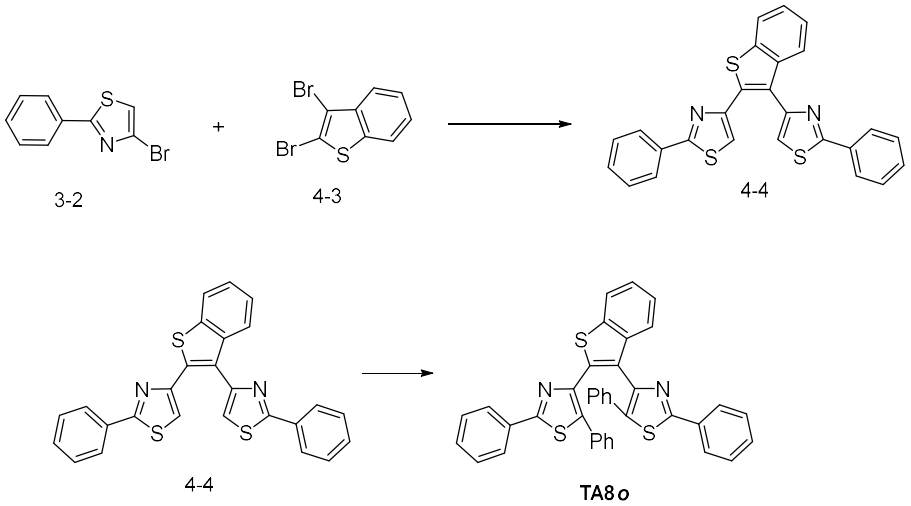

Scheme 4-2. Synthesis of **TA8*o***: a) $[Pd(PPh_3)_4]$, PPh_3, 2 M K_3PO_4, water/1,4-dioxane, THF; b) Phenylboronic acid, $(^tBu)_2PMeHBF_4$, pivalic acid, Cs_2CO_3, $Pd(OAc)_2$.

4.2.2 Optical property measurement

Table 4-2 summarizes the optical and photochemical properties of the eight compounds. Upon illumination with UV light (365 nm), acetonitrile solutions of the **o**-form of all compounds turn blue or red, indicating photocyclization to the **c**-form. The **o**-forms of terarylenes showed strong

light absorption in the UV region below 400 nm with high absorption coefficients over 10^4 $M^{-1}cm^{-1}$ at wavelength of maximum absorbance ($\lambda_{o,\,max}$).

Table 4-2 Optical and photochemical properties

	o–$\lambda_{o,\,max}$ / nm (ε)[a]	$\phi_{o\text{-}c}$ [b]	$t_{1/2}$ (s) [c]
TA1o	313(2.20)	0.61	1.2 x 10^6
TA2o	294(3.12)	–	56
TA5o	273(2.21)	0.76	4.7 x 10^7
TA6o	249(2.20 [d])	0.57	1.4 x 10^7
TA7o[e]	307(2.9)	0.98	1.9 x 10^8
TA8o	303 (2.8)	0.63	2.6 x 10^6
TA9o[f]	327(3.21)	0.4	1.0 x 10^8
TA10o[f]	327 (3.40)	0.12	1.2 x 10^7

All measurements reported in acetonitrile unless otherwise specified. [a] $\boldsymbol{\varepsilon}$ in 10^4 $M^{-1}cm^{-1}$; [b] The cycloreversion quantum yield were estimatied using an absolute photoreaction quantum yield evaluation system.[118] ; [c] measured in hexane; [d] ε was estimated at 313 nm, measured in hexane; [e] data from ref.[31], measured in hexane; [f] data from ref.[40];

The effect of the phenyl substituents on the reactive carbon atoms was almost negligible in the absorption onset for the **o**-forms, probably because of the free rotation over the side-aryl-phenyl bonds disrupting the effective π-conjugation, while the additional aromatic rings enhanced the light absorptivity in the UV region. The UV-vis spectral changes of newly synthesized compounds **TA6** and **TA8** are shown in Figure 4-4. (see also Chapter 3 Figure 3-12 about **TA1**, **TA2** and **TA5**)

The introduction of phenyl rings on the reactive carbon atoms was found to reduce the photocyclization reactivity ($\phi_{o\text{-}c}$) as well as the half-lifetimes of the **c**-forms. The introduction of bulky substituents on the reactive carbon atoms should interrupt the stabilization of the photoreactive conformation, leading to the suppressed $\phi_{o\text{-}c}$ values. The bulky substituents at these positions were also reported to have an effect on accelerating the thermal cycloreversion reaction due to their steric effect on the planar fused ring of the **c**-forms. However, it should be noted that the $\phi_{o\text{-}c}$ values around 0.6 for **TA6** and **TA8** are still remarkable for ordinary diarylethene derivatives and much more efficient compared to those of azobenzene and norbornadiene systems. The half-life time over 10^6 s (> 10 days) also seems to be enough for the practical use of **TA6** and **TA8** in heat storage. Terthiazole based **TA9** and **TA10** gave a relatively small $\phi_{o\text{-}c}$ values due to the preferential adoption of photochromic inactive conformation.[40] The half-lifetimes of **TA2** which is l56 s may be too short for the MOST application.

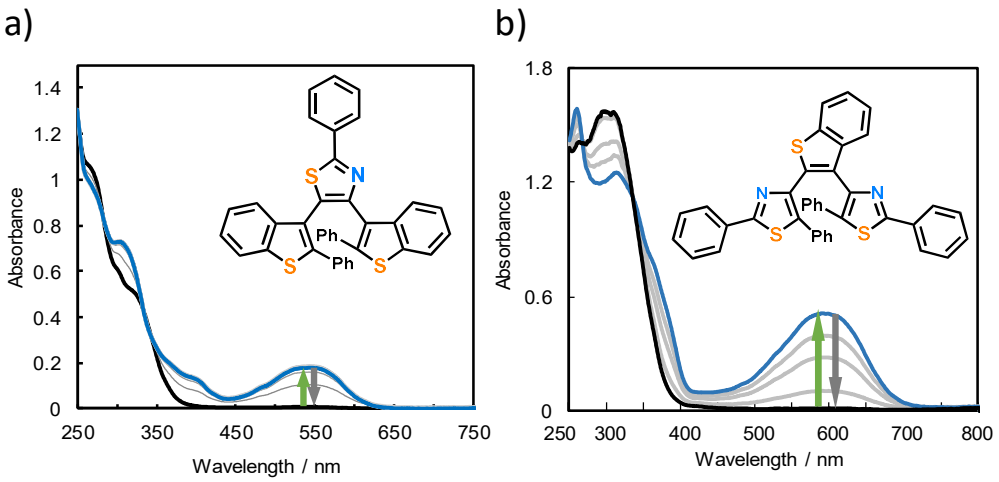

Figure 4-4 Spectral changes of a) **TA6**; b) **TA8** upon irradiation with UV light at 365 nm in acetonitrile. Each spectrum was taken after irradiation for 30 s. Visible light irradiation turns them back to the **o**-form. Concentration of **o**-form = a) 2.8 x 10^{-5} M; b) 5.3 x 10^{-5} M.

4.3.2 DFT calculations for $\Delta H_{c\text{-}o}$ and estimation of MOST

In estimation of MOST efficiency, the energy of photon at 380 nm (315 kJ mol^{-1}) to activate the photoresponsive molecules was assumed. $\Delta H_{c\text{-}o}$ was computationally estimated based on the

density functional theory (DFT) calculations using the B3LYP functional with the 6-31G(d) basis set. Table 2 summarizes the simulated $\Delta H_{c\text{-}o}$ and η values for terarylene derivatives.

Table 4-3 Summary of DFT calculations and theoretical MOST efficiency

	$\Delta H_{c\text{-}o}$ [a] / kJ mol^{-1}	Eff[b] / %
TA1	98.3	19
TA2	165	---
TA5	76.7	20
TA6	136	26
TA7	74.3	23
TA8	129	27
TA9	86.9	8.8
TA10	143	11
Ref 1	55	6.6
Ref 2	74	11

[a] data from DFT calculation B3LYP/6-31G(d); [b] calculation from Eq 2, irradiation at 380 nm t = 2.88 x 10^4 / s (8 hours), r.t. The quantum yield was refer to Table 4-2; [c] data from ref.[13] data from ref.

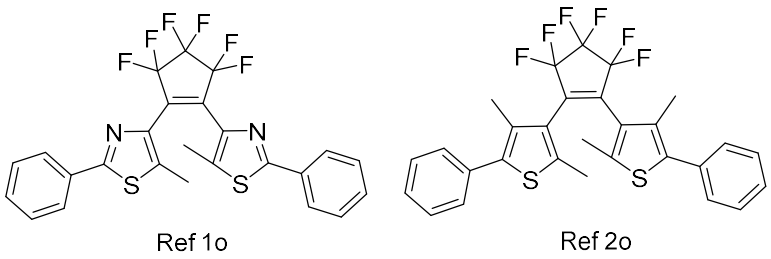

Figure 4-5 Target molecules for enhancement of MOST efficiency.

Compounds **TA5**, **TA7** and **TA9** composed of benzo[*b*]thiophene and thiazole units with less aromatic stabilization energy than thiophene gave the smaller $\Delta H_{c\text{-}o}$ values than **TA1** having two thiophene rings. The DFT calculation result indicated that the introduction of phenyl groups at the reactive carbon atoms enhanced the $\Delta H_{c\text{-}o}$ value by approximately 60 kJ mol^{-1}. Since these

phenyl substituents are not involved in the photochemical reaction, they do not contribute to the change in the aromaticity between the **o**-form and **c**-form. Therefore, these phenyl groups are considered to destabilize the **c**-form selectively through their steric effect on the planer fused rings. Values of η at a single wavelength of 380 nm were then calculated based on the results of DFT and optical measurements.

In an ideal system where the effect of the thermal cycloreversion can be ignored, the estimated maximum MOST efficiency was as high as 26.6% for **TA8** with a dithiazolylbenzo[*b*]thiophene framework. This value is surprisingly high compared to the previous typical values reported for norbornadiene and azobenzene based substances. For the typical diarylethene molecules **Ref 1**, **Ref 2** (Figure 4-5), η was estimated to 6.6%, 11% with similar procedure. These values are much less than the terarylene. The simulation study thus supports the advantage of terarylene for MOST technology.

4.4 Thermal stability and practical $\Delta H_{c\text{-}o}$ for high MOST efficiency.

4.4.1 The kinetics of the non-photochemical cycloreversion reaction

The kinetic of thermal cycloreversion reaction from the **c**-form o-form is of importance in the storage of solar energy for a practical time range. The activation barrier (E_a) from **c**-form to **o**-forms is a critical parameter to extrapolate the storage performance of MOST-active molecules.

The E_a values for **TA1**, **TA2**, **TA5**, **TA6** and **TA8** were estimated by means of the Arrhenius relationship of temperature-dependent cycloreversion kinetics (Figure 4-6 and also see Table 4-4 for the parameters of thermal cycloreversion reaction for all compounds including previously reported compounds).

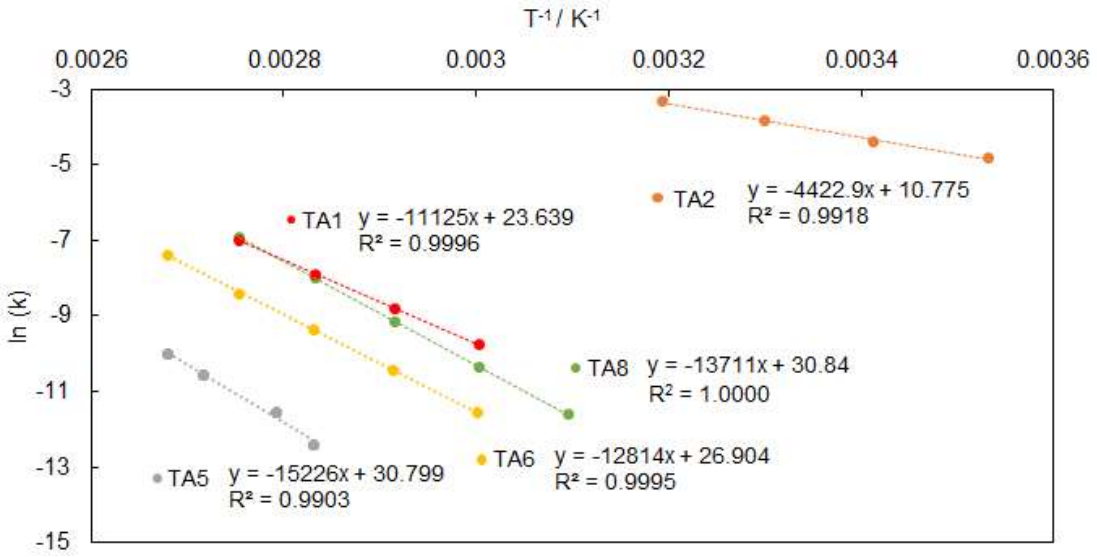

Figure 4-6 Arrhenius plots non-photochemical thermal of **c**-**o** conversion of **TA1**, **TA2**, **TA5**, **TA6** and **TA8**. Kinetic analyses for non-photochemical thermal conversion of **c**-**o** form. Solutions of each compound in toluene were heated to varying temperatures and spectra were recorded at different time intervals to yield the Arrhenius plot of thermal cycloreversion reaction.

Table 4-4 Half-lifetime of **c**-form via non-photochemical cycloreversion reaction and the ratio of remaining species (T)

	k / s^{-1} [a]	$Ea_{c\text{-}o}$ /kJ mol^{-1} [b]	A / s^{-1} [b]
TA1	6.5 x 10^{-7}	92	1.6 x 10^{10}
TA2	1.2 x 10^{-2}	37	4.3 x 10^{4}
TA5	1.0 x 10^{-8}	127	1.4 x 10^{8}
TA6	5.1 x 10^{-8}	106	4.8 x 10^{11}
TA7[c]	2.9 x 10^{-10}	137	5.3 x 10^{15}
TA8	3.8 x 10^{-7}	114	2.5 x 10^{13}
TA9[d]	5.8 x 10^{-4}	112	5.2 x 10^{16}
TA10[d]	4.9 x 10^{-3}	104	1.7 x 10^{26}

All measurements reported in toluene unless otherwise specified. [a] rate constant of a first-order decay at 20 °C; [b] the parameters of thermal cycloreversion reaction by means of Arrhenius relationship of temperature-dependent cycloreversion kinetics following Arrhenius's equation: $\ln k = \ln A - \frac{Ea}{RT}$ [c] data from Ref.[31]; [d] data from Ref.[40]

It is also possible that there is a correlation between the E_a and $\Delta H_{c\text{-}o}$ values considering Hammond's postulate. Figure 4-7 summarizes the plots of experimentally obtained E_a as a function of calculated $\Delta H_{c\text{-}o}$ values for **TA1**, **TA2** and **TA5-TA10**. The plots clearly demonstrate the trade-off relationship between the E_a and $\Delta H_{c\text{-}o}$ values. Furthermore, the plots are divided into two groups, in which the substituents on the reactive carbon atoms mark the difference. The plot for **TA1**, **TA5**, **TA7** and **TA9** showed a clear relationship with the slope of about –2.

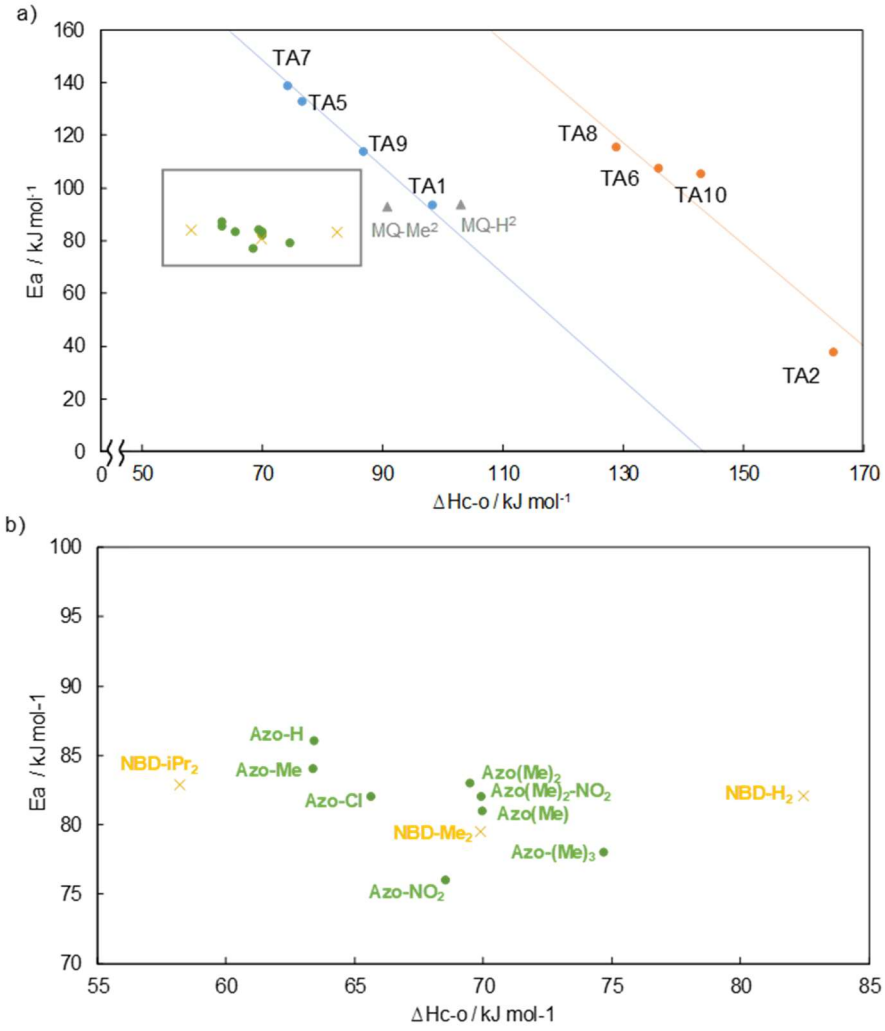

Figure 4-7 a) The plots of activation energy against $\Delta H_{c\text{-}o}$ for each compound. The data is from Table 4-3, 4-4. The molecular structure of reference data is described in Figure 4-8. ΔH_{iso} of references azobenzene derivatives are calculated as same method as table 4-2 using the B3LYP functional with the 6-31G(d) basis set. The reference data is from Ref.[44a,123] b) Enlarged view of Figure 4-7a.

Similar linear relationship on E_a-$\Delta H_{c\text{-}o}$ values was also observed for the phenyl-derivatives **TA2**, **TA6**, **TA8** and **TA10** with a similar slope of –2. This tendency may be explained based on the general principle of Linear-Freee Eneargy Relationship (LFER). The series of **TA1**, **TA5**, **TA7** and **TA9** have a same molecular framework of **TA2**, **TA6**, **TA8** and **TA10**, respectively. The substituents on the reactive carbon atoms are not involved in the photoconversion reactions. Therefore, the sum of aromatic stabilization energy of three aryl units in the terarylene framework might determine this E_a-$\Delta H_{c\text{-}o}$ relationship. In other words, the slope may be unique to the 6π-electrocyclization reaction system based on the present terarylene framework. The introduction of phenyl rings on the reactive carbon atoms did not change the slope but induced a parallel displacement of linear plot toward the lower-right direction. The phenyl substituents also increased $\Delta H_{c\text{-}o}$ and slightly decreased E_a. This clear trade-off relationship could be attributed to the nature of 6π-based reactions, which is likely a undesirable property for MOST-active molecules. A slight increase in the $\Delta H_{c\text{-}o}$ could lead to a remarkable decrease in E_a and decrease in the heat-storage capability. Meanwhile, from a viewpoint of MOST performance, the molecules with both high E_a and $\Delta H_{c\text{-}o}$ are desirable.

I explored over previous reports and delivers here reference data reported on azobenzene[44a] and norbornadiene derivatives.[123] Although both the photoresponsive scaffolds gave a less prominent E_a-$\Delta H_{c\text{-}o}$ relationship than that of terarylene derivatives, most of latter compounds displayed the better records both in E_a and $\Delta H_{c\text{-}o}$, suggesting the inherently superior characteristics of terarylenes for application in MOST.

a)

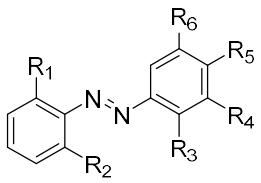

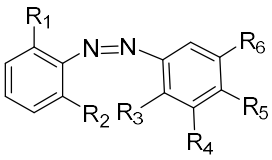

(E)-azobenzene derivatives

(Z)-azobenzene derivatives

	R_1	R_2	R_3	R_4	R_5	R_6
Azo-H	H	H	H	H	H	H
Azo-Me	H	H	H	H	Me	H
Azo-Cl	H	H	H	H	Cl	H
Azo-NO_2	H	H	H	NO_2	H	H
Azo$(Me)_2$	Me	H	Me	H	H	H
Azo$(Me)_2$-NO_2	Me	H	Me	H	H	NO_2
Azo(Me)	Me	H	H	H	H	H
Azo$(Me)_3$	Me	Me	Me	H	H	H

b)

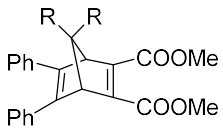

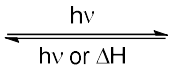

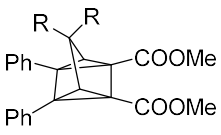

Norbornadiene derivatives (NBD-R_2)

Quadricyclane

	R
NBD-H_2	H
NBD-Me_2	Me
NBD-iPr_2	iPr
NBD-tBu_2	tBu

c)

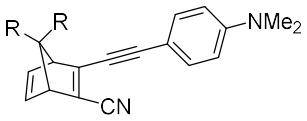

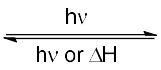

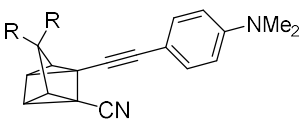

MQ-R_2

	R
MQ-H_2	H
MQ-Me_2	H

Figure 4-8 The molecular structure of reference data for a) azobenzene derivatives,[44a] b) Norbornadiene derivatives,[123] c) MQ-R_2 series.[123]

4.4.2 DSC measurement and estimation of actual MOST efficiency

I and coworkers then measured the $\Delta H_{c\text{-}o}$ value experimentally by means of differential scanning calorimetry (DSC). Compounds **TA1**, **TA5**, **TA6**, **TA7** and **TA8** with the relatively high $\phi_{o\text{-}c}$ and reasonable thermal stability were chosen for the DSC measurement as the promising candidate for the MOST application. The heating scan of the samples containing a considerable amount of the **c**-form induced a thermal cycloreversion reaction, releasing heat (Figure 4-9). The

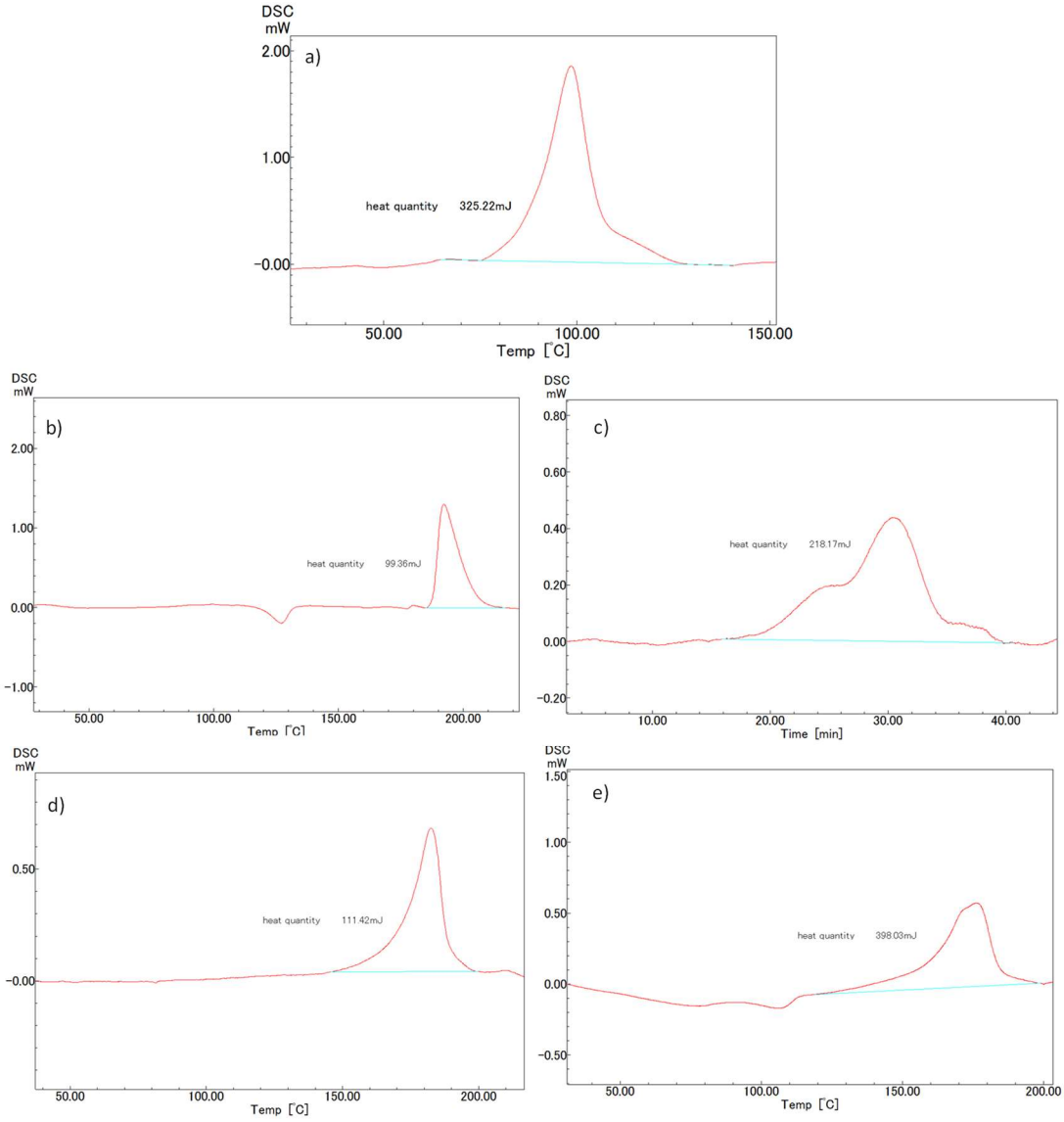

Figure 4-9 DSC of a) **TA1c/o**, b) **TA5c/o**, c) **TA6c/o**, d) **TA7c/o**, e) **TA8c/o**. The scan speed and the packed mass of powder in the DSC holder are a) 5 °C / min and 4.0 mg, b) 5 °C / min and 2.4 mg, c) 8 °C / min and 2.5 mg, d) 5 °C / min and 3.1 mg, e) 5 °C / min and 3.2 mg

released heat was detected as an exothermic peak in the DCS thermograms. The successive second scan gave no such exothermic peak for all samples, suggesting the observed exothermic peak correspond to the heat emission originating the thermal cycloreversion reaction of the **c**-form. From the peak integral and the content of **c**-form the $\Delta H_{c\text{-}o}$ values were estimated. These experimentally estimated values were smaller than the simulated ones based on the DFT calculation. Since the cycloreversion reaction of **c**-form does not take place in a cooperative manner unlike a phase transition such as melting, the exothermic peaks may not necessarily reflect the cycloreversion reaction of all the **c**-form molecules. The cycloreversion reaction of a non-negligible portion of **c**-form forms may be buried in the baseline noise of DCS thermograms. The net efficiency (η) of MOST was then estimated on the basis of these experimental $\Delta H_{c\text{-}o}$ values. Even with the underestimated values of $\Delta H_{c\text{-}o}$, those tested molecules afforded prominent η as high as 23%.

Table 4-5 Summary of DSC measurement

	Heat quantity[a] / mJ g^{-1}	Conversion rate of **c**-form[b]	$\Delta H_{c\text{-}o,measured}$[c] ($\Delta H_{c\text{-}o,theory}$)[d] / kJ mol^{-1}	Eff[e]/ %
TA1	81.3	0.62	70.6 (98.3)	13
TA5	41.4	0.58	32.7 (76.7)	8.3
TA6	87.3	0.45	114 (136)	22
TA7	35.9	0.70	24.8 (74.3)	7.7
TA8	124	0.69	109.6 (129)	23

[a] data are estimated by the integration for the peak of heat release in DSC measurement with a mass of each compound. [b] data are estimated using UV-vis spectrum by comparing of the **o**/**c** form of mixture powder dissolved in acetonitrile and the o-form induced by irradiation of visible light. [c] data are estimated with conversion rate of **c**-form. [d] data is from Table 4-3 [e] data is estimated by Eq 2.

4.5 Energy release via oxidative cascade reaction.

The release of stored energy in the terarylene-based MOST system is also possible to induce by the oxidative cycloreversion reaction, proceeding in a chain-reaction manner. The heat release demonstration was therefore performed by the addition of a small amount of chemical oxidant, Tris(4-bromophenyl)ammoniumyl hexachloroantimonate (TBPA), to a solution containing the **c**-form of **TA1** as previous report.[124] The surface temperature of the acetonitrile solution of **TA1** containing **c**-form (5.0 x 10^{-2} mM) was monitored by a thermography. As shown in Figure 5, after the addition of 5 mol%-equivalents of oxidant the solution temperature increased by 3 °C.

The temperature change was monitored continually using a thermocouple thermometer (Figure 4-10). The addition of the oxidant induced the heat release, with increase temperature from 27 °C to 30 °C. The temperature was kept for around 10 seconds at 30 °C, which seems to be at the

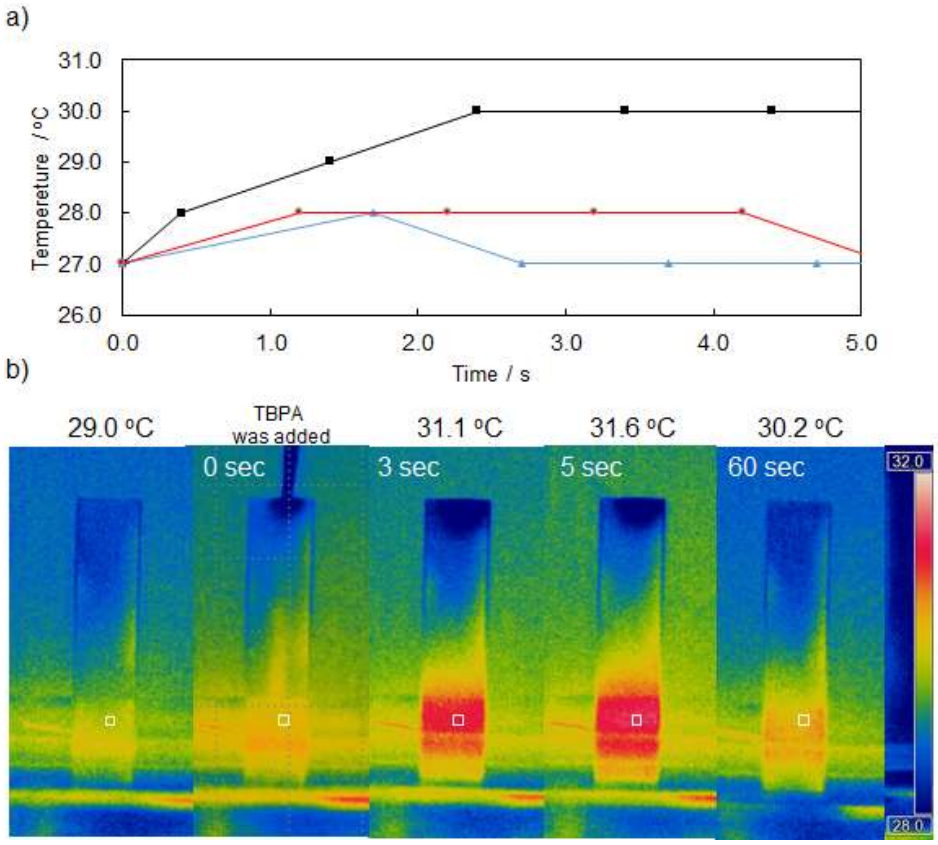

Figure 4-10 a) Temperature increase after adding 5 mol% of TBPA in acetonitrile (0.05 mL). Concentration of **c**-form = 5.0 x 10^{-2} M. b) Thermographic images after adding the TBPA in the same condition as Figure 4-10a.

balance between cooling by the air and the heat release. The change of the temperature was rather low because of the small energy density in comparison with the heat flow with the external environment. The concentration of the solution should be increased for future practical investigation. The ideal temperature increase calculated from the heat capacity of the solvent is 2.9 °C in this concentration of the **c**-form. The heating effect of initial oxidation is much smaller than the heat release by the **c**-form thanks to the cascade reaction capability. Electrochemical oxidation stimulation is expected to be used in future practical systems, which should be a subject of the next step of study. The present results indicate the possibility of efficient heat release through the oxidation cascade reaction system.

4.6 conclusion

Thermo-chemical response of the molecules toward molecular solar thermal storage and electro-chemical synergetic response inducing heat release is studied for eight targets, including two new compounds. Designs of terarylene framework in which the central ethene unit of diarylethene was replaced with another aromatic ring contributes to the efficiency by two major factors. One is the quantum yield of photoconversion related to the efficient use of photon energy. The other is an energy difference between the photoisomers (ΔH_{iso}) having a direct correlation with the amount of storage and released energy.

Intramolecular non-covalent interactions involving heteroatoms such as N-H, S-H and S-N interactions operating between the central and side aromatic units were reported to selectively stabilize the photochromic active conformation around the 6π-system. The target molecues of **TA7** achieving photon-quantitative cyclization reactivity. **TA1**, **TA5**, **TA7** and **TA8** achieved much larger $\phi_{o\text{-}c}$ values over 0.6 compared to the ordinary diarylethene derivatives and more efficient compared to those of azobenzene and norbonadiene systems. The $\Delta H_{c\text{-}o}$ stems from the loss of aromaticity in two or three aryl units constituting the diarylethene or terarylene framework upon the photoisomerization from **o**-form to **c**-form. The benzothiophene and thiophene as the aryl moiety and phenyl rings as bulky substituents at reactive carbon atoms resulted in the control of computationally estimated energy difference between **o**-form and **c**-form. In an ideal system where the effect of the thermal cycloreversion can be ignored, both deliberate approaches achieved the

estimated maximum MOST efficiency as high as 26.6% for **TA8**. We then measured the $\Delta H_{c\text{-}o}$ value experimentally by means of differential scanning calorimetry, resulting in prominent η as high as 23% for **TA8** compared with the other MOST molecules.

Meanwhile, in the general physicochemical consideration, the well-known Hammond's postulate implies the trade-off relation between the activation energy (E_a) and ΔH_{iso}. This fact has suggested the intrinsic difficulty to simultaneously achieve both the large ΔH_{iso} and high thermal stability for the practical MOST materials. The experimentally obtained E_a clearly demonstrate the trade-off relationship against $\Delta H_{c\text{-}o}$ values, suggesting the sum of aromatic stabilization energy of three aryl units in the terarylene framework might determine this E_a-$\Delta H_{c\text{-}o}$ relationship. The E_a-$\Delta H_{c\text{-}o}$ relationship clearly distinguishes the substances into two groups, with methyl and phenyl groups at the reactive carbon atoms. The introduction of phenyl rings on the reactive carbon atoms did not change the slope but introduced a parallel displacement of linear plots in the direction of low-right. This likely stems from non-involved substituent effect in the aromatic-non-aromatic photoconversion. The desirable molecules with both high E_a and $\Delta H_{c\text{-}o}$ for the application in MOST are achieved by means of inherent characteristics of terarylenes.

4.7 Experimental

General

General

^{1}H and ^{13}C NMR (300, 400, and 600 MHz) spectra were recorded on JEOL JNM-AL300, JEOL JNM-ECP400, and JEOL JNMECA600 spectrometers, respectively. Reversed-phase HPLC separation was performed with a LaChrom Elite apparatus (Hitachi). Mass spectrometry and high-resolution mass spectrometry were performed on JEOL JMS-Q1000TD and JMS-700 MStation JMS-S3000 spectrometers, respectively. UV/Vis spectra, quantum yields of photochromic reactions (ϕc-o and ϕo-c) and photo-induced fading reaction were measured using a JASCO V-660, V-760 spectrophotometer and a Shimadzu QYM-01 set-up, respectively. For kinetic thermal analyses, the temperature was controlled by a JASCO ETC 505 T temperature controller. Stopped-flow measurements were conducted with a rapid-scan stopped-flow spectroscopic system (Unisoku).

Oxidative cycloreversion experiments

Oxidative cycloreversion experiments were performed by mixing the requisite amounts of the oxidising agent tris(4-bromophenyl)ammonium hexachloroantimonate with the closed forms of 1, 3, 4 and 5 in acetonitrile and monitoring the evolution of absorbance at λmax, with constant stirring to avoid the effect of diffusion on the electron transfer.

Synthesis

TA6o and **TA8o** were prepared according to the route depicted in Scheme **4-1** and Scheme **4-2**. Compounds **3-1** and **3-2** were prepared in Chapter 3 and compound **4-1** was commercially available. Compound **4-3** was synthesized as previously reported.[31] The structures have all been successfully characterized using NMR and MS spectral methods.

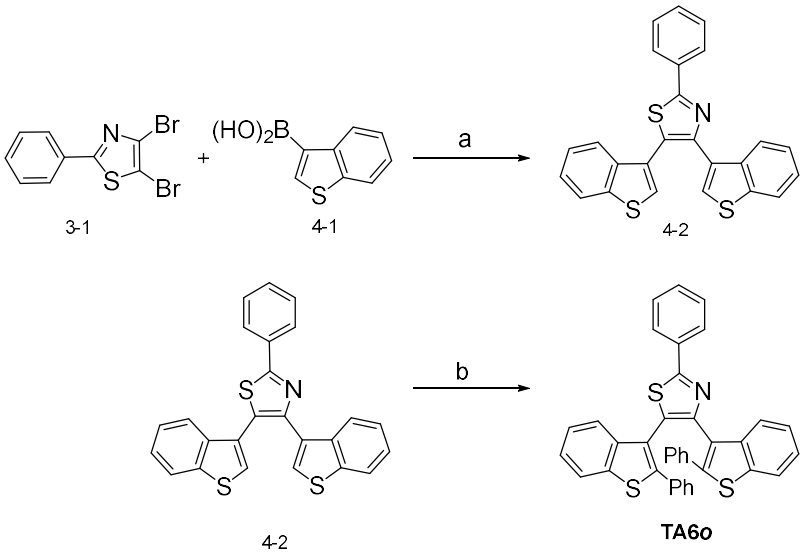

Scheme 4-1. Synthesis of **TA6*o***: a) [$Pd(PPh_3)_4$], PPh_3, 2 M K_3PO_4, water/1,4-dioxane, THF; b) Phenylboronic acid, ($^tBu)_2PMeHBF_4$, pivalic acid, Cs_2CO_3, $Pd(OAc)_2$.

4,5-bis(benzothiophen-3-yl)-2-phenylthiazole (**4-2**) A A two-necked flask was charged with 4,5-dibromo-2-phenylthiazole (**3-1**) (0.48 g, 2.0 mmol), benzothiophen-3-ylboronic acid (**3-2**) (1.28 g, 4.4 mmol), PPh_3 (0.26 g, 1.0 mmol) and 2 M aqueous K_3PO_4 (15 mL) in 1,4-dioxane (15 mL). After 15 minutes of stirring under N_2 atmosphere, $Pd(PPh_3)_4$ (0.34 g, 0.2 mmol) was added and stirred under N_2 atmosphere at 110 °C for 24 hours. After that, The organic layer was then extracted with chloroform, and the combined extracts were washed with water and dried over anhydrous sodium sulfate. The sample was then filtered, and the filtrate was concentrated in vacuo. Gel Permeation Chromatography (chloroform) afforded 4,5-bis(benzothiophen-3-yl)-2-phenylthiazole (**4-2**) as a white powder (0.59 g, 1.3 mmol, 65% yield). ^{1}H-NMR (300 MHz, $CDCl_3$, TMS/25 °C) δ (ppm) 7.42-7.50 (m, 7H), 7.81 (s, 2H), 7.86-8.18 (m 6H), HR-MS (MALDI-TOF): *m*/*z* calcd for $C_{37}H_{23}NS_3$ $[M]^+$: 657.168; found 657.149

4,5-Bis(2,5-diphenylthiazol-4-yl)-2-phenylthiazole (**TA6o**): A two-necked flask was charged with 4,5-bis(benzothiophen-3-yl)-2-phenylthiazole (**4-2**) (0.10 g, 0.23 mmol), bromobenzene (0.08 g, 0.51 mmol), di-*tert*-butylmethylphosphine tetrafluoroborate (0.011 g, 0.046 mmol), Cs_2CO_3 (0.30 g, 0.92 mmol), $Pd(OAc)_2$ (0.10 g, 0.046 mmol) and pivalic acid (0.011 g, 0.11 mmol) in mesitylene (2 mL). The mixture was heated under reflux at 150 °C for 16 hours.

Thereafter, it was filtered through celite, extracted with ethyl acetate, and the combined extracts were washed with water and dried over anhydrous sodium sulfate. Gel Permeation Chromatography (chloroform) afforded **TA6o** (0.019 g, 0.032 mmol, 14% yield) as a colorless powder. ^{1}H-NMR (600 MHz, $CDCl_3$, TMS/25 ºC) δ (ppm) 8.16 (d, J = 6.2 Hz, 2H), 7.60 (dd, J = 18.9, 7.9 Hz, 2H), 7.51 (dt, J = 18.6, 7.2 Hz, 3H), 7.33 (s, broad, 1H), 7.25 (s, 1H), 7.21-7.15 (m, 2H), 7.09 (m, 2H), 6.88 (d, J = 8.2 Hz, 2H), 6.84 (d, J = 8.2 Hz, 2H), 6.69 (s broad, 4H), 6.53 (s broad, 2H); ^{13}C NMR (151 MHz, CD_2Cl_2, TMS/25 ºC) δ = 167.0, 149.0, 143.1, 139.8, 139.5, 139.1, 138.9, 134.1, 133.8, 133.3, 130.6, 129.4, 129.0, 128.2, 128.2, 127.9, 127.8, 126.7, 124.7, 124.5, 124.3, 124.2, 124.0, 123.4, 122.2, 121.8, 121.5, 54.2, 54.0, 53.8, 53.6, 53.4 ppm; HR-MS (ESI): m/z calcd. for $C_{37}H_{23}NS_3$: 577.0993 [M^+]; found: 577.0998.

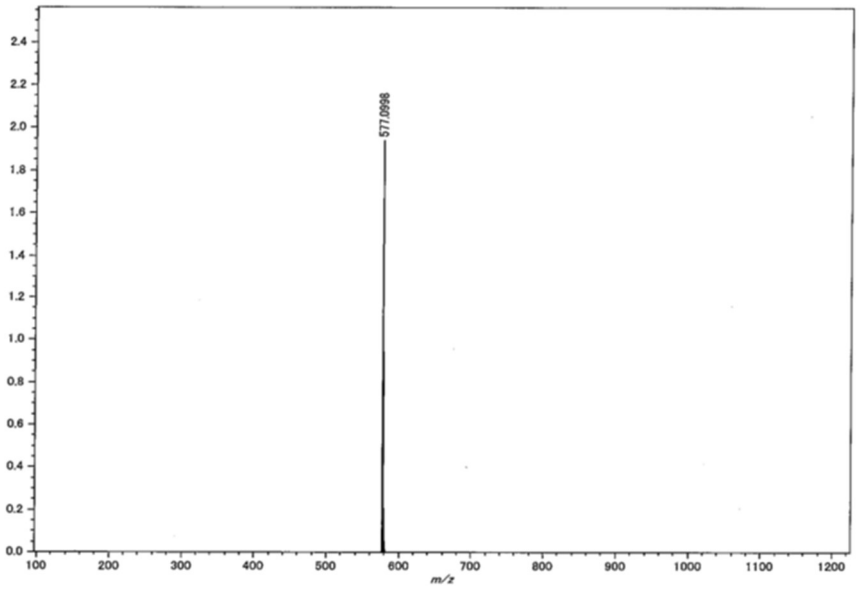

Figure 4-13 HR-MS data of **TA6o**. MALDI Spiral TOF system (JEOL, JMS-S3000).

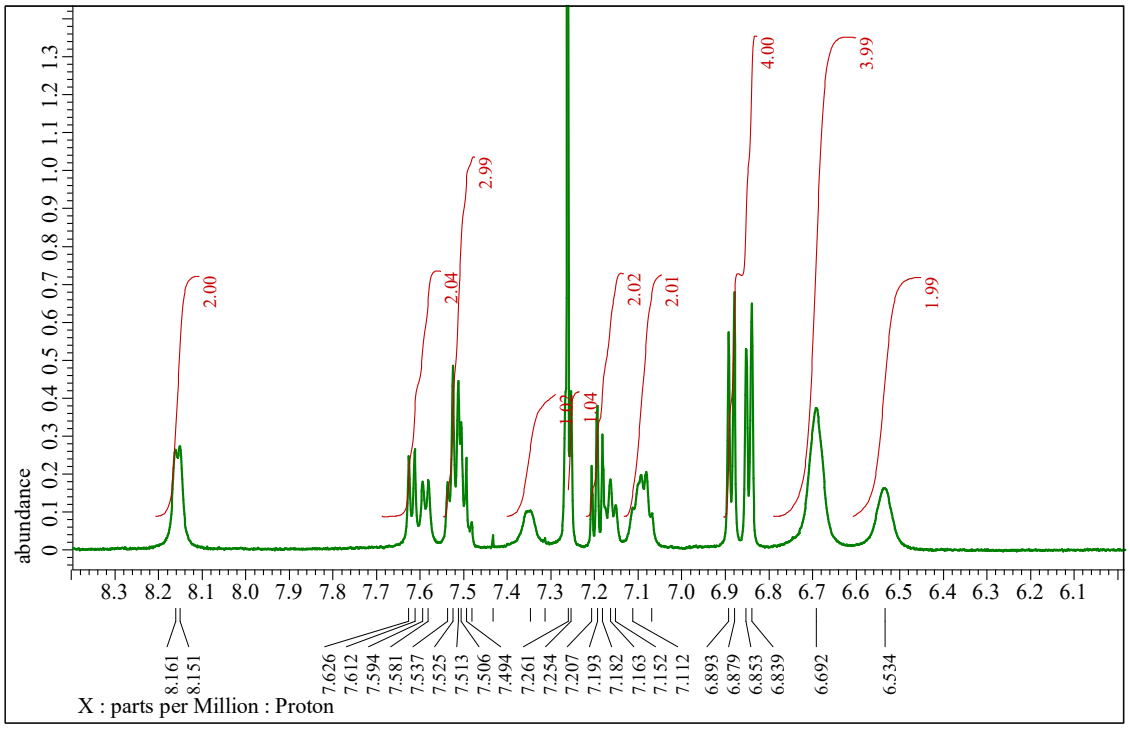

Figure 4-11 ^{1}H NMR spectrum of **TA6o** (600 MHz, $CDCl_3$, TMS/25 °C).

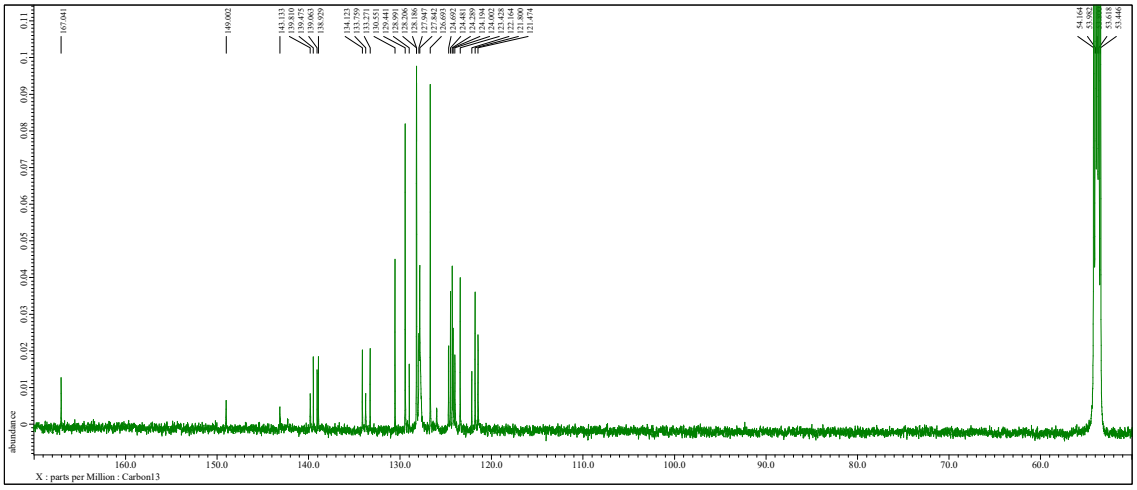

Figure 4-12 ^{13}C NMR spectrum of **TA6o** (151 MHz, CD_2Cl_2, TMS/25 °C).

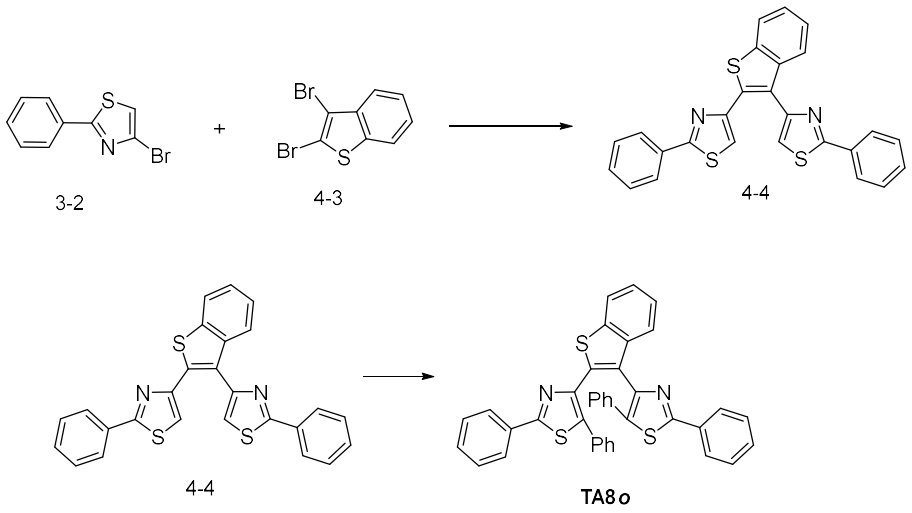

Scheme 4-2. Synthesis of **TA8*o***: a) [$Pd(PPh_3)_4$], PPh_3, 2 M K_3PO_4, water/1,4-dioxane, THF; b) Phenylboronic acid, ($^tBu)_2PMeHBF_4$, pivalic acid, Cs_2CO_3, $Pd(OAc)_2$.

4,4'-(benzo[b]thiophene-2,3-diyl)bis(2-phenylthiazole) (**4-4**) A two-necked flask was charged with 2-phenyl-4-(4,4,5,5-tetramethyl-1,3,2-dioxaborolan-2-yl)thiazole (**3-2**) (660 mg, 2.3 mmol), 2,3-dibromobenzo[b]thiophene (**4-1**) (321 mg 1.1 mmol,), PPh_3 (43 mg, 0.165 mmol) and 2 M aqueous K_3PO_4 (10 mL) in 1,4-dioxane (10 mL). After 60 minutes of stirring under N_2 atmosphere, $Pd(PPh_3)_4$ (80 mg, 0.047 mmol) was added and stirred under N_2 atmosphere at 110 °C for 24 hours. The organic layer was then extracted with chloroform and the combined extracts were washed with water and dried over anhydrous sodium sulfate. The sample was then filtered, and the filtrate was concentrated in vacuo. Gel Permeation Chromatography (chloroform) afforded 4,4'-(benzo[b]thiophene-2,3-diyl)bis(2-phenylthiazole) (**4-4**) (0.35 g, 0.7 mmol, 70% yield) as a white powder. ^{1}H-NMR (300 MHz, $CDCl_3$, TMS/25 °C) δ (ppm) 8.10-8.07 (m, 2H), 8.02-7.99 (m, 2H), 7.91-7.88 (m, 1H), 7.72-7.70 (m, 1H), 7.49-7.43 (m, 7H), 7.41-7.37 (m, 2H), 7.16 (s, 1H).

4,4'-(benzo[b]thiophene-2,3-diyl)bis(2,5-diphenylthiazole) (**TA8o**): A two-necked flask was charged with 4,4'-(benzo[b]thiophene-2,3-diyl)bis(2-phenylthiazole) (**4-4**) (0.20 g, 0.44 mmol), bromobenzene (0.16 g, 1.04 mmol), di-tert-butylmethylphosphine tetrafluoroborate (0.021 g, 0.09 mmol), Cs_2CO_3 (0.054 g, 1.7 mmol), $Pd(OAc)_2$ (0.019 mg, 85 μmol) and pivalic acid (0.026 g, 0.25 mmol) in mesitylene (1.5 mL). The mixture was heated under reflux at 150 °C for 16 hours. Thereafter, it was filtered through celite, extracted with ethyl acetate and the combined extracts

were washed with water and dried over anhydrous sodium sulfate. Gel Permeation Chromatography (chloroform) afforded **TA8o** (0.050 g, 0.083 µmol, 16% yield) as a white powder. ^{1}H NMR (600 MHz, $CDCl_3$, TMS/25 °C) δ (ppm) 7.86 (d, J = 7.9 Hz, 2H), 7.80 (d, J = 7.9 Hz, 2H), 7,79 (d, J = 6.6 Hz), 7,78 (d, J = 6.6 Hz), 7.71 (dd, J = 7.9, 1.7 Hz, 2H), 7.41-7.33 (m, 8H), 7.07 (dd, J = 7.2 Hz, 1,4 Hz, 2H), 7.03 (t, J = 7.2 Hz, 2H), 7,00 (d, J = 7.8 Hz), 6.96-6.91 (m, 4H); ^{13}C NMR (151 MHz, $CDCl_3$, TMS/25 °C) δ (ppm) 165.0, 145.3, 143.8, 139.8, 136.2, 136.0, 135.8, 133.8, 133.4, 131.2, 130.5, 129.8, 129.6, 128.8, 128.7, 128.6, 128.4, 128.4, 128.3, 128.1, 127.7, 126.5, 126.4, 124.9, 124.5, 122.0, 77.2, 77.0, 76.8, 0.0 ppm; HR-MS (ESI): m/z calcd. for $C_{38}H_{24}N_2S_3$: 604.1096 [M^+] ; found: 604.1097.

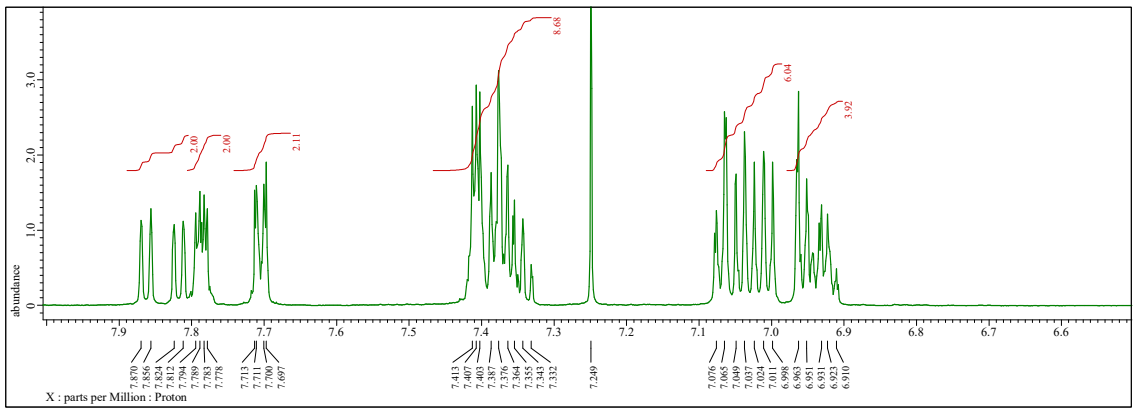

Figure 4-14 ^{1}H-NMR spectrum of **TA8o** (600 MHz, $CDCl_3$, TMS/25 °C).

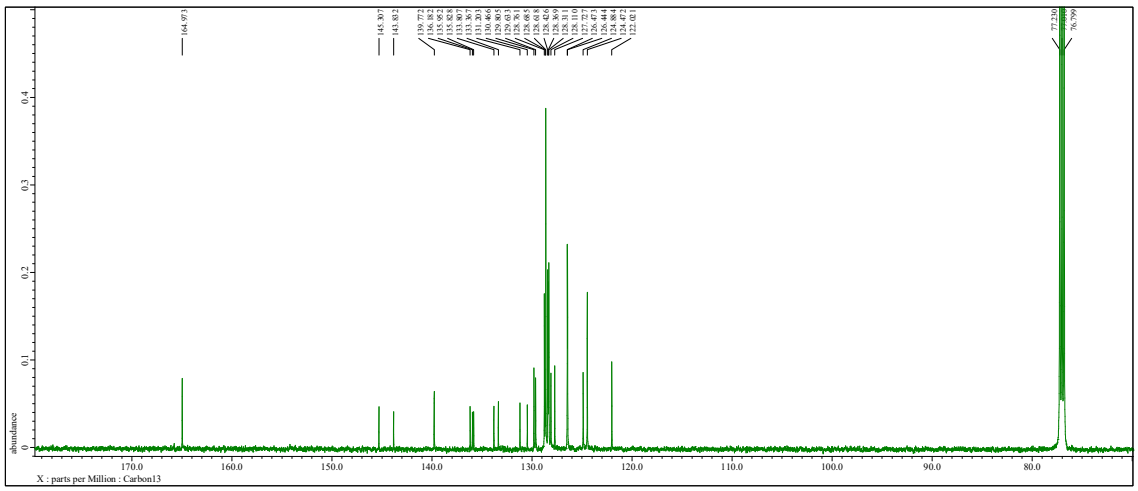

Figure 4-15 ^{13}C NMR spectrum of **TA8o** (151 MHz, $CDCl_3$, TMS/25 °C).

5. Conclusions and Prospects

The above chapters described the experimental and computational study on the functional activity of photochromic terarylenes and derivatives. In the following, each chapter is briefly summarized.

In chapter 1, general background of photochromic molecules especially diarylethene and their derivatives were presented, followed by the recent progress in terarylene chemistry. For further clarifying targets of the present study, progress in some other topics are also briefly reviewed, such as molecular machines, MOST storage, and radio-chromic molecules.

In chapter 2, a new type of molecular motor functionalized with a terarylene photochromic fragment was designed for developing photo-triggered breaking on the molecular rotator, taking into account a computational estimation and the inherent properties of terarylene. Careful design of terarylene with the additional aryl group preserves the high photoreactive nature of diarylethene derivatives and allows for peculiar substitution sites not related to photocyclization. The terarylene photochromic core frameworks can be conjugated to the cyclopentadiene rotor part of the motor through the linkage at the central aromatic units but not one of the peripheral side rings, this structure is advantageous to control precisely the steric interactions with the stator part. After the computational study, terarylene fragment was designed, synthesized and fully characterized. The NMR study showed that the rotation of the functionalized cyclopentadienyl ligand becomes slowly restrained when the **c**-form is generated by light irradiation, suggesting that upon photocyclization it acted as a brake. Afterward, the system was left in the dark for seven days to allow the ring-opening to occur thermally. NMR analysis showed the successful reversion to the **o**-form, indicating full thermodynamic release of the `brake` over time. Further investigations by STM are necessary to get a deeper insight into the complementary functionality of photoswitching to block the electron-induced rotation.

In chapter 3, photo and radio-chemical synergetic responses are developed for sensitive UV and X-ray sensing. The previous work suggested that the central aromatic ring of terarylene may play a major role in reactions in the cationic state, resulting in highly efficient cycloreversion reactions using the electron transfer cascade process. Meanwhile, high-energy photons such as

UV and X-rays, which act as radical generators in chloroform, are shown to initiate the cascade reaction. These considerations motivated the study of the sensitive detection of UV and X-ray via the cascade reaction. Five photoswitching terarylenes, including three new compounds, showing cyclization and cycloreversion with high quantum yield and complete recyclability, have been prepared. Three of them showed highly efficient cycloreversion reactions using the electron transfer cascade process. The introduction of a single phenyl unit on a carbon atom at the photoreactive reaction center significantly amplified efficiency. UV irradiation in a non-halogenated solvent allows for the inducing of coloration, converting to the thermally stable **c**-form, while UV irradiation in the presence of chloroform induces a highly efficient cycloreversion reaction from the closed-form to the **o**-form. This reaction kinetics represents a chain reaction process. Estimating this UV-induced quantum chain reaction showed it to be significantly higher than unity in total (3,300%). This value of photochemical reaction quantum yield is the highest among reversible photoisomerization reactions to my best knowledge. This photochemical quantum was observed in the present experimental condition for the mixture of both isomers. That is, the apparent maximum quantum yield might be 6,000% to 7,000% under appropriate conditions. The electron-donating phenyl thiophene or diphenyl thiophene units consisting in the present compounds would support the photo-oxidation capability by stabilizing the cationic radical intermediates, resulting in the UV-induced cascade reaction being observed. Indeed, light-triggered cascade reaction was not observed for conventional terthiazole derivatives with low oxidation activity and the other terarylenes, although they show efficient cascade reactions initiated by chemical and electrochemical oxidations. The fading reaction was also observed even with very low doses (mGy level) of X-rays, which was carefully assigned to produce the colorless **o**-form. The limit of detection (LOD) of 0.3 mGy is the highest sensitivity among organic X-ray color-changing materials. This LOD is attributed to a minimal change in the linear sensitivity due to X-ray irradiation; thus, the large change in absorbance with X-ray irradiation is mainly due to a very efficient charge transfer cascade reaction mechanism for cycloreversion. This presented the high utility of efficient photosynergetic reactions for highly sensitive detection or accuracy of absorbance measurements. These novel compounds provided a new approach to the development of future visually detectable dosimeters that could signal the presence of low-level radiation doses

through color fading. It is still challenging to make this cascade chemical system in a solid or film, by means of gelation, for example.

In chapter 4, from a thermo-chemical perspective, the advantages of terarylene as a MOST material were presented. Eight terarylenes, including two new compounds, are investigated. The terarylene framework was designed by considering energy difference between the photoisomers ($\Delta H_{c\text{-}o}$), which corresponds to amount of stored heat in each molecule. The $\Delta H_{c\text{-}o}$ likely stems from i) the increasing steric hindrance around the substituent groups on the reaction center carbon atoms and ii) the loss of aromatic stabilization energy upon the photoisomerization from **o**- to **c**-forms. The additional aromatic aryl unit of terarylene thus enhances $\Delta H_{c\text{-}o}$. The constituting benzothiophene as aryl moiety having high aromaticity and phenyl rings as a bulky substituent at reactive carbon atoms, **TA8** and **TA6**, were efficient to enhance $\Delta H_{c\text{-}o}$. High photo-cyclization quantum yield (ϕ_{iso}) is achieved by locking the **o**-form in its photoreactive conformation using intramolecular non-bonding interactions inherent in terarylene. These high $\Delta H_{c\text{-}o}$ and ϕ_{iso} are responsible to the maximum MOST efficiency as high as 23% for **TA8** and 22% for **TA6**.

In the general physicochemical consideration for photochromic molecules, the well-known Hammond's postulate implies the trade-off relation between the activation energy (E_a) and $\Delta H_{c\text{-}o}$. This has underlined the intrinsic difficulty to achieve both a large ΔH_{iso} and high thermal stability at the same time for photoresponsive molecules in practical MOST applications. The experimentally obtained E_a clearly exhibits the trade-off relationship against $\Delta H_{c\text{-}o}$ for the terarylenes. However, most of the present terarylenes showed significantly stable thermal-storage capability with sufficient E_a value. The sum of aromatic stabilization energy of the three aryl units in the terarylene framework seems predominantly to determine the E_a - $\Delta H_{c\text{-}o}$ relationship. The E_a - $\Delta H_{c\text{-}o}$ relationship plots readily show the terarylenes can be devided into two groups, depending on the nature of the substituent on the reactive carbon atoms, methyl or phenyl. The substitution of the methyl group with phenyl rings on the reactive carbon atoms did not change the slope but introduced a parallel displacement of the linear plot in the direction of lower-right. The study of terarylene having high quantum yield and high storage capacity ($\Delta H_{c\text{-}o}$) with relatively high E_a, suggests them as prospects for practical MOST applications.

Locking of the conformation through non-bonding intramolecular interactions allowed the high photocyclization quantum yields. The latter could be thanks to the symmetric forbidding in the

cycloreversion reaction in the ground state, which allowed enhancement of $\Delta H_{c\text{-}o}$ while maintaining a high enough activation barrier. These results may further encourage us to explore efficient MOST substances by optimization of the molecular structure. Considering the energy capacity of the terarylene molecule, the present highest $\Delta H_{c\text{-}o}$ is 114 kJmol^{-1} for **TA6,** which is surprisingly as high as about one-third of the photon energy at 380 nm. Some recently proposed MOST materials are based on phase transitions and utilize rather weak van der Waals interaction as the origin of heat storage capacity. The stored energy for **TA6** is based on alteration of covalent bonding and thus is an order of magnitude higher than those in the phase-changing systems. Terarylene is also advantageous as being highly photoreactive with excellent recyclability even in amorphous and crystalline solids,[30] which may provide immense energy density equivalent to fuels requiring combustion.[44a] The development of MOST materials based on terarylene will offer great progress in energy technology.

Despite the chemical structure of terarylenes being a rather simple extension of diarylethenes, they become much advantageous in some aspects. As described in chapter 1, there are four major points of advantages of terarylenes with the extension of π-conjugation system at the central part; 1) expanding the diversity of structures with combinations of heteroaromatics, 2) additional possibility to connect them to other units through the central aromatic units while preserving the central moieties responsible for photocyclization, 3) specific stabilization of the **o**-form due to additional aromatic units, 4) enhanced redox capability forming stable charged states supported by the extended π-conjugation system. These significant new finding of the nature of terarylene potentially delivers mechano-, radio- and thermo-chemical responses, resulting in new perspectives for on-off switches of a molecular motor rotation; extremely sensitive X-ray detectors using cascade reaction and highly efficient solar storage.

Looking at all the results from a higher perspective, the structural optimizations of terarylene based on a thermo-chemical point of view has further potential to pioneer not only a highly efficient MOST system but also various functional molecular systems. The accelerating the thermo-cycloreversion reaction rate achieves full thermodynamic release of the rotor-braking function, which could be achieved by optimizing the terarylene framework with a bulky substituent at reactive carbon atoms. I am further confident that the fundamental understanding the physicochemical nature of organic molecules in the ground, photo-excited and even charges

states will **o**-various new and impactful aspects of future chemical science and engineering, which should highlight the future of our society much brighter.

These challenges are expected to contribute to future macroscopic functionality based on molecular level action. The essential step for the pioneering and breakthrough development of future molecular materials is believed to be achieved through a fundamental understanding of their molecular-level properties.

Scientific production

Publications

1. C. J. Martin, M. Minamide, J.P.D.C Calupitan, R. Asato, J. Kuno, T. Nakashima, G. Rapenne, T. Kawai, "Terarylenes as Photoactivatable Hydride Donors". J. Org. Chem. 83, 13700 (2018).

2. R Mizutsu, R Asato, C. J. Martin, M Yamada, Y Nishikawa, S Katao, M Yamada, T Nakashima, and T Kawai, "Photo-Lewis Acid Generator Based on Radical-Free 6π PhotoCyclization Reaction" J. Am. Chem. Soc., 141, 20043−20047 (2019).

3. C.J. Martin, J.P. Calupitan, M. Minamide, R. Asato, Y. Goto, G. Rapenne, T. Nakashima, T. Kawai, "Systematic studies of structural variations in terarylene photohydride generators", J. Photochem. Photobiol. A 397 1125942 (2020).

4. R. Asato, C.J. Martin, J.P. Calupitan, R. Mizutsu, T. Nakashima, G Okada, N. Kawaguchi, T. Yanagida, T. Kawai "Photosynergetic amplification of radiation input: from efficient UV induced cycloreversion to sensitive X-ray detection" Chem. Sci. 11, 2504–2510 (2020).

5. T. Kawai, R. Asato, Review article, Isotope News, 722, December (2020).

6. R. Asato, C. J. Martin, S.Abid, Y. Gisbert, F. Asanoma, T. Nakashima, C. Kammerer, T. Kawai and G. Rapenne, "An Electron-fueled Molecular Motor Functionalized with a Photoresponsive Brake" in press (2020).

7. R. Asato, C. J. Martin, Y. Gisbert, S. Abid, T. Kawai, C Kammerer and G. Rapenne, "Ruthenium complexes of sterically-hindered pentaarylcyclopentadienyl ligands", under review.

8. R. Asato, T. Nakashima, J. P. Calupitan, C. J. Martin, Gwénaël Rapenne, Tsuyoshi Kawai, "E-type Photochromic Molecules for Efficient Solar Energy Storage and On-demand Heat Release" to be submitted.

Conference presentations

Oral presentations

International

1. Ryosuke Asato, Jan Patrick Calupitan, Go Okada, Takuya Nakashima, Noriaki Kawaguchi, Takayuki Yanagida, Gwénaël Rapenne, Tsuyoshi Kawai, “X-ray induced amplified cycloreversion of photochromic Terarylene” Photo IUPAC, Ireland, July 2018.

2. Ryosuke Asato, “Design and synthesis of molecular machines with photoinduced brake based on photochromic diarylethenes” the Mid-Term Student Research Evaluation Symposium 2019, Nara, Japan, Novenver, 2019.

Domestic

3. Ryosuke Asato, Ryosuke Asato, J. P. Calupitan, Takuya Nakashima, Jyh-Chiang Jiang, Tsuyoshi Kawai, “Molecular Solar Energy Storage and Thermal release of Photochlomic Terarylene” The 65th Japan Society of Applied Physics,Tokyo, Japan March, 2018 (Young Scientist Presentation Award).

4. Ryosuke Asato, Ryosuke Asato, J. P. Calupitan, Takuya Nakashima, Jyh-Chiang Jiang, Tsuyoshi Kawai, “Molecular Solar Energy Storage and Thermal release of Photochlomic Terarylene” The 79th Japan Society of Applied Physics,Nagoya, Japan September, 2018 (Invited).

5. Ryosuke Asato, Jan Patrick Calupitan, Ryo Mizutsu, Takuya Nakashima, Jiang Jyh-Chiang, Tsuyoshi Kawai, “Molecular Thermal Strage (MOST) and theraml release with Photochlomic Teralylene”, Annual Meeting on Photochemistry 2018, Nishinomiya, Japan, September 2018 (English).

6. Ryosuke Asato, Ryosuke Asato, J. P. Calupitan, Takuya Nakashima, Jyh-Chiang Jiang, Tsuyoshi Kawai, “Functional Solar Energy Storage and Thermal Release using Organic Photochromic Molecules” The 66th Japan Society of Applied Physics,Tokyo, Japan March, 2019 (English).

7. Ryosuke Asato, Colin J. Martin, Takuya Nakashima, Claire Kammerer, Tsuyoshi Kawai, Gwénaël Rapenne, “A molecular motor functionalized with a photochromic Terarylene brake’ Annual” Meeting on Photochemistry 2020, on Web, September 2020 (English).

Poster presentations

International

1. Ryosuke Asato, Jan Patrick Calupitan, Go Okada, Takuya Nakashima, Noriaki Kawaguchi, Takayuki Yanagida, Tsuyoshi Kawai. “UV-light and X-ray induced efficient cycloreversion reaction of Terarylene”, 10th Asian Photochemistry Conference, Taiwan, December 2018.

2. Ryosuke Asato, Colin J. Martin, Ryo Mizutsu, Takuya Nakashima, Gwénaël Rapenne and Tsuyoshi Kawai, “Molecular Design of Photochromic Terarylene for Solar Thermal Fuels”, 9th International Symposium On Photochromism Paris, France, September 2019.

Domestic

3. Ryosuke Asato, Takuya Nakashima, Takayuki Yanagida, Go Okada, Noriaki Kawaguchi, Tsuyoshi Kawai, “Domino-chromic reaction for X-ray sensitive molecular material” The 65th Japan Society of Applied Physics, Kanagawa, Japan March, 2018 (Poster award).

Patent

Number in Japanese 2017-037748 date 2017/2/28 Tsuyoshi Kawai, **Ryosuke Asato,** Takayuki Yanagida、Takuya Nakashima, Go Okada. Preparation for PCT patent.

Acknowledgments

All of my research was supported and carried out in the Photonic Molecular Science Laboratory - Graduate School of Material Science - Nara Institute of Science and Technology (NAIST, Nara), the NAIST-CEMES International Collaborative Laboratory for Supraphotoactive Systems - Centre d'Elaboration de Matériaux et d'Etudes Structurales (CEMES, Toulouse) and the Doctoral School Sciences de la matière - Université Toulouse III - Paul Sabatier (Toulouse).

I would like to express my sincere gratitude to Prof. Tsuyoshi Kawai, Prof. Gwénaël Rapenne, and Dr. Takuya Nakashima, who not only served as my research supervisors but also as great mentors as well. Their invaluable guidance was most instrumental in my formation as a scientist. I greatly appreciate Prof. Yo Shimizu, Dr. Claire Kammerer, Dr. Mihoko Yamada, Dr. Colin J. Martin, Dr. Marine Louis, Dr. Seifallah Abid, and Dr. Yoshiyuki Nonoguchi for their guidance and contribution to my formation.

Special thanks to the examination committee members Dr. Jeanne Crassous, Dr. Joanne Xie, Prof. Eric Benoist, Prof. Kenji Matsuda, and Prof. Shun Hirota, who will read and give constructive comments to the manuscript.

Prof. Takayuki Yanagida is acknowledged for collaboration work on the X-ray detection and serving as a supervisor during my studies in NAIST. Dr. Suzanne Fery-Forgues is also acknowledged for serving as an external advisor during my studies in Paul Sabatier.

To members of the Photonic Molecular Science, I thank all of you for making my academic life memorable. Especially, Mr. Junpei Kuno and Mr. Daiya Shimizu who were in the same grade from master to the doctoral course and always good competitors. They supported me anytime and gave me so many memories; Mr. Ryo Mizutsu and Mr. Hiroto Yoshida also worked with me for four years and gave me a lot motivations for research and dinner. Thank you so much. My research and life went well thanks to all the members of the Photonic Molecular Science Laboratory in the past and at present, Dr. Rui Kanazawa, Dr. Yuichiro Hashimoto, Dr. Ruiji Li, Dr. Motohiro Nakano, Dr. Jan Patrick. D. C. Calupitan, Dr. Ramarani Sethy, Dr. Yuki Taniguchi, Dr. Tan Yan Bing, Mr. Yu Ihara, Mr. Yuki Kita, Ms. Akiko Hayashide, Mr. Tommohiro Ikeda, Mr. Kouhei Fujiwara, Mr. Takao Takishita, Ms. Kasumi Shigekawa, Ms. Miho Minamide, Mr. Keita Kojiyama, Mr. Naoya Takeuchi, Mr. Takuya Kitano, Ms. Ami Takada, Ms. Shiori Matsuoka, Mr.

Hajime Yamamoto, Ms. Kanae Oi, Mr. Ryuta Okumiya, Mr. Yuma Kita, Mr. Junichi Komoto, Mr. Daichi Nishi, Mr. Yuki Sekiguchi, Mr. Shunpei Yonezawa, Mr. Florencio D. de los Reyes, Mr. Joy Ann Panis, Mr. Yuki Sekiguchi, Mr. Yora Goto, Mr. Tomoya Sawazaki, Mr. Katsuki Shigita, Mr. Satoki Taniguchi, Mr. Riku Tanibe, Mr. Ryosuke Tano, Ms. Tomoko Yagi, Mr. Masashi Iriguchi, Mr. Tetsuhiro Ota, Ms. Fumina Tsutsui, Ms. Ayaka Demise, Ms. Masato Nishi, Ms. Tomoki Fujitani, Dr. Jatish Kumar and Mr. Wataru Ishii, thank you very much. I would also like to acknowledge the technical staff, especially Ms. Chigusa Goto, Ms. Tomoko Murayama, and Ms. Miku Yamada, who helped me in my research and individual advice. Ms. Kyoko Kato, Ms. Toko Hishikawa, Ms. Noriko Takenae, and Ms. Junko Shimohira, are current and former staff who made administrative procedures accessible to me, thank you so much. My scientific thanks also go to technical staff from NAIST, especially Mr. Fumio Asanoma for NMR measurement and Ms. Yoshiko Nishikawa for HR-MS spectra measurements. To the friends in NAIST who give me much chances to go to eat ramen, thank you.

To all members of the Groupe Nanosciences in CEMES, especially: Dr. Erik Dujardin, the head of the group; the chemists Dr. Andre Gourdon, Dr. Jacques Bonvoisin, Prof. Jean-Pierre Launay, Christine Viala, Dr. Andrej Jancarik, Dr. Jan Holec, Dr. Michael Kleinwaechter, Dr. Lenka Pallova, Dr. Guillaume Erbland, with whom I shared many memorable times and give me some of the reasons why Toulouse is memorable to me, for the laughter and the friendship, thank you very much. Mr, Yohan Gisbert has collaborated with me on DFT calculations and has always been an inspiration to me; thank you very much. Their views and perspectives in science, literature, philosophy, academic life, and the greater scheme of things shaped me in several ways.

I would also like to thanks my research collaborators, Dr. Noriaki Kawaguchi and Dr. Go Okada.

Finally, my academic life couldn't have been led without my family, and thank you, Eiji Asato, Kana Asato, Yusuke Asato, Koichi Takata, and my wife Naoko Asato, for their selfless contribution and full support.

Ryosuke Asato

朝戸良輔

References

[1] Heck, R. F.; Nolley, J. P. J. Org. Chem. 37, 2320–2322 (1972).

[2] Negishi, E. Acc. Chem. Res. 15, 340–348 (1982).

[3] Suzuki. A. ; Yamamoto. Y. Chem. Lett. 40, 894901 (2011).

[4] Schertler, G F. X.; Villa, C. Henderson, R. Nature, 362, 770-772. (1993).

[5] Irie, M. *Chem. Rev.* 5, 100 (2000).

[6] Hartley, G. S.; *Nature*, 140, 281 (1937).

[7] Fischer, E.; Hirshberg, Y. J. Chem. Soc. 4522 (1952).

[8] Irie M.; and Mohri, M. *J. Org. Chem* 53, 803–808 (1988).

[9] a) Solomons, T. W. G.; Fryhle, C. B.; Snyder, S.A. Solomons' Organic Chemistry, 12th Edition, Global Edition. b) Fleming, I. Pericyclic Reactions. Oxford University Press (1999).

[10] a) Woodward, R. B.; Hoffmann, R. Angew. Chem. Internat. Edit. 8, 781-853 (1969). b) Fukui, K. Acc. Chem. Res. 4, 57 (1979).

[11] Fleming, I. Frontier Orbitals and Organic Chemical Reactions. John Wiley & Sons, Ltd. (1976).

[12] Clayden, J.; Greeves, N.; Warren, S. Organic Chemistry 2nd Edition (2012).

[13] Irie, M.; Fukaminato, T.; Matsuda, K.; Kobatake, S. Photochromism of Diarylethene Molecules and Crystals: Memories, Switches, and Actuators Chem. Rev. 114, 12174– 12277 (2014).

[14] Santiago, A.; Becker, R. S.; J. Am. CHem. Soc., 90, 3654 (1968).

[15] a) Stobe, H. Ber., 38, 3673 (1905), b) Stobe, H. Ann., 380, 1 (1911).

[16] a) Darcy, J.P.; Heller, G.H.; Strydom, J.P.; Whittall J.; J. Chem. Soc., Perkin Trans. 1. 202 (1981). b) Paetzold, H.-D. R.; Ilge, J. Signal 2, 93 (1975). c) H.G. Heller, Chem. Ind. 193, (1978). c) Heller, H.G. IEE Proceedings, 130, Part I, 209 (1980).

[17] a) Mallry F. B.; Gourdon, J. T.; Wood, C. S. J. Amer. Chem. Soc. 85, 828 (1963). b) Mallry F. B.; Wood, C. S.; Gourdon, J. T. J. Amer. Chem. Soc. 85, 828 (1963). c) Muszkat, K. A.; Fischer, F. J. Chem. Soc. 662 (1967).

[18] Calvert, J. G.; Pms, J. N.; John, JR.; Photochemistry. Wiley and Sons Inc. (1966).

[19] a) Nakamura, S.; Yokojima, S.; Uchida, K.; Tsujioka, T.; Goldberg, A.; Murakami, A.; Shinoda, K.; Mikami, M.; Kobayashi, T.; Kobatake, S.; Matsuda, K.; Irie, M. J. Photochem. Photobiol., A, 200, 1, 10–18 (2008). b) S. Nakamura, M. Irie, J. Org. Chem. 53, 6136–6138 (1988).

[20] a) Meng, F. et al. Orthogonally modulated molecular transport junctions for resettable electronic logic gates. Nat. Commun. **5**, 3023 (2014). b) Leydecker, T. et al. Flexible non-volatile optical memory thin-film transistor device with over 256 distinct levels based on an organic bicomponent blend. Nat. Nanotechnol. **11**, 769–775 (2016). c) Andréasson, J. et al. All-photonic multifunctional molecular logic device. J. Am. Chem. Soc. **133**, 11641–11648 (2011). d) Bälter, M., Li, S., Nilsson, J. R., Andréasson, J.; Pischel, U. An all-photonic molecule-based parity generator/checker for error detection in data transmission. J. Am. Chem. Soc. 135, 10230–10233 (2013).

[21] a) Meng, F. et al. Orthogonally modulated molecular transport junctions for resettable electronic logic gates. Nat. Commun. **5**, 3023 (2014). b) Leydecker, T. et al. Flexible non-volatile optical memory thin-film transistor device with over 256 distinct levels based on an organic bicomponent blend. Nat. Nanotechnol. **11**, 769–775 (2016).

[22] (a) Miyasaka, H.; Murakami, M.; Itaya, A.; Guillaumont, D.; Nakamura, S.; Irie, M. J. Am. Chem. Soc. 2001, 123, 753– 754 (b) Murakami, M.; Miyasaka, H.; Okada, T.; Kobatake, S.; Irie, M. J. Am. Chem. Soc. 126, 14764– 14772. (2004)

[23] (a) Ishibashi, Y.; Mukaida, M.; Falkenström, M.; Miyasaka, H.; Kobatake, S.; Irie, M. Phys. Chem. Chem. Phys. 2009, 11, 2640– 2648 (b) Piard, J.; Ishibashi, Y.; Saito, H.; Metivier, R.; Nakatani, K.; Gavrel, G.; Yu, P.; Miyasaka, H. J. Photochem. Photobiol., A 2012, 234, 57– 655

[24] Sotome, H.; Nagasaka, T.; Une, K.; Morikawa, Tetsuro Katayama, Seiya Kobatake, Masahiro Irie, and Hiroshi Miyasaka. Cycloreversion Reaction of a Diarylethene Derivative at Higher Excited States Attained by Two-Color, Two-Photon Femtosecond Pulsed Excitation. Journal of the American Chemical Society 139, 47, 17159-17167 (2017).

[25] Roubinet, B. et al. Fluorescent photoswitchable diarylethenes for biolabeling and single-molecule localization microscopies with optical superresolution. J. Am. Chem. Soc. 139, 6611–6620 (2017).

[26] Xiong, Y. et al. Spironaphthoxazine switchable dyes for biological imaging. Chem. Sci. 9, 3029–3040 (2018).

[27] Reisinger, B. et al. Exploiting protein symmetry to design light-controllable enzyme inhibitors. Angew. Chem. Int. Ed. 53, 595–598 (2014).

[28] a) Babii, O. et al. Direct photocontrol of peptidomimetics: an alternative to oxygen-dependent photodynamic cancer therapy. *Angew. Chem. Int. Ed.* **55**, 5493–5496 (2016). b) Simeth, N. A., Kneuttinger, A. C., Sterner, R.; König, B. Photochromic coenzyme Q derivatives: switching redox potentials with light. *Chem. Sci.* **8**, 6474–6483 (2017).

[29] Kawai, T.; Iseda, T.; Irie, M. Chem. Commun. 72– 73 (2004).

[30] Nakashima, T.; Atsumi, K.; Kawai, S.; Nakagawa, T.; Hasegawa, Y.; Kawai, T. Eur. J. Org. Chem. 3212– 3218 (2007).

[31] Fukumoto, S.; Nakashima, T.; Kawai, T. Photon-Quantitative Reaction of a Dithiazolylarylene in Solution. Angew. Chem., Int. Ed. 50, 1565– 1568 (2011)

[32] Mizutsu, R.; Asato, R.; Martin, C. J.; Yamada, M.; Nishikawa, Y.; Katao, S.; Yamada, M.; Nakashima, T.; Kawai, T. Photo-Lewis Acid Generator Based on Radical-Free 6π Photo-Cyclization Reaction. J. Am. Chem. Soc. 141, 51, 20043–20047 (2019)

[33] a) Nakashima, T.; Tsuchie, K.; Kanazawa, R.; Li, R.; Iijima, S.; Galangau, O.; Nakagawa, H.; Mutoh, K.; Kobayashi, Y.; Abe, J.; Kawai, T. Self-Contained Photoacid Generator Triggered by Photocyclization of Triangle Terarylene Backbone. J. Am. Chem. Soc. 137, 22, 7023–7026 (2015). b) Li, R.; Nakashima, T.; Kanazawa, R.; Galangau, O.; Kawai Efficient Self-Contained Photoacid Generator System Based on Photochromic Terarylenes. Chem. - Eur. J. 22, 16250– 16257. (2016). c) Galangau, O.; Delbaere, S.; Ratel-Ramond, N.; Rapenne, G.; Li, R.; Calupitan, D. C. J. P.; Nakashima, T.; Kawai, T. Dual Photochemical Bond Cleavage for a Diarylethene-Based Phototrigger Containing both Methanolic and Acetic Sources. J. Org. Chem. 2016, 81, 11282–11290. d) Li, R.; Nakashima, T.; Kawai, T. A Self-Contained Photoacid Generator for Super Acid Based on Photochromic Terarylene. Chem. Commun. 53, 4339– 4341 (2017).

[34] Nakashima, T.; Imamura, K.; Yamamoto, K.; Kimura, Y.; Katao, S.; Hashimoto, Y.; Kawai, T. Chem. Eur. J. 20 (2014) 13722-13729.

[35] Nakashima, T.; Yamamoto, K.; Kimura, Y.; Kawai, T. Chiral photoresponsive tetrathiazoles giving snapshots of folding states, Chem. Eur. J.19, 16972-16980 (2017).

[36] Hashimoto, Y.; Nakashima, T.; Shimizu, D.; Kawai, T. Photoswitching of an intramolecular chiral

stack in a helical tetrathiazole, Chem. Commun. 52, 5171-5174 (2016).

[37] Nakagawa T. Hasegawa Y. Kawai T J. Phys. Chem. A 112 50966-5103 (2008)

[38] (a) T. Koshido , T. Kawai and K. Yoshino , J. Phys. Chem., 99 , 6110-6114 (1995). (b) Moriyama, Y.; Matsuda, K.; Tanifuji, N.; Irie, S.; Irie, M. Electrochemical cyclization/cycloreversion reactions of diarylethenes, Org. Lett. 7, 3315-3318 (2005). (c) A. Peters and N. R. Branda , J. Am. Chem. Soc. 125 , 3404-3405 (2003). (c) W. R. Browne, J. J. D. de Jong, T. Kudernac , M. Walko , L. N. Lucas , K. Uchida , J. H. van Esch and B. L. Feringa , Chem.–Eur. J., 11 , 6414-6429 (2005). (d) Gorodetsky, B.; Branda, N. R.; Adv. Funct. Mater. 17, 786–796 (2007). (e) G. Guirado, C. Coudret and J.-P. Launay, J. Phys. Chem. C. 111, 2770 -2776 (2007). (f) A. Staykov, J. Areephong, W. R. Browne, B. L. Feringa and K. Yoshizawa, ACS Nano. 5, 1165-1178 (2011). (g) Lee, S.; You, Y.; Ohkubo, K.; Fukuzumi, S.; Nam, W.; Chem. Sci. 5, 1463 (2011). (h) Lee, S.; You, Y.; Ohkubo, K.; Fukuzumi, S.; Nam, W.; Angew. Chem. Int. Ed. 2012, 51, 13154–13158. (i) Akita, M.; Organometallics. **29**, 43–51 (2011). (g) A. Mulas, X. He, Y.-M. Hervault , L. Norel , S. Rigaut and C. Lagrost , Chem.–Eur. J., 2017, 23 , 10205-10214.

[39] Nakashima, T.; Kajiki, Y.; Fukumoto, S.; Taguchi, M.; Nagao, S.; Hirota S.; Kawai, T. J. Am. Chem. Soc.134, 19877-19883. (2012).

[40] Calupitan, J.P.; Nakashima, T.; Hashimoto, Y.; Kawai, T. Chem. Eur. J. 22, 10002-10008 (2016).

[41] Nakashima, T.; Goto, M.; Kawai, S.; Kawai, T. Photomodulation of ionic interaction and reactivity: reversible photoconversion between imidazolium and imidazolinium, J. Am. Chem. Soc. 130, 14570-14575 (2008).

[42] Kanazawa, R.; Nakashima, T.; Kawai, T. Photophysical properties of a terarylene photoswitch with adonor-acceptor conjugated bridging unit, J. Phys. Chem. A, 121, 1638-1646 (2017).

[43] Kawai, S.; Nakashima, T.; Atsumi, K.; Sakai, T.; Harigai, M.; Imamoto, Y.; Kamikubo, H.; Kataoka, M. Chem. Mater. 2007, 19, 3479– 3483

[44] Kucharski, T. J.; Tian, Y.; Akbulatov, S.; Boulatov, R. Chemical solutions for the closed-cycle storage of solar energy. Energy Environ. Sci. Review. 2011, 4, 4449 (b) Kathan, M.; Hecht, S. Chem. Soc. Rev., 2017, 46, 5536

[45] Balzani, V.; Credi, A.; Venturi, M. Molecular Devices and Machines – Concepts and perspectives for the Nanoworld, Wiley-VCH, Weinheim, 2nd ed. 2008.

[46] Rapenne, G.; Launay, J.-P.; Joachim, C.; J. Phys.: Condens. Matter. 2006, 18, S1797–S1808.

[47] (a) Sauvage, J.-P. Angew. Chem. Int. Ed., 2017, **56**, 11080; (b) Stoddart, J. F. Angew. Chem., Int. Ed., 2017, **56**, 11094; (c) Feringa, B. L. Angew. Chem., Int. Ed., 2017, **56**, 11060.

[48] Breslow, R.; J. Biol. Chem. 2008, 284, 1337–1342.

[49] (a) Chance, J. M.; Geiger, J. H.; Mislow, K. J. Am. Chem. Soc., 1989, 111, 2326; (b) Clayden, J.; Pink, J. H. Angew. Chem., Int. Ed., 1998, 37, 1937; (c) Carella, A.; Jaud, J.; Rapenne, G.; Launay, J.-P. Chem. Commun., 2003, 2434; (d) Chiaravalloti, F.; Gross, L.; Rieder, K. H.; Stojkovic, S.; Gourdon, A.; Joachim, C.; Moresco, F. Nat. Mater., 2007, 6, 30.

[50] (a) R. A. Bissel, E. Co´ rdova, A. E. Kaifer and J. F. Stoddart, Nature, 1994, 369, 133; (b) J.-P. Collin, P. Gavin˜ a and J.-P. Sauvage, Chem. Commun., 1996, 2005; (c) N. Armaroli, V. Balzani, J.-P. Collin, P. Gavin˜ a, J.-P. Sauvage and B. Ventura, J. Am. Chem. Soc., 1999, 121, 4397; (d) V. Balzani, A. Credi, F. M. Raymo and J. F. Stoddart, Angew. Chem., Int. Ed., 2000, 39, 3348.

[51] (a) M. C. Jimenez-Molero, C. O. Dietrich-Buchecker and J.-P. Sauvage, Angew. Chem., Int. Ed., 2000, 39, 3284; (b) J. C. Chambron, C. O. Dietrich-Buchecker, G. Rapenne and J.-P. Sauvage, Chirality, 1998, 10, 125; (c) M. Barboiu, G. Vaughan, N. Kyritsakas and J.-M. Lehn, Chem.–Eur. J., 2003, 9, 763.

[52] von Delius, M.; Geertsema, E. M.; Leigh, D. A.; Tang, D.-T. D.; J. Am. Chem. Soc. 2010, 132, 16134–16145.

[53] Kammerer, C.; Erbland, G.; Gisbert, Y.; Nishino, T.; Ya-suhara, K.; Rapenne, G.; Chem. Lett. 2019, 48, 299–308.

[54] L. Grill, K. H. Rieder, F. Moresco, G. Rapenne, S. Stojkovic, X. Bouju and C. Joachim, Nat. Nanotech., 2007, 2, 95.

[55] Y. Shirai, J.-F. Morin, T. Sasaki, J. M. Guerrero and J. M. Tour, Chem. Soc. Rev., 2006, 6, 1043 and references therein.

[56] (a) G. Rapenne and G. Jimenez-Bueno, Tetrahedron, 2007, 63, 7018; (b) L. Grill, K. H. Rieder, F. Moresco, G. Jimenez-Bueno, C. Wang, G. Rapenne and C. Joachim, Surf. Sci., 2005, 584, 153.

[57] Muraoka, T.; Kinbara, K.; Kobayashi, Y.; Aida, T.; J. Am. Chem. Soc. 2003, 125, 5612–5613.

[58] (a) Hounshell, W. D.; Johnson, C. A.; Guenzi, A.; Cozzi, F.; Mislow, K.; Proc. Natl. Acad. Sci USA 1980, 77, 6961–6964. (b) Kawada, Y.; Iwamura, H.; J. Org. Chem. 1980, 45, 2547–2548. (c) Frantz, D. K.; Linden, A.; Baldridge, K. K.; Siegel, J. S.; J. Am. Chem. Soc. 2012, 134, 1528–1535. (d) Ube, H.; Yasuda, Y.; Sato, H.; Shionoya, M.; Nature Commun. 2017, 8, 14296.

[59] (a) Jacquot de Rouville, H.-P.; Garbage, R.; Ample, F.; Nickel, A.; Meyer, J.; Moresco, F.; Joachim, C.; Rapenne, G.; Chem. Eur. J. 2012, 18, 8925–8928. (b) Joachim, C.; Rapenne, G.; ACS Nano 2013, 7, 11–14.

[60] Gisbert, Y.; Abid, S.; Bertrand, G.; Saffon-Merceron, N.; Kammerer, C.; Rapenne, G.; Chem. Commun. 2019, 55, 14689–14692.

[61] Badjić, J. D.; Credi, A.; Silvi, S.; Stoddart, J. F.; Science 2004, 303, 1845–1849.

[62] Kassem, S.; Lee, A. T. L.; Leigh, D. A.; Markevicius, A.; Solá, J.; Nature Chem, 2016, 8, 138–143.

[63] (a) Kelly, T. R.; Silva H. D. and Silva, R. A. Nature, 1999, 401, 150; (b) Koumura, N.; Zijlstra, R. W. J.; van Delden, R. A.; Harada N. and Feringa, B. L. Nature, 1999, 401, 152; (c) Leigh, D. A.; Wong, F. J. K. Y.; Dehez and Zerbetto, F. Nature, 2003, 424, 174; (d) Kottas, G. S.; Clarke, L. I.; Horinek D. andMichl, J. Chem. Rev., 2005, 105, 1281; (e) Kay, E. R.; Leigh D. A. and Zerbetto, F. Angew. Chem., Int. Ed., 2007, 46, 72 and references therein.

[64] (5) a) Kelly, T. R.; Silva, H. D.; Silva, R. A. Unidirectional rotary motion in a molecular system. Nature 1999, 401, 150–152. b) Koumura, N.; Zijlstra, R. W. J.; van Delden, R. A.; Harada, N.; Feringa, B. L. Light-driven monodirectional molec-ular rotor. Nature 1999, 401, 152–155. c) Leigh, D. A.; Wong, J. K. Y.; Dehez, F.; Zerbetto, F. Unidirectional rotation in a mechanically interlocked molecular rotor. Nature 2003, 424, 174–179. d) Kottas, G. S.; Clarke, L. I.; Horinek, D.; Michl, J. Artificial molecular rotors. Chem. Rev. 2005, 105, 1281–1376. e) Kay, E. R.; Leigh, D. A.; Zerbetto, F. Synthetic molecular motors and mechanical machines. Angew. Chem. Int. Ed. 2007, 46, 72–191.

[65] a) Zhang, Y.; Kersell, H.; Stefak, R.; Echever-ria, J.; Iancu, V.; Perera, U. G. E.; Li, Y.; Deshpande, A.; Braun, K.-F.; Joachim, C.; Rapenne, G.; Hla, S.-W. Simultane-ous and coordinated rotational switching of all molecular rotors in a network. Nature Nanotechnol. 2016, 11, 706–713. b) Kassem, S.; van Leeuwen, T.; Lubbe, A. S.; Wilson, M. R.; Feringa, B. L.; Leigh, D. A. Artificial molecular motors. Chem. Soc. Rev. 2017, 46, 2592–2621. c) García-López, V.; Liu, D.; Tour, J. M. Light-activated organic molecular motors and their applications. Chem. Rev. 2020, 120, 79–124. d) Goswami, A.; Saha, S.; Kumar Biswas, P.; Schmittel, M. (Nano)mechanical motion triggered by metal coordination: from functional devic-es to networked multicomponent catalytic machinery. Chem. Rev. 2020, 120, 125–199. e) Baroncini, M.; Silvi, S.; Credi, A. Photo- and redox-driven artificial molecular motors. Chem. Rev. 2020, 120, 200–268.

[66] Perera, U. G. E.; Ample, F.; Echeverria, J.; Kersell, H.; Zhang, Y.; Vives, G.; Grisolia, M.; Rapenne, G.; Joachim, C.; Hla, S.-W. Controlled clockwise and anticlockwise rotational switching of a molecular motor. Nature Nanotechnol. 2013, 8, 46–51.

[67] Vives, G.; Jacquot de Rouville, H.-P.; Carella, A.; Launay, J.-P.; Rapenne, G.; Chem. Soc. Rev. 2009, 38, 1551–1561.

[68] Zhang, Y.; Calupitan, J. P.; Rojas, T.; Tumbleson, R.; Erbland, G.; Kammerer, C.; Ajayi, T.M.; Wang, S.; Curtiss, L.C.; Ngo, A.T.; Ulloa, S.E.; Rapenne, G.; Hla, S.W.; Nature Commun. 2019, 10, 3742.

[69] Lentz T. L. Cell fine structure, Philadelphia, 1971,

[70] a) Cova, S.; Bertolaccini M. and Bussolati, C. The measurement of luminescence waveforms by single photon techniques, Phys. Status Solidi A, 1973, 18 , 11-62. b) Kume, H. Koyama, K.: Nakatsugawa, K. Suzuki S. and Fatlowitz, D. Ultrafast microchannel plate photomultipliers, Appl. Opt., 1988, 27 , 1170-1178

[71] a) R. B. Emmons J. Appl. Phys., 1967, 38, 3705. b) S. Cova, A. Lacaita , M. Ghioni , G. Ripamonti and T. A. Louis , Rev. Sci. Instrum., 1989, 60 , 1104-1110. c) H. Dautet , P. Deschamps , B. Dion , A. D. MacGregor , D. MacSween , R. J. McIntyre , C. Trottier and P. P. Webb , Appl. Opt., 1993, 32 , 3894-3900. d) S. Cova, M. Ghioni , A. Lacaita , C. Samori and F. Zappa , Appl. Opt., 1996, 35 , 1956-1976

[72] Arai, T.; Karatsu, T.; Sakuragi H.; Tokumaru, K.; Tetrahedron Lett., 1983, 24 , 2873-2876

[73] Yorozu, T.; Yoshida, K.; Hayashi, K.; Irie, M.; J. Phys. Chem., 1981, 85, 459-462

[74] Kuzmanich, G.; Gard, M. N.; Garcia-Garibay, M. A.; J. Am. Chem. Soc., 2009, 131, 11606-11614

[75] Han. J.-M.; Xu, M.; Wang, B.; Wu, N.; Yang, X.; Yang, H.; Salter, B. J.; Zang, L. J. Am. Chem. Soc., 2014, 136, 5090-5096

[76] (a) Sohma, J; Kashiwabara, H.; Komatsu, T.; Takahashi, T.; Bull. Fac. Eng., 1964, 35, 511-519. (b) Alger, R. S.; Anderson T. H.; Webb, L. A.; J. Chem. Phys., 1959, 30, 695-706. (c) Ayscough, P. B.; Thomson, C.; Trans. Faraday Soc., 1962, 58, 1477-1494.

[77] Fitzgerald Jr., E. A.; Wuelfing Jr., P.; Richtol, H.; J. Phys. Chem., 1971, 75, 2737-2741.

[78] (a) Meyer, W. C.; J. Phys. Chem., 1970, 74, 2118-2121. (b) Davis K. M. C.; Farmer, M. F.; J. Chem. SOC. B, 1967, 28-32.

[79] R. Fazel, H. M.; Krumholz, Y.; Wang, J. S.; Ross, J.; Chen, H.; H. Ting, N. D.; Shah, K.; Nasir, Einstein, A. J.; Nallamothu, B. K. N. Engl. J. Med., 2009, 361, 849–857.

[80] a) Brenner D. J.; Hall, E. J. N. Engl. J. Med., 2007, 357, 2277–2284.

[81] Kamiya, K.; Ozasa, K.; Akiba, S.; Niwa, O.; Kodama, K.; Takamura, N.; Zaharieva, E. K.; Kimura Y.; Wakeford, R. Lancet, 2015, 386, 469–478.

[82] a) Rodnyi P. A. Physical Processes in Inorganic Scintillators, CRC Press, Boca Raton, 1997, b) Shani G. Radiation Dosimetry: Instrumentation and Methods, CRC Press, Boca Raton, 2000,

[83] Yanagida T. Opt. Mater., 2013, 35, 1987-1992. Yanagida T.; J. Lumin., 2016, 169 , 544-548.

[84] Rodnyi, P. A.; Physical Processes in Inorganic Scintillators, CRC Press, Boca Raton, 1997.

[85] Su, Y. B.; Wei, Y. Q.; Cai, L. Z.; Li, P. X.; Wang, M. S.; Guo, G. C.; Chem. Commun., 2018, 54, 12349–12352.

[86] a) Irie, S.; Kim, M.S.; Kawai, T.; Irie, M. Bull. Chem. Soc. Jpn., 2004, 77, 1037. b) K. Asai,; M. Koshimizu, Y. Fujimoto and K. Asai, Radiat. Meas., 2017, 106, 166-169. c) K. Takahashi, M. Koshimizu.

[87] (a) Y. Fujimoto and K. Asai, Nucl. Instrum. Methods Phys. Res., Sect. A, 2019. (b) K. Kinashi, Y. Miyashita, K. Ishida and Y. Ueda, J. Phys. Org. Chem., 2012, 25, 427-430. (c) K. Kinashi, Y. Miyamae, R. Nakamura, W. Sakai, N. Tsutsumi, H. Yamane, G. Hatsukano, M. Ozaki, K. Jimbo and T. Okabe, Chem. Commun., 2015, 51, 11170-11173. (d) K. Kinashi, T. Iwata, H. Tsuchida,

W. Sakai and N. Tsutsumi, ACS Appl. Mater. Interfaces, 2018, 10, 11926-11932. (e) Y. B. Su, Y. Q. Wei, L. Z. Cai, P. X. Li, M. S. Wang and G. C. Guo, Chem. Commun., 2018, 54, 12349-12352.

[88] (a) BP statistical review of world energy, Workbook, London, 2020. (b) Cook, T. R.; Dogutan, D. K.; Reece, S. Y.; Surendranath, Y.; Teets, T. S.; Nocera, D. G. Chem. Rev. 110, 6474-6502 (2010).

[89] Shockley, W.; Queisser H.J. Detailed balance limit of efficiency of p-n Junction Solar Cells. J. Appl. Phys. 32, 510-519 (1960).

[90] Battaglia, C.; Cuevas, A.; Woolf, S.D. High-efficiency crystalline silicon solar cells: status and perspectives. Energy Environ. Sci. 9, 1552-1576 (2016).

[91] Lewis, N. S. Toward Cost-Effective Solar Energy Use. Science 315, 798-801 (2007).

[92] (a) Albrecht, S. et al. Monolithic perovskite/silicon-heterojunction tandem solar cells processed at low temperature. Energy Environ. Sci. 9, 81-88 (2016), (b) Lumb, M. et al. GaSb-based solar cells for full solar spectrum energy harvesting. Adv. Energy Mater. 7, 1700345 (2017).

[93] Semonin, O. et al. Peak external photocurrent quantum efficiency exceeding 100% via MEG in a quantum dot solar cell. Science, 334, 1530-1533 (2011).

[94] Matthew, S. et al. Dye-sensitized solar cells with 13% efficiency achieved through molecular engineering of porphyrin sensitizers. Nat. Chem. 6, 242-247 (2014).

[95] M. Pagliaro, A. G. Konstandopoulos, R. Ciriminna and G. Palmisano, Energy Environ. Sci., 2010, 3, 279. (b) T. R. Cook, D. K. Dogutan, S. Y. Reece, Y. Surendranath, T. S. Teets and D. G. Nocera, Chem. Rev., 2010, 110, 6474–6502.

[96] (a) Ausfelder, F. et al. Energy Storage as Part of a Secure Energy Supply. Chem. BioEng. Rev. 4, 144-210 (2017). (b) Cook, T. R., Dogutan, D. K., Reece, S. Y., Surendranath, Y., Teets, T. S., Nocera, D. G. Chem. Rev. 110, 6474-6502 (2010).

[97] (a) L. Schnatbaum, Eur. Phys. J. Spec. Top., 2009, 176, 127–140. 12 M. Roeb, M. Neises, N. Monnerie, C. Sattler and R. Pitz-Paal, Energy Environ. Sci., 2011, 4, 2503. (b) N. Piatkowski, C. Wieckert, A. W. Weimerc and A. Steinfeld, Energy Environ. Sci., 2011, 4, 73. (c) A. Gil, M. Medrano, I. Martorell, A. Lazaro, P. Dolado, B. Zalba and L. F. Cabeza, Renewable Sustainable Energy Rev., 2010, 14, 31. (d) B. Coelho, A. C. Oliveira and A. Mendes, Energy Environ. Sci., 2010, 3, 1398.

[98] G. Jones, II, S.-H. Chiang and P. T. Xuan, J. Photochem., 1979, 10, 1–18.

[99] (a) Dubonosov, A. D.; Bren V. A. and Chernoivanov, V. A. Russ. Chem. Rev., 2002, 71, 917–927. (b) H. Taoda, K. Hayakawa, K. Kawase and H. Yamakita, J. Chem. Eng. Jpn., 1987, 20, 265–270. (c) Pouliquen, J.; Wintgens, V.; Toscano, V.; Jaafar, B. B.; Tripathi, S.; Kossanyi J. and Valat, P. Can. J. Chem., 1984, 62, 2478– 2486. (d) Olmsted, J.; Lawrence III, J. and Yee, G. G. Sol. Energy, 1983, 30, 271–274. (e) Bren, V. A.; Dubonosov, A. D.; Minkin V. I. and Chernoivanov, V. A.Russ. Chem. Rev., 1991, 60, 451-469

[100] Bren, V. A.; Dubonosov, A. D.; Minkin V. I. and Chernoivanov, V. A. Russ. Chem. Rev., 1991, 60, 451-469

[101] (a) Ishiba, K., et al. Photoliquefiable ionic crystals: a phase crossover approach for photon energy storage materials with functional multiplicity, Angew. Chemie. Int. Ed. 54, 1532-1536 (2014). (b) Kolpak, A. M. and Jeffrey C. Grossman, Azobenzene-Functionalized Carbon Nanotubes As High-Energy Density Solar Thermal Fuels, Nano Lett. 11, 3156–3162 (2011). (c) Kucharski, T. J. et al. Templated assembly of photoswitches significantly increases the energy-storage capacity of solar thermal fuels, Nat. Chem. 6, 441-447 (2014). (d) N. Nishimura, T. Sueyoshi, H. Yamanaka, E. Imai, S. Yamamoto and S. Hasegawa, Bull. Chem. Soc. Jpn., 1976, 49, 1381–1387.

[102] (a) Bandarab, H. M. D. and Burdette, S. C. Chem. Soc. Rev., 41, 1809–1825 (2012). (b) Brummel, O. ChemSusChem 9, 1424 – 1432 (2016).

[103] (a) Dreos, A.; et al. Exploring the potential of a hybrid device combining solar water heating and molecular solar thermal energy storage, Energy Environ. Sci. 10, 728-734 (2017). (b) Moth-Poulsen K.; et al. Molecular solar thermal (MOST) energy storage and release system, Energy Environ. Sci. 5, 8534-8537 (2012).

[104] (a) Kitagawa, D.; Kobatake, S. Chem. Rec. 2016, 16, 2005–2015. (b) Kobatake, S.; Uchida, K.; Tsuchida, E.; Irie, M. Chem. Lett. 2000, 1340–1341. (d) Chen, D. Z.; Wang, Z.; Zhang, H.; J. Mol. Struct.: THEOCHEM 2008, 859, 11–17.

[105] (a) Shirinian, V. Z.; Lvov, A. G.; Krayushkin, M. M.; Lubuzh, E. D.; Nabatov, B. V. J. Org. Chem. 2014, 79, 3440–3451 (b) Liu, G.; Pu, S.; Wang, R. Org. Lett. 2013, 15, 980–983.

[106] Gilat, S. L.; Kawai, S. H.; Lehn, J. M. Chem. Eur. J. 1995, 1, 275–284.

[107] Hammond, G. S. A correlation of reaction rates. J. Am. Chem. Soc. 77, 334-338 (1955).

[108] Perera, U. G. E.; Ample, F.; Echeverria, J.; Kersell, H.; Zhang, Y.; Vives, G.; Grisolia, M.; Rapenne, G.; Joachim, C.; Hla, S.-W. Controlled clockwise and anticlockwise rotational switching of a molecular motor. Nature Nanotechnol. 2013, 8, 46–51.

[109] (a) Chantzis, A.; Cerezo, J.; Perrier, A.; Santoro, F.; Jacquemin, D., J.; Chem. Theory Comput. 2014, 10, 3944-3957. (b) Li, X.; Zou, Q.; Ågren, H. J.; Phys. Chem. A 2015, 119, 9140-9147.

[110] Carella, A.; Launay, J.-P.; Poteau, R.; Rapenne, G.; Chem. Eur. J. 2008, 14, 814–8156.

[111] Yang, Y.; Weaver, M. N.; Merz, Jr., K. M.; J. Phys. Chem. A 2009, 113, 9843–9851.

[112] Uzelac, E. J.; Rasmussen, S. C.; J. Org. Chem. 2017, 82, 5947−5951.

[113] Erbland, G.; Gisbert, Y.; Rapenne, G.; Kammerer, C.; Eur. J. Org. Chem. 2018, 34, 4731–4739.

[114] Kutsunugi, Y.; Kawai, S.; Nakashima, T.; Kawai, T.; New J. Chem. 2009, 33, 1368–1373.

[115] Nakashima, T. ; Atsumi, K. ; Kawai, S. ; Nakagawa, T.; Hasegawa Y.; Kawai, T.; Eur. J. Org. Chem., 2007, 2007, 3212–3218.

[116] (a) Galangau, O.; Nakashima, T.; Maurel, F.; Kawai, T.; Chem. Eur. J., 2015, 21, 8471–8482.

[117] Calupitan, J. P. D. C.; Galangau, O.; Guillermet, O.; Coratger, R.; Nakashima, T.; Rapenne G.; Kawai, T.; Eur. J. Org. Chem., 2017, 2017, 2451–2461.

[118] Nakashima, T.; Tsuchie, K.; Kanazawa, R.; Li, R.; Iijima, S.; Galangau, O.; Nakagawa, H.; Mutoh, K.; Kobayashi, Y.; Abe J.; Kawai, T.; J. Am. Chem. Soc., 2015, 137, 7023-7026.

[119] Xie, J.; Wang, Y.; Liu, W.; Yin, X.; Chen, L.; Zou, Y.; Diwu, J.; Chai, Z.; Albrecht-Schmitt, T. E.; Liu, G.; Angew. Chem., Int. Ed., 2017, 56, 7500-7504

[120] (a) T. J. Kucharski, Y. Tian, S. Akbulatov, R. Boulatov, Energy Environ. Sci. 4, 4449–4472 (2011). (b) Lennartson, A. & Moth-Poulsen K. Molecular solar-thermal storage: molecular design and functional devices in Molecular devices for solar energy conversion and storage (eds. Tian, H., Boshcloo, G., Hagfeldt, A.) 327-352 (Springer, 2018). (c) Lennartson, A. Roffey, K. Moth-Poulsen, Tetrahedron Lett. 56, 1457–1465 (2015). (d) Ishiba, K., et al. Photoliquefiable ionic crystals: a phase crossover approach for photon energy storage materials with functional multiplicity, Angew. Chemie. Int. Ed. 54, 1532-1536 (2014). (e) Kucharski, T. J. et al. Templated assembly of photoswitches significantly increases the energy-storage capacity of solar thermal fuels, Nat. Chem. 6, 441-447 (2014). (f) Kolpak, A.M. and Jeffrey C. Grossman,

Azobenzene-Functionalized Carbon Nanotubes As High-Energy Density Solar Thermal Fuels, Nano Lett. 11, 3156–3162 (2011) (g) Wang, Z. et al. Evaluating Dihydroazulene-Vinylheptafulvene Photoswitches for Solar Energy Storage Applications, ChemSusChem 10, 2998 (2017), (h) Alexandru Vlasceanu et al. Photoswitchable Dihydroazulene Macrocycles for Solar Energy Storage: The Effects of Ring Strain, J. Org. Chem. (2017) (i) Ambra Dreos et al. Exploring the potential of a hybrid device combining solar water heating and molecular solar thermal energy storage, Energy Environ. Sci. 10, 728-734 (2017) (j) Kasper Moth-Poulsen et al., Energy Environ. Sci. 5, 8534-8537 (2012),

[121] (a) Nyulászi, L. Chem. Rev.2001, 101, 1229.; Katritzky, A. R.; Jug, K.; Oniciu, D. C. Chem. Rev. 2001, 101, 1421. (b) Havenith, R. W. A.; Fowler, P. W.; Steiner, E.; Shetty, S.; Kanhere D.; Pal, S. Phys. Chem. Chem. Phys.2004, 6, 285.

[122] (a) Balaban, A. T.; Oniciu, D. C.; Katritzky, A. R. Chem. Rev.2004, 104, 2777. (b) Minkin, V. I.; Glukhovtsev, M. N.; Simkin, B. Ya. Aromaticity and Antiaromaticity. Electronic and Structural Aspects; Wiley: New York, 1994.

[123] Jorner, K. et al. Unraveling factors leading to efficient norbornadiene–quadricyclane molecular solar-thermal energy storage systems. J. Mater. Chem. A. 5, 12369–12378 (2017).

[124] Asato, R.; Martin, C.J.; Calupitan, J.P.; Mizutsu, R.; Nakashima, T.; Okada, G.; Kawaguchi, N.; Yanagida, T.; Kawai T. “Photosynergetic amplification of radiation input: from efficient UV induced cycloreversion to sensitive X-ray detection” Chem. Sci. 11, 2504–2510 (2020).

Abstract

Molecular switching materials that modulate physical properties through an external trigger have received much attention in the development of new devices. They require precise switching performance and large scale propagation on single and multiple molecular levels. Diarylethene has attracted much attention due to its excellent photoswitching properties. These molecules photocyclize from the open (o) form to the closed (c) form with UV light, with visible light inducing reversion to the o form. Terarylene structures have been optimized for switching in areas including photoreaction quantum yields, thermal stability and desorption of functional groups upon structural change. In this thesis the focus is placed upon a single photoswitching reaction and the affect this has on local geometry and physical properties. First, this thesis shows that a small number of photoswitching reactions on a terarylene subunit can stop or start dynamic movement, namely the rotation of a molecular motor. The rotation was activated depending on which part of the rotor is approached by an electron injecting STM tip; with light irradiation offering a second independent control input. A new motor containing a terarylene substituent was designed in which the flexible open form can be converted to its rigid closed form to block rotation via steric interactions thus acting as a light-induced brake. With the initial target unit for this motor chosen using computational calculations of these interactions. A new synthetic methodology for the introduction of the photoswiching unit into the motor is presented and then the rotational control was discussed using spectral changes in the NMR upon irradiation. In the second part of this thesis, the effect c to o form isomerization of terarylenes has on nearby molecules through synergetic effects are presented. Work to enhance the quantum yield of the isomerization provides new applications using alternative stimulus without light irradiation. Examples including chemical or electrochemical oxidation proceed with high efficiency in a (electro)catalytic way, with apparent reaction efficiency exceeding 100% through a cascade reaction. By introducing aromatic groups on the reactive carbons of a photoreactive system, the efficiency of the electrocatalytic cycloreversion reaction was increased to 100000% and applied to the amplified detection of a small amount of high energy photons such as X-rays. In the third part, new molecular solar thermal (MOST) fuel is presented using the cascade reaction. MOST fuel systems capture photonic energy, retaining photocurrent in the formed chemical bond, instead of battery based electrochemical storage. The high energy density of MOST fuel offers large heat release, with cycloreversion via bond disassociation at levels equivalent to artificial photosynthesis without environmental impact. A small amount of electrochemical or chemical oxidation can induce the cascade release of stored thermal energy. In addition, a storing process of the light energy optimized by introduction of phenyl rings on the terarylene reactive carbon atoms has been developed. These present high MOST efficiency and the results are supported by a detailed computational study.

Résumé

Les matériaux photo-commutation moléculaires qui modulent les propriétés physiques via un stimulus externe ont reçu beaucoup d'attention dans le développement de nouveaux appareils. Les diaryléthènes sont particulièrement intéressants en raison de leurs excellentes propriétés de photoswitching. Ces molécules photocyclisent de la forme ouverte (o) à la forme fermée (c) sous rayonnement UV, la lumière visible permettant de revenir à la forme o. Les structures de type terarylène ont été optimisées pour présenter des rendements quantiques de photoréaction important ainsi qu'un bonne stabilité thermique. Dans cette thèse, l'accent est mis sur une seule réaction de photoswitching et son effet sur la géométrie locale et les propriétés physiques de la molécule obtenue. Dans la première partie, cette thèse montre qu'un petit nombre de réactions de photoswitching sur une sous-unité de terarylène peut arrêter ou déclencher le mouvement de rotation d'un moteur moléculaire à deux étages. La rotation est activée par l'injection d'électrons sur le rotor par une pointe STM. La lumière offre donc une deuxième entrée de commande indépendante. Un nouveau moteur contenant un substituant terarylène a été conçu dans lequel la forme ouverte flexible peut être convertie en sa forme fermée rigide pour bloquer la rotation via des interactions stériques agissant ainsi comme un frein induit par la lumière. L'introduction du fragment photochrome a nécessité une nouvelle voie synthétique dans le moteur est présentée et le contrôle de rotation est démontré par RMN à température variable et suivi de l'irradiation par spectroscopie UV-Visible. Dans la deuxième partie de cette thèse, il est démontré que l'isomérisation des terarylènes peut se propager aux molécules voisines. Il est donc possible d'améliorer le rendement quantique de l'isomérisation pour de nouvelles applications sans qu'il y ait besoin de stimulus lumineux. Des exemples comprenant une oxydation chimique ou électrochimique se déroulent avec une efficacité élevée de manière (électro) catalytique, avec une efficacité de réaction apparente dépassant largement 100% par une réaction en cascade. En introduisant des groupes aromatiques sur les carbones réactifs du système photochrome, l'efficacité de la réaction de cycloréversion électrocatalytique a été augmentée à 100 000 %. Un nouveau système thiophényl riche en électrons a aussi été conçu pour augmenter la stabilité cationique. Il permet de détecter de faible quantité de photons à haute énergie tels que les rayons X. Dans la troisième partie est proposé un nouveau système de combustible solaire thermique moléculaire (MOST) utilisant également la réaction en cascade. La plupart des systèmes de carburant capturent l'énergie photonique, conservant le photocourant sous forme de liaison chimique, au lieu d'un stockage électrochimique couramment utilisé dans les batteries. La densité d'énergie élevée du combustible MOST offre un dégagement de chaleur important, avec une cycloréversion par dissociation des liaisons à des niveaux équivalents à la photosynthèse artificielle sans impact environnemental. Une petite quantité d'oxydation électrochimique ou chimique peut induire la libération en cascade de l'énergie thermique stockée. De plus, un procédé de stockage de l'énergie lumineuse optimisé par l'introduction de cycles phényle sur les atomes de carbone réactifs au terarylène a été développé. Ceux-ci présentent une efficacité MOST élevée et les résultats sont soutenus par une étude théorique détaillée.